THE IMPACT OF INFLAMMATION ON THE REGULATION OF INTRACELLULAR CALCIUM IN CUTANEOUS NOCICEPTIVE NEURONS

by

Nicole Newell Scheff

Bachelor of Science in Chemistry, University of Kentucky, 2009

Submitted to the Graduate Faculty of

University of Pittsburgh School of Medicine in partial fulfillment

of the requirements for the degree of

Doctor of Philosophy

University of Pittsburgh

2014

UNIVERSITY OF PITTSBURGH

SCHOOL OF MEDICINE

This dissertation was presented

by

Nicole Newell Scheff

It was defended on

June 26th, 2014

and approved by

Dr. Gerald Gebhart, PhD, Professor, Department of Anesthesiology

Dr. Brian Davis, PhD, Professor, Department of Neurobiology

Dr. William de Groat, PhD, Professor, Department of Pharmacology and Chemical Biology

Dr. Stephen Meriney, PhD, Professor, Department of Neuroscience

Dr. Yuriy Usachev, PhD, Professor, Department of Pharmacology

Dissertation Advisor: Dr. Michael S. Gold, PhD, Professor, Department of Anesthesiology

THE IMPACT OF INFLAMMATION ON THE REGULATION OF INTRACELLULAR CALCIUM IN CUTANEOUS NOCICEPTIVE NEURONS

Nicole Newell Scheff, B.S.

University of Pittsburgh, 2014

The most effective way to treat clinical pain is to target the subpopulation of primary afferent neurons responsible. However, clinical pain is heterogeneous, reflecting, in part, differences in the relative contribution of different subpopulations of afferents. The functional heterogeneity of primary afferents is reflected in the heterogeneous regulation of intracellular Ca^{2+} ($[Ca^{2+}]_i$). Because the regulation of $[Ca^{2+}]_i$ contributes to neuronal function, injury-induced changes in neuronal function may be due to dysregulation in the regulation of $[Ca^{2+}]_i$. Thus, the persistent inflammation-induced increase in the magnitude and duration of depolarization-evoked Ca^{2+} transient in a subset of putative nociceptive cutaneous DRG neurons served as the focus of this thesis. I first ruled out the contribution of Ca^{2+}-induced Ca^{2+} release to the inflammation-induced increase in the evoked Ca^{2+} transient. Results of these experiments also indicated the presence of tightly segregated Ca^{2+} regulatory domains where Ca^{2+} transients evoked via Ca^{2+} influx and release from intracellular stores are functionally isolated. Parametric analysis demonstrated that inflammation-induced changes in evoked Ca^{2+} had a high threshold for activation, thus I focused on low affinity Ca^{2+} extrusion mechanism, Na^{+}/Ca^{2+} exchanger (NCX). I demonstrated that NCX regulates the decay of the evoked transient in the same subset of putative nociceptive afferents modified by inflammation, and can influence axonal $[Ca^{2+}]_i$ levels, resting membrane potential, and nociceptive threshold. Finally, I confirmed a role for NCX in response to persistent inflammation, such that the increase in the duration of the evoked

transient is due to a loss of NCX in the cell body due to an increase in unidirectional NCX3 trafficking to the peripheral terminals. These observations serve as the basis for my current working hypothesis that the inflammation-induced changes in trafficking of NCX3, underlie three major aspects of the inflammatory response: an increase in transmitter release from the central terminal to contribute to inflammatory hyperalgesia, a change in gene expression secondary to altered Ca^{2+} transients in the cell body, and a decrease in the neurogenic inflammatory response in the periphery secondary to a decrease in transmitter release. Increasing NCX function may be a potentially novel therapeutic strategy for treatment of inflammatory pain.

TABLE OF CONTENTS

LIST OF TABLES

LIST OF FIGURES

PREFACE

I would like to thank a number of individuals for the guidance and support during the completion of my graduate training. First and foremost, I would like to express the highest amount of gratitude and appreciation to my thesis advisor, Dr. Michael Gold, for his continual support over the past 5 years. It was truly a pleasure (most days) to be able to interact with someone so driven and intrigued by science, regardless of the subject. I am extremely grateful for the substantial amount of time and energy spent by Dr. Gold, to break me down and remold me into a critical thinker, academic scientist, and master of the perfectly crafted run-on sentence, as demonstrated in the subsequent pages of this dissertation.

I would also like to show my appreciation to my thesis committee, comprised of Drs. Chet de Groat, Brian Davis, Steve Meriney, and Jerry Gebhart for time and valuable feedback regarding my project and manuscripts. Their knowledge and expertise during this process has been instrumental in my success. I would like to show special appreciation to Dr. Gebhart for serving as my committee chair and Dr. Davis for kindly agreeing to step in as member of the committee late in the process. I would also like to give a special thanks to Dr. Yuriy Usachev for serving as my outside examiner.

There are no suitable words to describe the magnitude of appreciation I have for my parents, Steve and Sue Scheff, as none of this could have been possible without their love and guidance. I would like to especially thank my father for teaching me how to fall in love with

research, that tomorrow is another day and a positive outlook can make all the difference. He is truly an inspiration and I could not be more proud to be his daughter and follow in his footsteps. I would also like to thank my wonderful fiancé, Marvin Devers, for putting up with all the late nights and weekends spent in lab and for the constant encouragement and entertainment during this process. Lastly, I would like to thank all of my fantastic friends, especially Jennifer Deberry, Lisa McIlvreid, Jamey Maniscalco and Michelle Failla for adding in the perfect amount of hilarity to the day to day insanity of this process.

1.0 INTRODUCTION

One of the most vital functions of the nervous system is to integrate information about the occurrence and threat of injury. Pain, as a submodality of somatic sensations, has been defined by the International Association for the Study of Pain as an unpleasant sensory and emotional experience associated with actual or potential tissue damage. Pain is modulated by past experiences, setting, affect, cognitive influences, gender and even cultural expectations, and thus is always subjective (Merskey, 1994). Accordingly, the central nervous system (CNS) must be intact for pain to be perceived. However, while pain can originate from within the central nervous system (e.g stroke), the vast majority of pain experienced, including chronic pain associated with nerve injury and inflammatory disorders, arises from activity in primary afferent neurons. Under normal conditions, only stimulus modalities (mechanical, thermal, and chemical) extreme enough to potentially injure tissues are capable of initiating the neural process of encoding noxious stimuli, referred to as nociception, and ultimately the perception of pain. Noxious stimuli are detected by specialized sensory neurons referred to as nociceptors, which then relay this information to the CNS. This process is referred to as transduction, and major progress has been made in understanding the molecular mechanisms underlying this process within nociceptive primary afferents. There has also been significant progress in our understanding of the subsequent steps in the process including transmission, perception and modulation. We chose to focus on the role of the primary afferent in pain because of overwhelming evidence indicating that in the presence of ongoing pain, a reduction in the relevant primary afferent activity or block of their input to the CNS can attenuate or completely

relieve the complex sensory and emotional consequences of the noxious input. This has been found to be true not only for acute pain associated with tissue injury, but for many types of chronic pain as well (Gracely et al., 1992, Verne et al., 2003, Price et al., 2009, Staud et al., 2009).

While pain is often discussed as a singular entity, it is clearly more complex. Even in experimental settings, intense heat to the foot can be easily dissected into an initial component, referred to as first pain that is described as lancinating, stabbing, or pricking, and a second component referred to as second pain described as burning, throbbing, cramping, or aching (Price and Dubner, 1977). More relevantly, in clinical settings, patients can complain of a variety of different "types" of pain. For example, ongoing pain is the most common feature of neuropathic pain, and is manifest in the absence of any other stimuli. Movement-evoked pain is most bothersome to patients suffering from osteoarthritis, who feel pain in their knees when attempting to walk. Patients may also complain of increased sensitivity to shifts in temperature, where cool or warm stimuli can be perceived as painful; the latter is most commonly manifest in burn patients. Additionally, the source of the pain is also associated with unique perceptual components such that, for example, sore muscles feel nothing like the cramping associated with distention of the colon.

The available evidence indicates that specific nociceptive primary afferents mediate these different conditions. For example, the more rapidly conducting A-δ fibers have been shown to mediate first pain, while more slowly conducting C-fibers mediating second pain (Price and Dubner, 1977, Fang et al., 2005). Similarly, ongoing pain must reflect the emergence of ongoing activity in afferents. There is a distinct population of mechanically sensitive C-fibers that are relatively insensitive to mechanical stimuli in the absence of tissue injury, referred to as "silent"

nociceptors. However, in the presence of injury these silent afferents become spontaneously active and show robust mechanical sensitivity suggesting that these afferents mediate ongoing pain in neuropathic pain patients. Nociceptive afferents, by definition, can be sensitized. Sensitization, which typically develops as a consequence of tissue insult and inflammation, is defined as a reduction in the threshold and an increase in the magnitude of a response to noxious stimulation (Bessou and Perl, 1969). Since not all nociceptive afferents are mechanically sensitive, a subpopulation of mechanically sensitive afferents must mediate the pain of osteoarthritis. A subset of C-fibers that transduces noxious levels of heat has been shown to be essential for thermal sensitivity associated with most types of tissue injury, whereas two other distinct populations appears to underlie cold sensitivity following sensitization versus after injury (Bautista et al., 2007, Karashima et al., 2008). Furthermore, there is additional evidence that subpopulations of visceral nociceptors might underlie different types of visceral pain such as hypersensitivity to organ filling, acidic or burning pain, bloating and gas sensations (Robinson and Gebhart, 2008). Even more interesting, and potentially important from a clinical perspective, there is evidence to suggest that there are two parallel but distinct nociceptive pathways that code for the affective emotional component of pain versus sensory discriminative components (Braz et al., 2005). All of these data suggest that to most effectively treat clinical pain, it may not only be possible, but necessary, to target the subpopulation of afferents responsible for the type of pain and thus, identification of the nociceptive afferent subpopulation responsible for a particular type of pain is an active area of investigation.

1.1 HETEROGENEITY OF CUTANEOUS PRIMARY AFFERENTS

The first major theme of this dissertation is the molecular mechanism underlying pain in the presence of inflammation. Cutaneous (skin) afferents were chosen for three major reasons. First, while deep tissue pain is more common, sensory receptors in the skin have been more thoroughly studied, most likely due to the relative ease of accessibility, than receptors in any other tissue, thereby providing a broader context within which to interpret the experimental results. Second, the opportunity to perform correlative studies in animals and humans allows for powerful inferences to be made regarding function and the more rapid translation of preclinical observations to the clinic. Significant insights into the cellular and molecular basis of cutaneous nociception have been realized from studies on conscious humans and animal models (Le Bars et al., 2001, Namer et al., 2009) and furthermore, the morphology of sensory nociceptive nerve endings is highly conserved in animals from rodents to humans (Raja et al., 1988, Lewin and Moshourab, 2004). Third, cutaneous pain still has clinical significance as diseases associated with small-fiber neuropathies (e.g. postherpetic neuralgia) have profound effects on cutaneous sensory function often leading to severe pain.

While, there is considerable heterogeneity among nociceptive afferents, all sensory afferents are pseudo-unipolar neurons with an axon arising from the soma and then bifurcating. One branch gives rise to peripheral axons that ultimately terminate in somatic tissue in what is referred to as a free nerve ending, due to the absence of specialized cells around the terminal. The second branch gives rise to the central projection, terminating in the superficial dorsal horn of the spinal cord. The cell bodies reside in a cluster referred to as the dorsal root ganglia (DRG) positioned on either side of the spinal cord providing the innervation pattern, referred to as dermatomes, mapped onto the spinal cord (Raja et al., 1988).

Despite the clinical need, there is currently no single criterion that can reliable identify specific subpopulations of nociceptive afferents. Nevertheless, attempts have been made to classify these neurons based on their anatomy, physiology, and biochemical content (Koerber et al., 1988, Lawson, 2002). One criterion, as alluded to above, is conduction velocity. The sensory neurons thought to transmit nociceptive input can be divided into two classes: 1) small diameter cell bodies and slowly conducting unmyelinated axons (C fibers) and 2) medium diameter cell bodies and faster conducting lightly myelinated axons (Aδ fibers) (Harper and Lawson, 1985, Lawson, 2002). There also is evidence that cell body diameter can be used to distinguish these two classes as neurons with a small cell body diameter tend to give rise to C-fibers, while those with a large diameter cell body tend to give rise to A-beta fibers (Harper and Lawson, 1985). A second criterion is the noxious sensory modalities to which nociceptors respond, such that afferents that respond to mechanical, thermal, and chemical stimuli are referred to as polymodal, whereas others are only activated by a subset (e.g. mechano-heat). However, these classes are neither functionally nor anatomically homogeneous (Caterina and Julius, 1999). Alternatively, as a third criterion, neurochemical studies have revealed a variety of different markers based on the histological/neurochemical properties. The most common of these is the presence of the neuropeptides, substance P and calcitonin gene related peptide (CGRP). The subpopulation of nociceptors that express these peptides are referred to as peptidergic, while those without are referred to as non-peptidergic. Neurotrophic receptors are also widely used to distinguish subpopulations of nociceptive afferents, where one group is defined by the presence of the receptor for nerve growth factor (NGF), trkA, and others are defined by the presence of receptors for different members of the glial cell line-derived family of neurotrophic factors (GDNF). Alternatively, neurons were screened with a panel of plant lectins that demonstrated distinct

patterns of staining within the DRG (Acosta et al., 2014). Of these, the most commonly used is the lectin, alpha-D-galactose-specific isolectin B4 (IB4), from the plant *Griffonia Simplicifolia*. At least in cutaneous neurons, IB4 appears to primarily bind to non-peptidergic neurons that give rise to C-fibers. However, there are still limitations using these criteria. For example, there is a subpopulation of IB4+ C-fibers that coexpress Ret and TrkA and are therefore responsive to both GDNF and NGF (Orozco et al., 2001). Substance P has also been observed in myelinated Aα/β fibers (Koerber and Mendell, 1988, Lawson et al., 1997) thought to be involved in non-nociceptive transduction.

A fifth criterion is based on the chemosensitivity of the neuron. For example, different subpopulations of nociceptive afferents are responsive to ATP, decreases in pH, or nicotine. In this context, capsaicin, the chemical ingredient in hot peppers responsible for the burning sensation (Caterina and Julius, 1999), has been used most widely to identify nociceptors, as the most prominent perception in response to capsaicin application to the skin is pain (Acosta et al., 2014). Importantly, the advantage of this last criterion is that it is easily used on dissociated neurons *in vitro*, where in the absence of a peripheral axon to enable functional characterization of the afferent in question, capsaicin sensitivity can be used to identify a nociceptor. The receptor for capsaicin is transient receptor potential vanilloid 1 (TRPV1), shown to underlie inflammatory thermal sensitivity. However, the downside of TRPV1-mediated chemosensitivity is that it encompasses a large variety of nociceptive subtypes. Localization studies with TRPV1 show expression in 75% of IB4+ and 59-65% of CGRP expressing neurons from rat (Michael and Priestley, 1999, Popovich et al., 1999). Furthermore, genetic deletion of TRPV1 in mice only partially reduced noxious heat sensitivity in behavioral assays, and had no effect on heat responsiveness of C-fibers tested (Caterina et al., 2000, Davis et al., 2000, Woodbury et al.,

2004) suggesting that, at least in mice, there exists a subset of fibers other than those expressing TRPV1 that contribute to thermal pain.

1.2 CUTANEOUS NONPEPTIDERGIC C-FIBERS

Of interest for the work described in the subsequent chapters is the C fiber nonpeptidergic subpopulation of nociceptors that innervate the skin. In order to establish a "neurochemical profile" for this subpopulation at the level of the isolated cell body and due to the limitations surrounding individual criteria, multi-criterion approach was utilized. A retrograde tracer was used to identify the neurons in the lumbar DRG that innverate the glabrous skin. The cell body diameter was used to identify the C-fiber subpopulation based on data indicating that there is a rough correlation between cell body (soma) size and axon conduction velocity (Harper and Lawson, 1985). IB4 binding was used to distinguish peptidergic from non-peptidergic fibers. Lastly, capsaicin was applied to identify capsaicin-sensitive putative nociceptive neurons.

The IB4+ population of cells has recently been the focus of many studies in rodents (Stucky and Lewin, 1999, Braz et al., 2005, Lu et al., 2010) and ultimately proved to be the most important subpopulation studied in the subsequent chapters. There are unique properties of this subpopulation, found to be very distinct from the IB4-, presumably peptidergic, subpopulation. While both classes are believed to respond to all noxious stimulus modalities, they appear to have distinct innervation patterns in the spinal cord as well as specialized multisynaptic connectivity in the CNS. IB4+ fibers terminate mainly in inner lamina II of the dorsal horn of the spinal cord and the neurons in the inner portion are rich in protein kinase C (PKC). Transgenic animals that lack the gamma isoform of PKC showed normal acute pain responses but attenuated

response to neuropathic pain (Malmberg et al., 1997). Alternatively, peptidergic fibers are found to terminate in the most superficial layers, lamina I, as well as deeper lamina III/IV. The resident neurons in these lamina express the receptor for substance P, neurokinin 1 (NK1). However, ablation of these neurons with a substance P-conjugated neurotoxin had no effect on baseline responses to noxious mechanical and heat stimuli and instead, the hypersensitivity induced by capsaicin was significantly attenuated (Mantyh et al., 1997). These fundamental differences in the patterns of termination suggest that they engage different CNS pain transmission circuitry. Braz and colleagues found that in distinct contrast to the peptidergic nociceptors, which communicate with projection neurons of lamina I (Gauriau and Bernard, 2002), the IB4+ population predominately engages the limbic regions of the brain, via projection neurons in the deep dorsal horn, suggesting a parallel pain pathway to brain regions that process affect and emotional aspects of pain (Braz et al., 2005).

Studies have also demonstrated functional differences in efferent activity of primary afferents, that is involved in regulation of vasculature and immune cells within the skin necessary to maintain general tissue health and bone integrity (Pierce et al., 1995, Offley et al., 2005). Peptidergic afferents in particular appear to be the major effectors of this efferent mechanism, referred to as neurogenic inflammation (Cao et al., 1998). The hallmarks of inflammation are redness (rubor), swelling or edema (tumor), pain (dolor), and warmth (calor). CGRP and substance P are released from primary afferents into the skin and cause vasodilation (redness) and plasma extravasation (swelling), respectively, in addition to immune cell activation and recruitment, release of pro-inflammatory cytokines, and production of new immune cells. Neurogenic inflammation is thought to accelerate healing (Lynn et al., 1996). However, in some

situations, it can exacerbate tissue damage/pain by indirectly facilitating interplay between components of pro-inflammatory mechanisms and nociception (Chiu et al., 2012).

The extent to which there is an efferent function for IB4+ afferents is not currently clear. However, recent evidence suggests that IB4+ neuron may be the major source of glutamate release in the periphery as proteins considered essential for vesicular uptake and exocytotic release of glutamate are not expressed at detectable levels in most peptidergic neurons (Morris et al., 2005). Glutamate has been shown to have a major role in signaling in the skin, regulating the release of adenosine, CGRP, and nitric oxide in the periphery from primary afferent nerve terminals (Jackson and Hargreaves, 1999, Beirith et al., 2002). While there is little evidence that glutamate directly contributes to signs of inflammation, when released from nociceptors or exogenously applied it produces nociceptive effects in animals and painful responses in humans (Miller et al., 2011). Results from animal studies show analgesic benefit from regulation of the peripheral glutamatergic system (Aley and Levine, 2002, Jang et al., 2004) and clinical studies show potential for relieving some aspects of chronic pain (Quan et al., 2003, Takahashi et al., 2008, Miller et al., 2011). However, more evidence is needed to better understand the role of efferent glutamate signaling and pain.

Although much remains to be learned regarding the functional importance of the specializations among nociceptors, the existing data provides a framework for study. A more complete understanding of how nociceptor heterogeneity contributes to the discriminative properties of the pain pathway will aid the continued search of more specialized therapeutic approaches to prevent chronic pain.

1.3 REGULATION OF INTRACELLULAR CALCIUM SIGNALING

The second major theme of this dissertation is the regulation of intracellular Ca^{2+} ($[Ca^{2+}]_i$). Ca^{2+} is a highly versatile second messenger within the cell that is involved in the regulation of a multitude of physiological processes, where kinetics, amplitude, and spatio-temporal patterning (Berridge et al., 2000). Ca^{2+} signaling begins when a neuron is stimulated, resulting in an increase in the concentration of free cytosolic Ca^{2+}. The increase can occur via influx (e.g. voltage-gated cation channels) or release from internal Ca^{2+} stores. Ca^{2+} then functions as a second messenger, interacting with different Ca^{2+} binding proteins to stimulate numerous Ca^{2+}-sensitive processes ranging from neurotransmitter release, neuronal excitability, gene transcription, and even apoptosis (Berridge et al., 2000). The brief increase in $[Ca^{2+}]_i$, referred to as the Ca^{2+} transient, is terminated by a series of buffers, re-uptake, and efflux mechanisms that remove Ca^{2+} from the cytoplasm to restore the resting state. These regulatory mechanisms, referred to as the "Ca^{2+} toolkit" (Berridge et al., 2003), serve to tightly regulate $[Ca^{2+}]_i$..

Ca^{2+} signaling has been described in virtually all cell types, but each cell type expresses a unique version of the toolkit, based on their function within the organism, in order to sculpt spatial and temporal properties of the transient to fit the precise needs of the cell. The influx and intracellular release pathways initiate the magnitude of the $[Ca^{2+}]_i$ transient. These pathways are comprised of plasma membrane Ca^{2+} channels, such as voltage gated Ca^{2+} channels (VGCC), whereas release is mediated by intracellular Ca^{2+} channels, such as Ins(1,4,5)P3 receptor (InsP3R) and ryanodine receptor (RYR) expressed on the endoplasmic reticulum (ER), an organelle responsible for protein synthesis and metabolic processes. Regulation of Ca^{2+} after the initial rise in $[Ca^{2+}]_i$ is mediated by a complex interplay between cytosolic Ca^{2+} buffer proteins,

mitochondria, an organelle responsible for a bulk of the cell's ATP production, and Ca^{2+} pumps and exchangers expressed on the internal stores and plasma membrane. The cytosolic Ca^{2+} buffers and mitochondria serve to rapidly sequester Ca^{2+}, thereby regulating the magnitude of the transient, and then slowly release it back into the cytosol to be further regulated. The Na^{+}/Ca^{2+} exchanger (NCX), a low affinity/high capacity extrusion mechanism located in the plasma membrane, the plasma membrane Ca^{2+} ATPase (PMCA), and the sarco-endoplasmic reticulum Ca^{2+} ATPase (SERCA), thought to be lower capacity pumps with a much higher affinity for Ca^{2+}, work in unison to pump Ca^{2+} out of the cell or into the ER, respectively. Together these mechanisms complete the recovery process and the maintenance of resting Ca^{2+} levels (Berridge et al., 2003). Under normal conditions, the buffering and extrusion mechanisms can reduce the Ca^{2+} transient introduced by different influx pathways, thus maintaining tight regulation of the magnitude and duration of the Ca^{2+} transient.

Another layer to the regulation of intracellular Ca^{2+} involves a concept, referred to as Ca^{2+} microdomains, in which a transient Ca^{2+} signal is focalized to a specific area of a cell and regulated by a unique combination of machinery. For example, Ca^{2+} microdomains have been implicated in the presynaptic regulation of transmitter release. Based on the classical mechanism of release, VGCC influx is associated with the exocytotic machinery to provide the localized pulse of Ca^{2+} that triggers exocytosis (Weiss and Zamponi, 2012). Grosche and colleagues (1999) found that exocytosis could also be triggered by a Ca^{2+} microdomain involving release from the ER found in the synaptic endings in neurons. The size of these microdomains depends on a number of aspects, such as the rate of signal generation, signal diffusion, and removal, and presumably the density and distribution of Ca^{2+} regulatory mechanisms. The presence of Ca^{2+} buffers helps to restrict brief pulses to small microdomains within the cytoplasm (Berridge,

2006). The global Ca^{2+} signal is thus a reflection of the integrated output of temporally and spatially restricted microdomains, which, if appropriately organized, may be able to sustain Ca^{2+} oscillations within the cytosol.

1.4 INFLAMMATION AND INTRACELLULAR CALCIUM SIGNALING

There is a large body of evidence establishing that the regulation of $[Ca^{2+}]_i$ contributes to neuronal function. Thus, a change in neuronal function, such as an increase in excitability or neurotransmitter release caused by injury or inflammation, may be reflected in the regulation of $[Ca^{2+}]_i$. This is supported by observations that traumatic nerve injury is associated with decreases in VGCC density (Baccei and Kocsis, 2000, Hogan et al., 2000, McCallum et al., 2003), a decrease in resting $[Ca^{2+}]_i$ and a decrease in both the magnitude and decay of evoked Ca^{2+} transients in DRG neurons after nerve injury (Fuchs et al., 2007). In contrast, Lu and colleagues (2008) assessed the impact of persistent inflammation on resting and evoked $[Ca^{2+}]_i$ and found that while there was no change in resting $[Ca^{2+}]_i$, there was a marked increase in the magnitude and duration of depolarization-evoked Ca^{2+} transients in putative nociceptive cutaneous DRG neurons. Despite subsequent work by these investigators (Lu and Gold, 2008, Lu et al., 2010), the underlying mechanisms and functional implications for this inflammation-induced change are currently unknown and thus served as the focus of this thesis.

Based on the earlier discussion regarding primary afferent signaling, it should not be surprising that there is extensive heterogeneity in the relative contribution of the various components of the Ca^{2+} toolkit among sensory DRG neurons. Lu and colleagues (2006) have done extensive work analyzing the contribution of individual Ca^{2+} regulatory mechanisms with

respect to the depolarization-evoked Ca^{2+} transient in the dissociated sensory neuron cell body. They demonstrated marked differences among subpopulations with respect to both the magnitude and duration of evoked Ca^{2+} transients. The magnitude of the evoked increase in $[Ca^{2+}]_i$ was the largest and the decayed the slowest in small diameter, IB4+ and capsaicin-responsive (CAP+) neurons. However, this population had the smallest high voltage activated (HVA) VGCC current density, suggesting differential contribution of other toolkit components are reflected in the kinetics of the evoked transient compared to the large diameter IB4- negative population (Lu et al., 2006).

The impact of inflammation was the most substantial in small diameter, IB4+, CAP+ neurons innervating the site of inflammation. Lu and colleagues used depolarization through application 30mM KCl (high K^+) to evoke a Ca^{2+} transient in the dissociated cell body. This technique results in a shift in resting membrane potential to -20 mV for the duration of high K^+ application, and demonstrated that there was no inflammation-induced change in either the magnitude of the depolarization or the number of action potentials evoked in response to depolarization, thereby ruling out an inflammation-induced shift in excitability as an underlying mechanism for this change. Furthermore, depolarization leads to Ca^{2+} influx through VGCC only, so while there may be inflammation-induced changes in other cation channels, such as NMDAR (Tan et al., 2008) and TRP channels (Koerber et al., 2010), these are not engaged by the stimulus used by Lu and colleagues. An increase in HVA current density has been identified in a number of chronic pain conditions and is associated with a decrease in nociceptive threshold (Bourinet et al., 2014). However, inflammation was associated with a paradoxical decrease in the density of HVA current in small and medium but not large diameter cutaneous DRG neurons innervating the site of inflammation (Lu and Gold, 2008). While this decrease is attributed, at

least in part, to an inflammation-induced trafficking of the α2δ1 subunit and CaV2.2 protein to the central nerves of L4 and L5 ganglia ipsilateral to the site of inflammation (Lu and Gold, 2008), it does not aid in understanding the underlying mechanism of the inflammation-induced increase in the evoked Ca^{2+} transient.

Release from intracellular stores via a mechanism referred to as Ca^{2+} induced Ca^{2+} release (CICR), is a potential player in the increase in the magnitude and/or duration of the Ca^{2+} transient in the presence of inflammation. The major intracellular Ca^{2+} channels mediating CICR are ryanodine receptors (RYR). Others have previously demonstrated that this mechanism contributes to the magnitude of evoked Ca^{2+} transients in some DRG neurons from naïve animals (Usachev et al., 1993, Usachev and Thayer, 1999, Eun et al., 2001). It has also been demonstrated that CICR is most prominent in large diameter DRG neurons (Jackson and Thayer, 2006, Lu et al., 2006) and contributes little to the high K^+-evoked Ca^{2+} transient in the small diameter, IB4+, CAP+ cutaneous subpopulation of afferents (Lu et al., 2006). Therefore, any change in CICR machinery or the coupling between Ca^{2+} influx via VGCC and CICR in these neurons could have a profound influence on the evoked transient, possibly underlying the inflammation-induced changes in the Ca^{2+} transient. In Chapter 1 of this dissertation, I assess the contribution of CICR to the inflammation-induced increase in the high K^+-evoked Ca^{2+} transient in small diameter putative nociceptive cutaneous DRG neurons.

The inflammation-induced changes in the duration of the evoked transient could be mediated by different buffers, pumps, and/or exchangers. There are many studies that have identified marked differences in the relative contribution of buffering mechanisms in DRG neurons, but a consensus has not yet been reached. For example, mitochondria, thought to shape both the magnitude, via uptake through a Ca^{2+} uniporter, and the decay, via release via

mitochondrial NCX (Berridge et al., 2003), have been shown to buffer (> 400 nM) Ca^{2+} loads in most DRG neurons (Werth and Thayer, 1994). However, Kostyuk et al demonstrated that mitochondria differentially impact the magnitude and decay of evoked Ca^{2+} transients in larger, but not small diameter DRG neurons. Furthermore, inhibition of mitochondria in DRG neurons resulted in a larger magnitude and slower decay of the high K^+-evoked Ca^{2+} transient (Shishkin et al., 2002) suggesting it may play a role in the presence of inflammation. However, disruption of mitochondria would lead to a loss in ATP production, which would in turn disrupt PMCA-mediated extrusion as well as other ATPase activity underlying resting membrane potential. Again, because there is no inflammation-induced change in resting $[Ca^{2+}]_i$ (Lu and Gold, 2008) and no apparent change in cell health, mitochondria are not highly likely to contribute to the changes in evoked Ca^{2+}.

The impact of PMCA and NCX in the extrusion of Ca^{2+} has also been controversial. Pottorf and Thayer (2002) suggested that PMCA, but not NCX, plays the major role in regulating the small (300 nM – 400 nM) evoked Ca^{2+} transient, while others suggest that the duration of depolarization-evoked Ca^{2+} transients in sensory neurons are determined, at least in part, by NCX activity (Verdru et al., 1997, Lu et al., 2006). While PMCA function appears to have a substantial impact on maintaining resting $[Ca^{2+}]_i$ (Gemes et al., 2012), there appears to be no inflammation-induced change in resting $[Ca^{2+}]_i$ (Lu and Gold, 2008), thus it is unlikely that PMCA is playing a role in the inflammation-induced increase in the durations of the transient. Alternatively, NCX is believed to have a low affinity for Ca^{2+} but has very high exchange capacity enabling it to function at the initiation of the recovery process to rapidly remove large quantities of Ca^{2+} (Khananshvili, 2013). While blocking NCX by removing Na^+ from the extracellular environment does not effect the magnitude, it results in a substantial increase in the

duration of the evoked transient (Lu et al., 2006) suggesting that this mechanism could be, at least in part, responsible for the inflammation-induced increase in the duration of the depolarization-evoked Ca^{2+} transient. Therefore in Chapter 2 and 3 of this dissertation the contribution of NCX to Ca^{2+} signaling is assessed in the naïve state and to the inflammation-induced increase in the high K^{+}-evoked Ca^{2+} transient respectively in small diameter putative nociceptive cutaneous DRG neurons.

2.0 CONTRIBUTION OF ENDOPLASMIC RETICULUM CALCIUM REGULATORY MECHANISMS TO THE INFLAMMATION-INDUCED INCREASE IN THE EVOKED CALCIUM TRANSIENT IN RAT CUTANEOUS DORSAL ROOT GANGLION NEURONS

2.1 ABSTRACT

Persistent inflammation results in an increase in the magnitude and duration of high K^+-evoked Ca^{2+} transients in putative nociceptive cutaneous dorsal root ganglion (DRG) neurons. The purpose of the present study was to determine whether recruitment of Ca^{2+}-induced Ca^{2+} release (CICR) contributes to these inflammation-induced changes. Acutely dissociated, retrogradely labeled cutaneous DRG neurons from naïve and complete Freund's adjuvant inflamed adult male Sprague Dawley rats were studied with ratiometric microfluorimetry. Ryanodine only attenuated the duration but not magnitude of the high K^+-evoked Ca^{2+} transient in neurons from inflamed rats. However, there was no significant impact of inflammation on the potency or efficacy of ryanodine-induced block of the caffeine-evoked Ca^{2+} transient, or the impact of sarco-endoplasmic reticulum ATPase (SERCA) inhibition on the high K^+-evoked Ca^{2+} transient. Furthermore, while there was no change in the magnitude, an inflammation-induced increase in the duration of the caffeine-evoked Ca^{2+} transient was only observed with a prolonged caffeine application. In contrast to the high K^+-evoked Ca^{2+} transient, there was no evidence of direct mitrochondrial involvement or that of the Ca^{2+} extrusion mechanism, the Na^+/Ca^{2+} exchanger, on

the caffeine-evoked Ca^{2+} transient, and block of SERCA only increased the duration of this transient. These results indicate the presence of tightly segregated Ca^{2+} regulatory domains in cutaneous nociceptive DRG neurons that isolate cytosolic Ca^{2+} increased via influx from release. Furthermore, our results suggest that changes in neither CICR machinery nor the coupling between Ca^{2+} influx and CICR are primarily responsible for the inflammation-induced changes in the evoked Ca^{2+} transient.

2.2 INTRODUCTION

We previously demonstrated that persistent inflammation of peripheral tissue is associated with an increase in the magnitude and duration of the high K^+-evoked Ca^{2+} transient in a subpopulation of putative nociceptive cutaneous dorsal root ganglion (DRG) neurons (Lu and Gold, 2008). Identifying the underlying mechanism(s) of this change in Ca^{2+} signaling is important as an alteration in intracellular Ca^{2+} signaling may contribute to the pain and hypersensitivity of persistent inflammation both directly via the facilitation of transmitter release (Richardson and Vasko, 2002) and indirectly via changes in the regulation of proteins critical for the control of neuronal excitability (Zhang et al., 2012b) and/or changes in gene expression (Fields et al., 2005).

In sensory neurons, the high K^+-evoked increase in the concentration of intracellular Ca^{2+} ($[Ca^{2+}]_i$) is initiated by a depolarization-induced activation of voltage-gated Ca^{2+} channels (VGCC) and further shaped by Ca^{2+} release from intracellular stores, sequestration into organelles, and extrusion from the cell (Usachev and Thayer, 1997, 1999, Jackson and Thayer, 2006, Lu et al., 2006, Gemes et al., 2011). Thus, there are a number of mechanisms that could

contribute to the inflammation-induced change in Ca^{2+} signaling, several likely candidates of which we have previously ruled out. In particular, the inflammation-induced change in the high K^+-evoked Ca^{2+} transient was neither the result of increased neuronal excitability nor an increase in the magnitude of the high K^+-evoked depolarization (Lu and Gold, 2008). We subsequently ruled out an increase in Ca^{2+} influx via VGCC as current density was selectively suppressed by inflammation in putative nociceptive cutaneous DRG neurons (Lu et al., 2010).

Another mechanism that may contribute to the inflammation-induced change in the regulation of $[Ca^{2+}]_i$ in cutaneous neurons is an increase in the relative contribution of Ca^{2+}-induced Ca^{2+} release (CICR) to the evoked transient. We (Lu et al., 2006) and others (Usachev et al., 1993) previously demonstrated that CICR contributes to the magnitude of evoked Ca^{2+} transients in some DRG neurons from naïve animals. However this mechanism contributes little to the high K^+-evoked Ca^{2+} transient in the subpopulation of afferents defined by a small cell body diameter (<30μM), IB4 binding and capsaicin sensitivity. This is also the subpopulation primarily impacted by inflammation (Lu and Gold, 2008). Thus, any change in CICR machinery or the coupling between Ca^{2+} influx and CICR in these neurons could have a profound influence on the evoked transient. Therefore, in the present study we assessed the contribution of CICR to the inflammation-induced increase in the high K^+-evoked Ca^{2+} transient.

Retrogradely labeled small diameter IB4 binding DRG neurons from naïve and inflamed rats were studied with ratiometric Ca^{2+} imaging in combination with a variety of pharmacological manipulations to assess the impact of inflammation on the mechanisms underlying CICR.

2.3 METHODS

Adult male Sprague-Dawley rats (Harlan, 220-300g) were used for all experiments. Animals were housed two per cage in a temperature and humidity controlled animal facility on a 12:12 light:dark schedule with food and water freely available. All procedures were approved by the University of Pittsburgh Institutional Animal Care and Use Committee and performed in accordance with National Institutes of Health guidelines for the use of laboratory animals in research.

Fourteen to 17 days prior to tissue harvest, the retrograde tracer 1,1'-dioctadecyl-3,3,3',3'-tetramethylindocarbo-cyanine perchlorate (DiI, Invitrogen, Carlsbad, CA) was injected into the glabrous skin of the hindpaw in order to label cutaneous afferents. The tracer was dissolved at 170 mg/mL in dimethylsufoxide (DMSO), diluted 1:10 in 0.9% sterile saline, and injected in 3-5 subcutaneous sites using a 30 g needle for a total volume of 10 μL per hindpaw under isoflurane (Abbott Laboratories, North Chicago, IL, USA) anesthesia. Three days prior to tissue harvest, rats were again anesthetized with isoflurane and inflammation was induced at the site of tracer injection in the left hindpaw with a 100 μL subcutaneous injection of complete Freud's adjuvant (CFA, Sigma-Aldrich, St Louis MO), diluted 1:1 in 0.9 % sterile saline). Prior to tissue removal, animals were deeply anesthetized with an intraperitoneal injection of a cocktail containing ketamine (55 mg/kg), xylazine (5.5 mg/kg) and acepromazine (1.1 mg/kg) and the L4-L5 DRG were removed ipsilateral to labeling and CFA-induced inflammation. Ganglia were enzymatically treated, mechanically dissociated, and plated on laminin- (Invitrogen, Carlsbad, CA; 1mg/ml) and poly-L-ornithine-coated (Sigma-Aldrich; 1 mg/ml) glass cover slips as previously described (Lu et al., 2006). All subsequent experiments were performed within 8 h of tissue harvest.

2.3.1 Calcium imaging

Neurons were incubated with 2.5 μM Ca^{2+} indicator fura-2 AM ester with 0.025 % Pluronic F-127 for 20min at room temperature. Neurons were then labeled with FITC-conjugated IB4 (10 μg/ml) for 10 min at room temperature. Labeled neurons were placed in a recording chamber and continuously superfused via a gravity fed system with normal bath solution (mM: 130 NaCl, 3 KCl, 2.5 CaCl2, 0.6 MgCl2, 10 HEPES, 10 glucose, pH 7.4, osmolality 325 mOsm) or a 'Ca^{2+}-free' bath solution (mM: 130 NaCl, 3 KCl, 10 MgCl2, 2 EGTA, 10 Hepes, 10 glucose, pH 7.4, osmolality 325 mOsm). Fluorescence data were acquired on a PC running Metafluor software (Molecular Devices, City State) via a CCD camera (Roper Scientific; model RTE/CCD 1300). The ratio (*R*) of fluorescence emission (510 nm) in response to 340/380nm excitation (controlled by a lambda 10–2 filter changer (Sutter Instrument, Novato, CA) was acquired at 1 Hz during drug application. $[Ca^{2+}]_i$ was determined from fura-2 ratio following in situ calibration experiments according to the following equation:

$$[Ca^{2+}]_i(nM) = K_d(\frac{S_{f2}}{S_{b2}})(\frac{R - R_{\min}}{R_{\max} - R})$$

Where K_d is the dissociation constant for fura-2 for Ca^{2+} at room temperature; S_{f2}/S_{b2} is the fluorescence ratio of the emission intensity excited by 380 nm signal in the absence of Ca^{2+}; R_{min} and R_{max} are the minimal and maximal fluorescence ratios respectively. Determination of these variables has been described in detail previously (Grynkiewicz et al., 1985, Kao et al., 1994, Lu et al., 2006). All drugs were applied through a computer-controlled perfusion fast-step system (switching time <20 ms; Warner Perfusion System, Hamden, CT, USA, Model SF-77B).

2.3.2 Chemical and Reagents

Cyclopiazonic acid (CPA) (10μM, 100mM stock in DMSO) was purchased from Calbiochem (La Jolla, CA, USA), 1,1'-dioctadecyl-3,3,3',3'-tetramethylindocarbo-cyanine perchlorate (DiI) was purchased from Invitrogen (Carlsbad, CA, USA). Fura-2 acetoxymethyl (AM) ester (2.5 μM) and Pluronic F-127 (0.025 %) were purchased from TEF Laboratories (Austin, TX, USA). Ryanodine (1-100 μM, 10 mM stock in DMSO) and H-89 (10μM, 100mM stock in DMSO) were purchased from R&D Systems (Minneapolis, MN, USA), FITC-conjugated IB4 (IB4, 10 ug/ml), caffeine (10 mM), carbonyl cyanide *m*-chlorophenyl hydrazone (CCCP) (10μM, 100mM stock in DMSO) were obtained from Sigma-Aldrich (St Louis, MO, USA).

2.3.3 Statistical Analysis

Data are expressed as mean ± s.e.m. Student's *t* test was used for simple comparisons between groups. For experiments involving the application of test compounds, vehicle controls were always included. A two-way ANOVA was used for analysis of more than two groups with the Holm-Sidak test used for post-hoc analysis. The response to repeated caffeine application in the presence of different concentrations of ryanodine was assessed with a mixed design 3-way ANOVA. Statistical significance was assessed at $p < 0.05$.

2.4 RESULTS

Data were collected from 315 cutaneous DRG neurons acutely dissociated from 54 male Sprague Dawley rats, of which 30 were control and 24 were subject to CFA-induced peripheral inflammation. Based on previous results indicating that the inflammation-induced increase in the high K^+-evoked Ca^{2+} transient was primarily manifest in small (<30 μm) diameter, cutaneous, IB4 binding, capsaicin sensitive DRG neurons, this subpopulation was the focus of the present study and is subsequently referred to as a subpopulation of putative nociceptive cutaneous neurons. Consistent with our previous results (Lu and Gold, 2008), inflammation was associated with a significant increase in the magnitude (as measured by a change from baseline) and duration (as measured by the time to a 50, 75 and 90, but not 25% decrease from peak (T50, T75, T90 and T25)) of the high K^+-evoked Ca^{2+} transient (Figure 1A & B and Table 1). These changes in the evoked Ca^{2+} transient were not associated with a change in resting $[Ca^{2+}]_i$, which was 139.09 ± 4.80 nM (n = 41) and 133.29 ± 6.33 nM (n = 39) in neurons from naïve and inflamed rats, respectively ($p > 0.05$).

Table 1: Changes in the decay of the high K^+-evoked Ca^{2+} transient in putative nociceptive DRG neurons

Treatment	n	T25 (s)	T50 (s)	T75 (s)	T90 (s)
Naïve	41	4.66 ± 0.5	19.43 ± 2.4	50.36 ± 8.2	184.45 ± 21.0
CFA	36	3.08 ± 0.3**	36.93 ± 5.2**	98.19 ± 13.4**	280.63±26.3**
Naïve Post CPA	13	15.37 ± 5.9**	82.45 ± 17.0**	167.7 ± 28.2**	273.75 ± 34.8
CFA Post CPA	12	9.25 ± 3.7	142.56 ± 39.3**	222.07 ± 47.4**	304.6 ± 61.8
Naïve Post CCCP	11	46.36 ± 6.8**	72.93 ± 11.0**	218.96 ± 58.2**	402 ± 38.7**
Naïve Post Na^+ Free	11	4.46 ± 0.6	31.29 ± 5.93	192.62 ± 33.77**	331.33±39.84**

Neurons were challenged with high K^+ (30 mM, 4s). T25, T50, T75 and T90 are the time to 25, 50, 75 and 90% decay of the peak increase evoked with high K^+. Using a mixed 2-way ANOVA, there is a significant main effect associated with time, treatment, and an interaction between the two ($p < 0.0001$). Post hoc analyses are provided within each time domain. * signifies $p < 0.05$ compared to naïve, Ψ signifies $p < 0.05$ compared to CFA treatment, and § signifies $p < 0.05$ between treatments (CPA, CCCP).

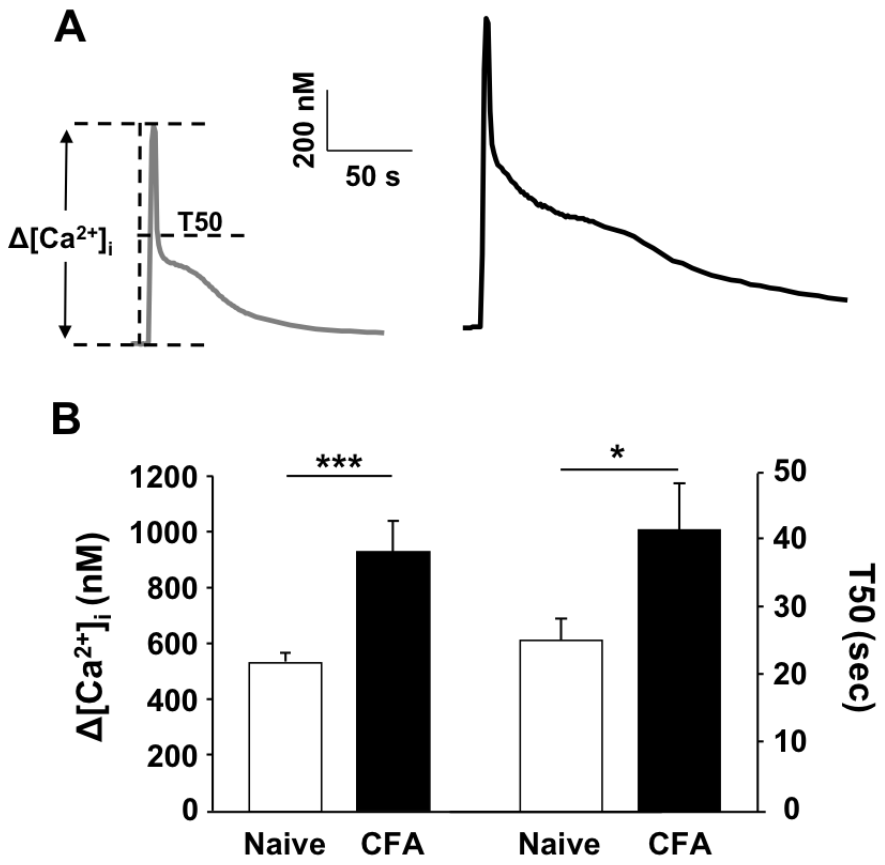

Figure 1: Inflammation increases the magnitude and duration of the high K^+-evoked Ca^{2+} transient in putative nociceptive cutaneous DRG neurons**.**

A) Typical high K^+-evoked Ca^{2+} transients in neurons from naïve (gray trace) and inflamed (black trace) rats. B) Pooled data for the magnitude (change from baseline (Δ $[Ca^{2+}]_i$)) and decay (quantified as the time to 50% of peak, or T50) of the high K^+ (30 mM for 4 sec) evoked Ca^{2+} transient in putative nociceptive DRG neurons from naïve (n = 32) and inflamed (CFA, n = 29) rats.* $p < 0.05$. ** $p < 0.01$.

2.4.1 Ryanodine attenuates the duration of the high K^+-evoked Ca^{2+} transient in cutaneous neurons from inflamed rats

To assess the presence of an inflammation-induced change in the relative contribution of CICR to the high K^+-evoked Ca^{2+} transient, high K^+ (30 mM, 4 sec) was applied to cutaneous neurons from naïve and inflamed rats before and after the application of the ryanodine receptor (RyR) blocker, ryanodine (10 μM). To establish steady-state RyR block, caffeine (10 mM, 4 sec) was applied 4 times with a 2.5 min inter-stimulus interval (ISI) after the application of ryanodine and before the last challenge with high K^+ (Figure 2A). A 4s application of 10mM caffeine was chosen based on the results of an analysis of the response to caffeine applied for durations ranging between 250 ms and 12 s: the magnitude of the caffeine-evoked Ca^{2+} transient saturated in all neurons tested ($\Delta[Ca^{2+}]_i$ = 453.48 ± 38.9 nM, n = 15) with a duration of application of 4s or greater. Of note, this change in magnitude was comparable to that evoked with high K^+ (Figure 1). Interestingly, in control experiments in which caffeine was applied 4 times between high K^+ applications in the absence of ryanodine, there was an increase in the T50 of decay of the second high K^+-evoked transient (Figure 2A, B and C). The response to high K^+ is highly reproducible with an ISI of at least 5 minutes, therefore, this increase in T50 of decay appears to be due to the actions of caffeine, possibly secondary to a shift in resting protein kinase A (PKA) activity as a result of caffeine-induced inhibition of phosphodiesterase (Leijten and van Breemen, 1984). To assess this possibility, we repeated the experiment with high K^+ applied before and after repeated application of caffeine in neurons pre-incubated (20min) with the PKA inhibitor, H-89 (10 μM). Consistent with the suggested involvement of PKA in the caffeine-induced increase in the duration of the high K^+-evoked Ca^{2+} transient, the presence of H-89 resulted in a significant

attenuation of the caffeine-induced increase in the duration of the high K^+-evoked transient from 164.59 ± 0.34 (n = 9) to 51.3 ± 0.34 (n = 7) %ΔT50 ($p < 0.05$). Regardless of the mechanism of the change in T50, because of its presence, the impact of ryanodine-induced RyR block was assessed relative to control neurons treated identically in the absence of ryanodine. Consistent with previous results indicating that the contribution of CICR to the high K^+-evoked transient in putative nociceptive cutaneous DRG neurons is minimal (Lu et al., 2006), ryanodine (10 μM) had no detectable influence on the magnitude or decay of the high K^+-evoked transient in neurons tested from naïve rats (Figure 2C). Comparable results were obtained with 100 μM ryanodine, where the high K^+-evoked Ca^{2+} transient in the presence of ryanodine (T50 = 60.27 ± 9.43 s, n = 4) was not different ($p > 0.05$) from that observed in control neurons the absence of ryanodine (T50 = 46.69 ± 11.85 s, n = 9). In contrast, while ryanodine had no significant influence on the magnitude of the high K^+-evoked Ca^{2+} transient in putative nociceptive cutaneous neurons from inflamed rats, the T50 of decay was significantly ($p < 0.001$) attenuated (Figure 2C). This observation is consistent with the recruitment of CICR as a mechanism contributing to at least part of the inflammation-induced change in the high K^+-evoked transient.

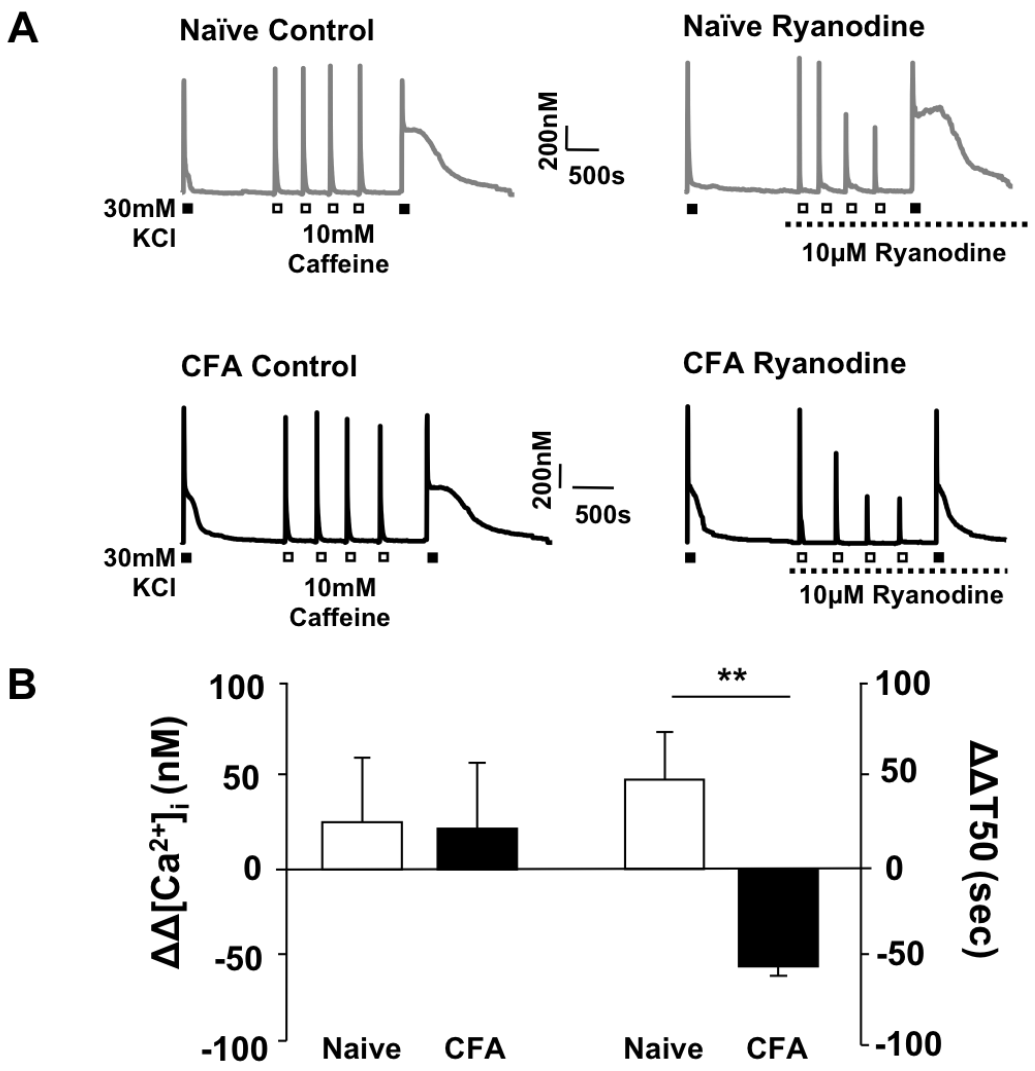

Figure 2: The impact of ryanodine on the inflammation-induced changes of the high K^+-evoked transient.

A) Evoked Ca^{2+} transients in neurons from naïve (gray traces) and inflamed (black traces) rats challenged with high K^+ (30 mM, 4 sec) before and after 4 applications of caffeine (10 mM, 4 sec). Neurons were challenged with caffeine in the presence (Ryanodine) or absence (Control) of ryanodine (10 μM). Note the increase in the duration of the high K^+-evoked transient in control neurons following repeated caffeine administration. B) The change in the magnitude (ΔΔ $[Ca^{2+}]_i$ (nM)) and decay (ΔΔ T50 (s)) of the high K^+-evoked Ca^{2+} transient associated with the application of ryanodine (10 μM) was assessed as the difference between the high K^+-evoked transients before and after the application of ryanodine. Control neurons (open bars, n = 12) treated with an identical protocol revealed a caffeine-induced increase in the T50 of decay, therefore, changes associated with ryanodine (black bars, n = 12) were assessed relative to control with a two way ANOVA. ** $p < 0.01$, * $p < 0.05$

Finally, recent evidence suggests that CICR via IP3 receptors contributes to the Ca^{2+} transient associated with transient receptor potential (TRP) channel activation in DRG neurons which appears to occur secondary to a Ca^{2+}-dependent activation of phospholipase C (Rohacs, 2005, Rohacs et al., 2008). Because we have previously demonstrated that IP3 receptor activation contributes minimally to the high K^+-evoked Ca^{2+} transient in putative nociceptive DRG neurons from naïve rats (Lu et al., 2006), we sought to rule out the possibility that recruitment of an IP3-dependent mechanism contributes to the inflammation-induced increase in the high K^+-evoked Ca^{2+} transient. As we have previously demonstrated that 100 μM 2-APB was sufficient to attenuate an UTP-evoked Ca^{2+} transient in DRG neurons (Lu et al., 2006), the same concentration of this IP3 receptor blocker was used in the present experiment. We observed no significant ($p > 0.05$, $n = 7$) difference in either the magnitude (-5.74 ± 0.08 %) or duration (11.47 ± 0.11 %) of the high K^+-evoked Ca^{2+} transient evoked in the presence or absence of 2-APB, respectively, in putative nociceptive cutaneous neurons from inflamed rats. These results argue against a role for IP3 receptor activation in the inflammation-induced changes in the high K^+-evoked Ca^{2+} transient.

2.4.2 No detectable influence of inflammation on the magnitude or duration of the caffeine-evoked Ca^{2+} transient

Given that CICR reflects the activation of Ca^{2+} activated Ca^{2+} channels (i.e., RyRs) on the endoplasmic reticulum (ER) which enable the release of Ca^{2+} loaded into the ER via sarco-endoplasmic reticulum Ca^{2+} ATPase (SERCA), there are several mechanisms that could account for the recruitment of CICR as a contributing factor to the inflammation-induced increase in the time of decay of the high K^+-evoked transient. These include: 1) an increase in releasable Ca^{2+}

stored in the ER, 2) a shift in the expression of RyR subtypes from a receptor such as RyR1 with a low open channel probability to one such as RyR3 with a high open channel probability (Meissner, 1994), 3) a decrease in the rate of SERCA uptake, 4) a shift in the coupling between VGCC Ca^{2+} influx and ER store release, and/or 5) a change in a SERCA/CICR-independent mechanism that enables the high K^{+}-evoked transient to engage CICR to further amplify the evoked transient. To address the first possibility, we analyzed caffeine-evoked transients in putative nociceptive cutaneous neurons from naïve and inflamed rats.

Results from the first set of experiments suggested that there was no inflammation-induced change in the magnitude or decay of the caffeine-evoked transient. An additional set of neurons (n = 36 naïve, n = 29 CFA) was used to study the caffeine-evoked transients directly to avoid the potential confound associated with an initial challenge with high K^{+}. Results with caffeine alone were consistent with our initial observations, indicating that there is no detectable influence of inflammation on either the magnitude or the decay of the caffeine-evoked transient (Figure 3A). To confirm that the caffeine-evoked transient was due to the release of Ca^{2+} from internal stores, caffeine was applied to neurons in the presence of Ca^{2+} free bath solution or following depletion of Ca^{2+} from the ER with the SERCA inhibitor, cyclopiazonic acid (CPA, 10 μM) (Figure 3B). In contrast to the results obtained in nodose ganglion neurons (Hoesch et al., 2001), there was no significant ($p > 0.05$) difference in the magnitude of the caffeine transient evoked in the presence or absence of extracellular Ca^{2+} (Figure 3B and C). Furthermore, the caffeine-evoked transient was completely blocked following depletion of ER stores with CPA (Figure 3B and C).

The concentration of caffeine used in these experiments is comparable to that used by other investigators (Eun et al., 2001, Lokuta et al., 2002, Cheng et al., 2010). However, to rule

out the possibility that inflammation altered either the potency or efficacy of caffeine, concentration response data were collected from another group of neurons (n = 15 naïve, n = 14 CFA). Increasing concentrations of caffeine were applied to each neuron with an ISI of 5 minutes. Data for each neuron was fitted with a Hill equation to determine the concentration resulting in a response 50% of maximal (EC50) as well as the maximal response (Emax). Results of this analysis indicated that inflammation has no detectable influence on either the potency or efficacy of the caffeine-evoked transient, with EC50's of 4.09 ± 0.39 and 5.29 ± 0.67 mM and Emax of 522.62 ± 58.93 and 500.84 ± 38.52 nM Ca^{2+} in neurons from naïve and inflamed rats, respectively (Figure 3D).

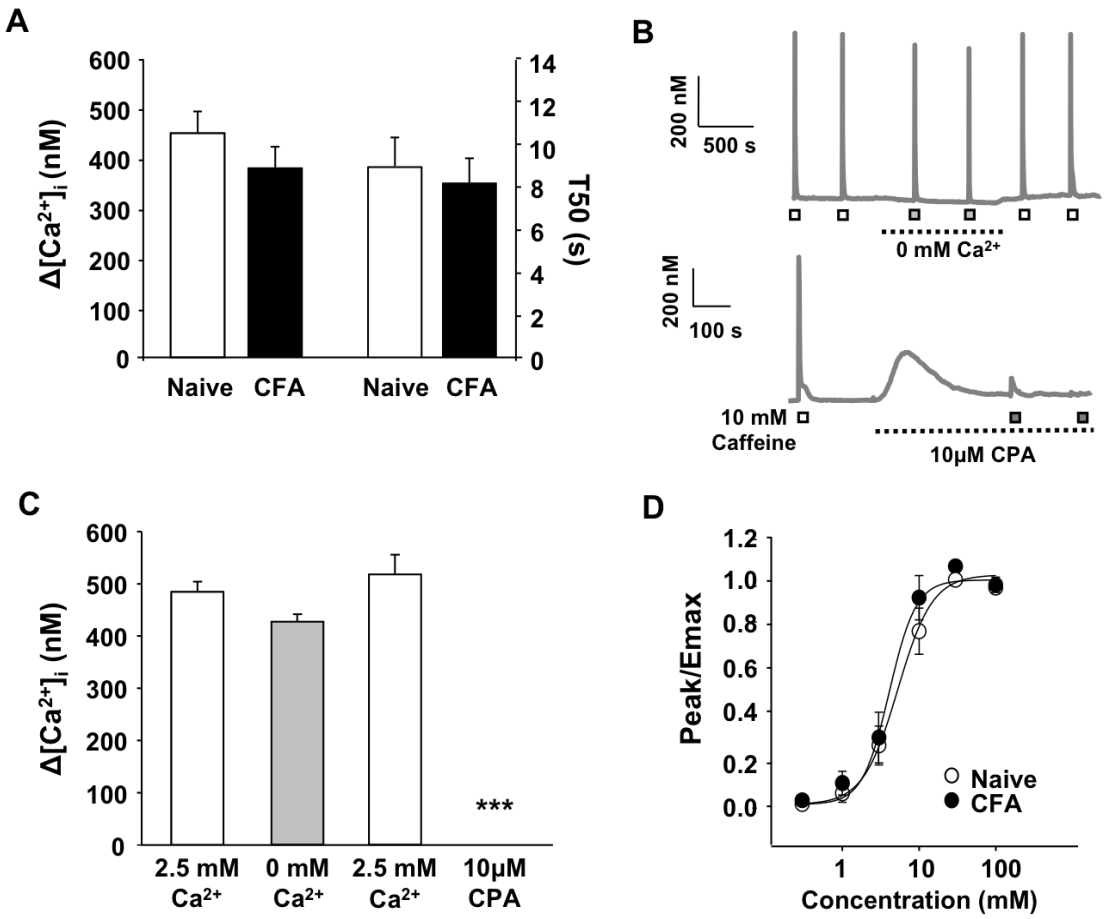

Figure 3: Inflammation did not change the magnitude or duration of the caffeine-evoked Ca^{2+} transient.

A) The magnitude (Δ $[Ca^{2+}]_i$) and duration (T50) of caffeine (10 mM for 4 sec) evoked Ca^{2+} transients were determined in a manner identical to that used for the high K^+-evoked transient. Pooled data from putative nociceptive cutaneous neurons from naïve (n = 36) and inflamed (n = 29) rats are plotted. B) Top: Example of caffeine-evoked Ca^{2+} transients in a neuron from a naïve rat in the presence (open square) and absence (closed square) of Ca^{2+} in the bath solution. Bottom: Example of caffeine-evoked Ca^{2+} transients in a neuron from a naïve rat before (open square) and after (closed square) the application of the SERCA inhibitor, CPA. C) Pooled data from neurons (n = 8) challenged with caffeine before and after the application Ca^{2+} free bath solution and from a second groups of neurons (n = 10) challenged before and after depletion of intracellular Ca^{2+} stores with CPA. D) Pooled concentration response data for neurons from naïve (n = 13) and inflamed (n = 14) rats challenged with increasing concentrations of caffeine. Data from each neuron were fitted with a modified Hill equation to estimate the maximal size of the evoked transient (Emax) and this value was used to normalize data prior to pooling. Pooled data are also fitted with a modified Hill equation. ***$p < 0.001$

2.4.3 Inflammation does not affect the balance of RyR-mediated Ca^{2+} release and SERCA-mediated Ca^{2+} re-uptake

The rapid decay of the caffeine-evoked Ca^{2+} transient highlights the possibility that a shift in the relative balance of Ca^{2+} release to re-uptake contributes to the inflammation-induced increase in the high K^+-evoked Ca^{2+} transient as it suggests that in putative nociceptive cutaneous neurons, release and re-uptake are tightly coupled. To determine whether inflammation is associated with a shift in the balance of these two processes, we assessed the extent of caffeine-induced depletion of intracellular stores in Ca^{2+} free bath solution. Results of this experiment indicated that even after 4 applications of 10 mM caffeine in Ca^{2+} free bath solution, there was no significant reduction in the caffeine-evoked transient (Figure 4A). Comparable results were obtained in neurons from naïve and inflamed rats (Figure 4B), arguing against an inflammation-induced shift in the balance of release and re-uptake, at least over a time frame relevant to the high K^+-evoked Ca^{2+} transient.

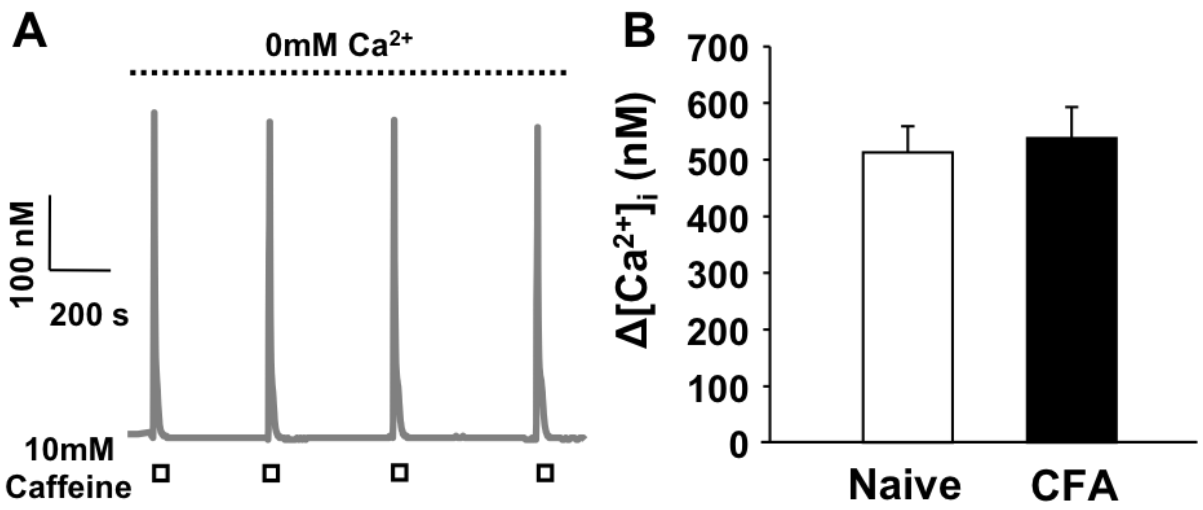

Figure 4: No significant reduction in the magitude of caffeine-evoked transient in the absence of extracellular Ca^{2+}. A) Caffeine-evoked Ca^{2+} transients in a putative nociceptive cutaneous neuron from a naïve rat. The neuron was continuously bathed in Ca^{2+} free bath solution. Caffeine was applied where indicated by the white boxes B) The magnitude of the caffeine-evoked Ca^{2+} transient in Ca^{2+} free bath solution was comparable in putative nociceptive cutaneous neurons from naïve (n = 37) and inflamed (n = 38) rats.

2.4.4 Heterogeneity among cutaneous neurons with respect to function RyR subtypes does not contribute to the inflammation-induced changes in Ca^{2+} signaling

To further determine whether a shift in the balance of functional RyR subtypes contributes to the inflammation-induced increase in the high K^+-evoked Ca^{2+} transient, we assessed the concentration dependence of ryanodine-induced block of the caffeine-evoked transient. Caffeine (10 mM) was applied before and then 4 times (ISI = 5 minutes) in the presence of 1, 10 or 100 μM ryanodine in Ca^{2+} free bath solution. Results of this experiment suggested the presence of at least 3 subpopulations of putative nociceptive cutaneous DRG neurons: those that were relatively resistant (resistant), those that were sensitive (sensitive), and those that were highly sensitive (highly sensitive) to ryanodine-induced block (Figure 5A and B). This difference between neurons was most readily apparent in the response to 10 μM ryanodine, depicted by plotting the magnitude of the transient evoked in response to the 4^{th} application of caffeine in the presence of ryanodine normalized to the response prior to the application of ryanodine (Figure 5B); 10 μM ryanodine produced only ~20% block in resistant neurons, ~65% block in sensitive neurons and ~100% block of highly sensitive neurons. These subpopulations appeared to be less well defined in neurons from inflamed rats (Figure 5B). However there was no statistically significant difference in the average block produced by 10 μM ryanodine. Plotting the fractional block as a function of caffeine application and ryanodine concentration (Figure 5C and D), suggests the presence of an inflammation-induced increase in the sensitivity to ryanodine-induced block of the caffeine response. However, statistical analysis (mixed design 3 way ANOVA) revealed no significant interaction between inflammation and ryanodine concentration despite significant main effects associated with caffeine application and ryanodine concentration.

To begin to assess the functional consequences of what appeared to be a differential distribution of RyRs among putative nociceptive cutaneous neurons, we analyzed the initial response to caffeine in subpopulations of neurons defined by their sensitivity to ryanodine-induced block. This analysis revealed that the magnitude of the Ca^{2+} transient in response to first caffeine application was significantly larger in the "highly sensitive" neurons (825.15 ± 113.05 nM) compared to those that were "sensitive" (501.33 ± 65.92 nM) or "resistant" (480.37 ± 67.38 nM) to the ryanodine-induced block. Nevertheless, while these results are consistent with a heterogeneous distribution of RyR subtypes among cutaneous nociceptive DRG neurons, there does not appear to be an inflammation-induced shift in this distribution.

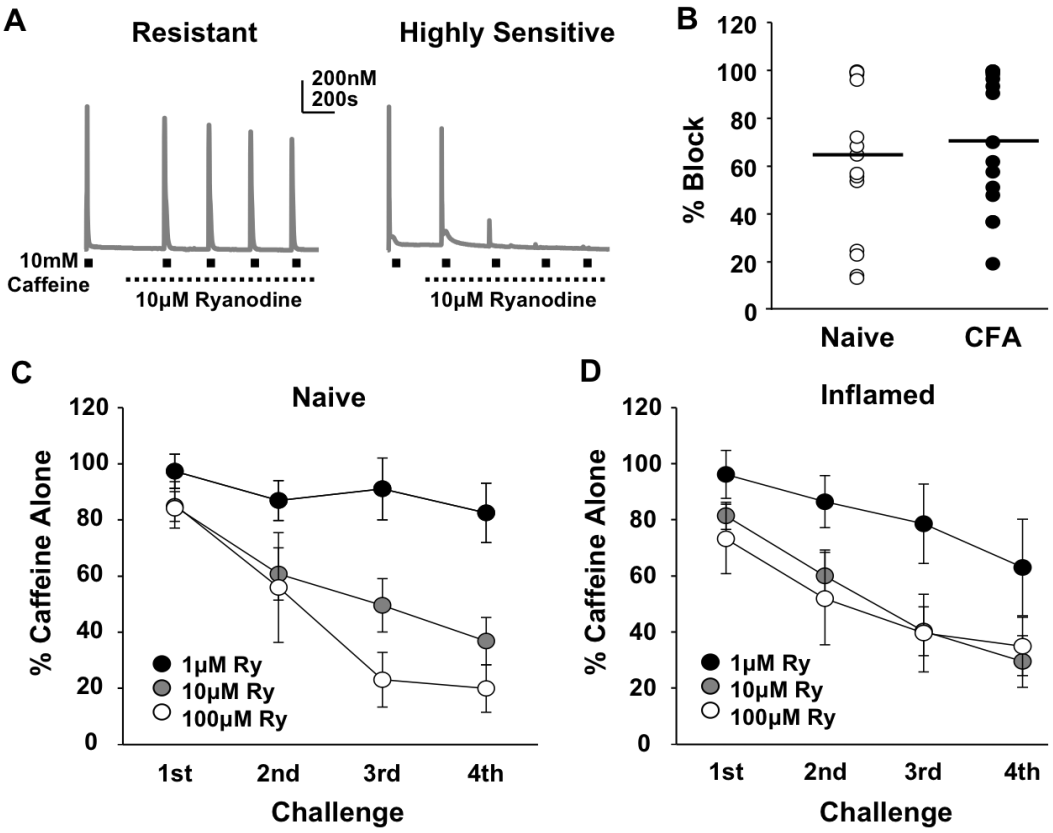

Figure 5: Heterogeneity in the ryanodine receptor activity in neurons from both naive and inflamed rats.

A) Examples of caffeine (caff)-evoked Ca^{2+} transients in putative nociceptive cutaneous neurons before and after the application of 10 μM Ry in Ca^{2+} free bath. The neuron on the left was relatively resistant to Ry-induced block, while that on the right was highly sensitive. B) The percent of Ry-induced block of the caff-evoked Ca^{2+} transient was calculated from the response evoked by the 4^{th} caffeine application relative to the response evoked prior to the application of Ry. Data from neurons from naïve (n = 15) and inflamed (n = 15) rats challenged with 10 μM Ry are plotted. C) Neurons (n = 31) from naïve rats were challenged with caff (10 mM) before and after the application of 1 of 3 concentrations of Ry. The response to each of 4 successive applications of caff was calculated as a percent of the response to caff prior to the application of caff. Pooled data over subsequent challenges are plotted relative to the concentration of Ry employed. D) Data from neurons (n = 33) from inflamed rats were collected and plotted as described in C. There was no significant interaction between inflammation and Ry concentration despite significant main effects associated with caff application and Ry concentration (Mixed 3 way ANOVA, $p > 0.05$).

2.4.5 No evidence of an inflammation-induced change in SERCA activity

While the results from the caffeine experiments suggest that the inflammation-induced increase in high K^+-evoked Ca^{2+} transients is not due to a change in the relative level of SERCA activity, we directly tested this possibility by comparing the magnitude and decay of the high K^+-evoked Ca^{2+} transient before and after the application 10 μM CPA in normal Ca^{2+}-containing bath solution. To confirm complete block of SERCA, caffeine (10 mM) was applied after resting $[Ca^{2+}]_i$ levels returned to baseline following CPA application (Figure 6A). Consistent with the suggestion that Ca^{2+} released from the ER does not engage the mechanisms underlying the inflammation-induced increase in the magnitude of the high K^+-evoked Ca^{2+} transient, the CPA-induced Ca^{2+} transient was comparable in neurons from naïve and inflamed rats ($p > 0.05$, Figure 6B). There was no significant change in the magnitude of the high K^+-evoked Ca^{2+} transient in neurons from either naïve or inflamed animals in the presence of CPA (Figure 6C). However, in both groups of neurons, the T50 of decay was significantly ($p < 0.01$) increased in the presence of CPA. Furthermore, the CPA-induced increase in T50 was significantly greater in neurons from inflamed rats than in neurons from naïve (Figure 6D). These results are consistent with our previous finding that in this subpopulation of neurons, SERCA plays a far more dominant role in the regulation of the duration of the Ca^{2+} transient than in the magnitude. They also argue against a role for an inflammation-induced change in SERCA activity as an underlying mechanism of the inflammation-induced increase in the high K^+-evoked Ca^{2+} transient because an inflammation-induced decrease in SERCA activity would have attenuated the CPA-induced increase in T50 in neurons from inflamed rats.

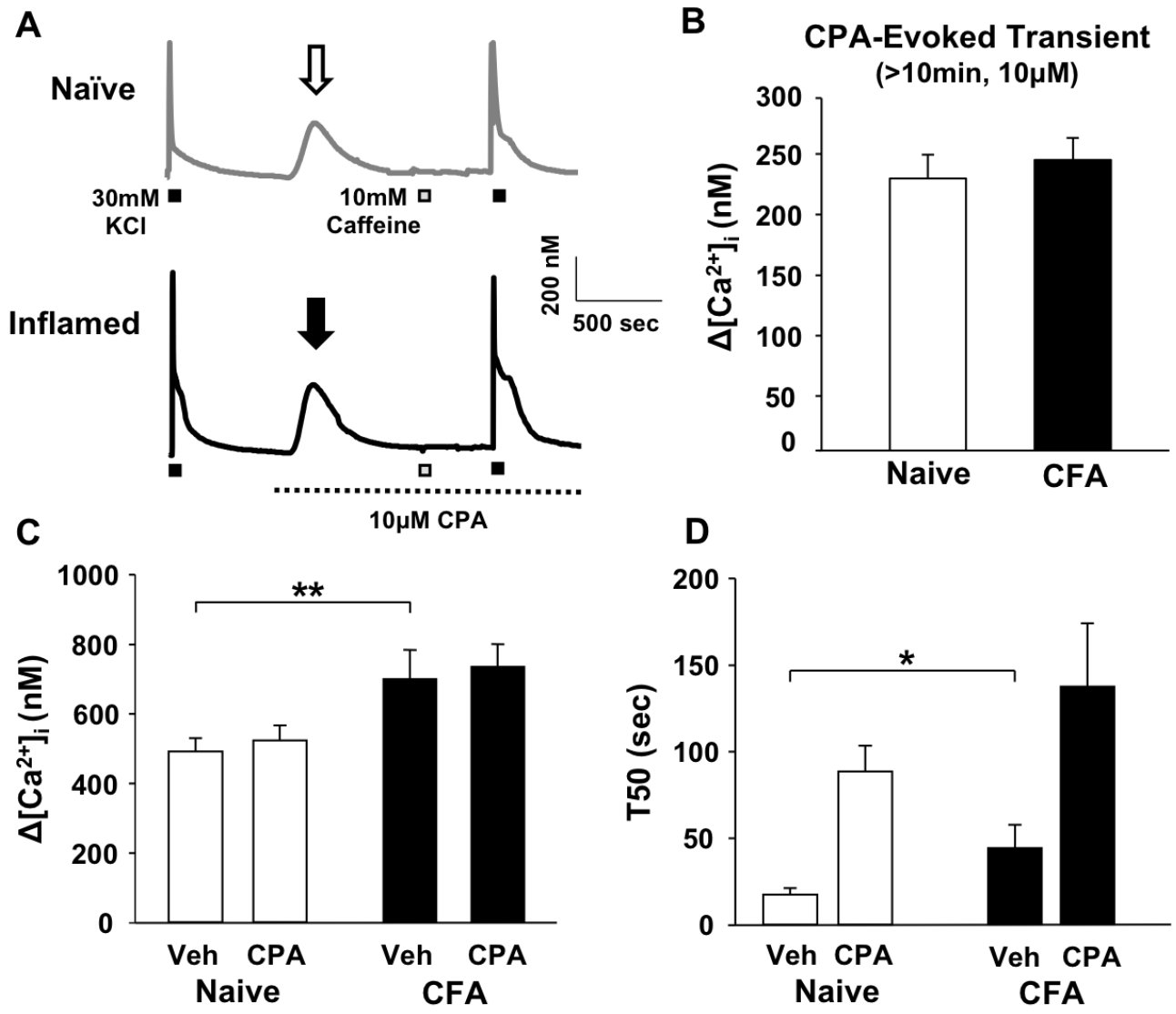

Figure 6: No inflammation-induced change in the influence of SERCA on the high K^+-evoked transient.

A) Ca^{2+} transients in neurons from a naïve (grey trace) and inflamed (black trace) rat evoked with high K^+ before and after the application of CPA. Both neurons were challenged with caffeine to confirm depletion of Ca^{2+} from intracellular stores. B) The magnitude of the CPA-evoked Ca^{2+} transient was comparable in neurons from naïve (n = 11) and inflamed (n = 9) rats. C) CPA had no influence on the magnitude of the high K^+-evoked Ca^{2+} transient, despite a significant main effect associated with inflammation (two-way ANOVA). Pooled data are responses obtained before (Veh) and after application of CPA. D) The decay of the high K^+-evoked Ca^{2+} transient was calculated, pooled and plotted as in C. There were significant main effects associated with CPA and inflammation but no statistically significant interaction (two-way ANOVA). * $p < 0.05$; ** $p < 0.01$.

2.4.6 Selective influence of inflammation on the decay of the Ca^{2+} transient evoked with prolonged caffeine application

Having largely ruled out a change in the machinery underlying CICR as a mechanism contributing to the inflammation-induced increase in the high K^+-evoked Ca^{2+} transient, we performed an experiment to begin to assess the presence of an inflammation-induced shift in the coupling between Ca^{2+} influx and release. The possibility of such a shift in coupling was suggested by the observation that the decay of the caffeine-evoked Ca^{2+} transient (average T50 = 9 sec) is much faster than that of the high K^+-evoked Ca^{2+} transient (average T50 = 45 sec) despite the fact that the magnitude of the transient evoked with these two stimuli were comparable ($p > 0.05$). This observation suggests that very different Ca^{2+} regulatory mechanisms are engaged by Ca^{2+} influx and Ca^{2+} release in this subpopulation of sensory neurons. It also raises the possibility that increasing the duration of the caffeine application would prolong the Ca^{2+} transient sufficiently to enable Ca^{2+} access to the mechanisms altered by inflammation that contribute to the inflammation-induced increase in the high K^+-evoked transient, where negative results would be consistent with a change in the association between influx and release. To test this possibility, caffeine was applied for 12 seconds to another group of neurons (n = 8 naïve, n = 10 CFA) (Figure 7A). Consistent with preliminary results indicating that the magnitude of the caffeine-evoked Ca^{2+} transient was saturated in response to caffeine applications of 4s or longer, there was not difference between a 4s and 12s application of caffeine with respect to the magnitude of the evoked transient in neurons from naïve and inflamed rats (Figure 7B). Interestingly, however, in contrast to the results obtained in neurons from naïve rats, where the T50 of decay to a 4 and 12 second application of caffeine were comparable ($p > 0.05$, Figure

7C), inflammation was associated with a significant ($p < 0.05$) increase in the T50 of decay in response to a 12 second caffeine application (Figure 7C).

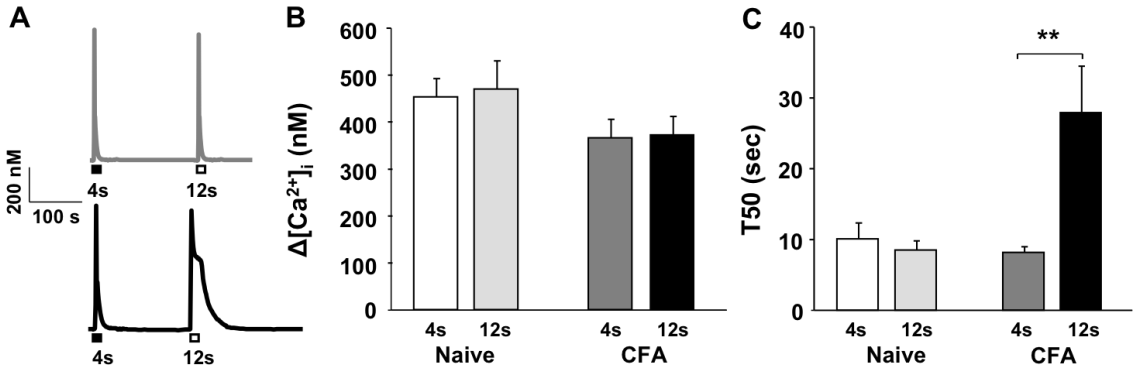

Figure 7: Ca^{2+} transients evoked in response to prolonged caffeine application.

Ca^{2+} transients evoked in a neuron from naïve (grey trace) and inflamed (black trace) rats with a 4 second (closed box) or 12 second (open box) application of caffeine (10 mM, ISI = 5 min). Pooled magnitude (B) and duration (C) data from neurons from naïve (n = 8) and inflamed (n = 10) rats stimulated with caffeine as described in A are plotted. **$p < 0.01$

2.4.7 Different Ca^{2+} regulatory machinery are engaged with Ca^{2+} transients evoked with caffeine and high K^+

The rapid decay of the caffeine-evoked Ca^{2+} transient not only suggests that in putative nociceptive cutaneous neurons ER Ca^{2+} release and re-uptake are tightly coupled, but that different Ca^{2+} regulatory machinery is engaged by Ca^{2+} influx via VGCC and release from the ER. The observation that repeated caffeine application results in an increase in the duration of the high K^+-evoked transient (Figure 2), but no change in the duration of the caffeine-evoked transient (with a T50 of decay of 6.2 ± 0.9s after the first application, and 7.0 ± 1.2s after the fourth application, $p > 0.05$, $n = 10$) is also consistent with the suggestion that the Ca^{2+} transients evoked by these stimuli engage distinct Ca^{2+} regulatory machinery. To further explore these suggestions, we performed three additional experiments: First, caffeine or high K^+ were applied in the presence of 10μM CCCP, a mitochondrial proton pump inhibitor; Second, caffeine was applied in the presence of SERCA inhibitor CPA; and third caffeine or high K+ were applied in the presence of Na^+ free bath to inhibit the Na^+/Ca^{2+} exchanger (NCX).

For the first experiment, CCCP was co-applied with caffeine or high K^+ to minimize the potential impact of a decrease in ATP on Ca^{2+} regulatory machinery. However, because CCCP was associated with a transient increase in intracellular Ca^{2+} which influenced the magnitude of the evoked transient relative to baseline, CCCP was first applied alone and the magnitude of the CCCP-evoked transient was subtracted from the caffeine or high K^+-evoked transient prior to calculating the percent change from the transient evoked in the absence of CCCP. Results of this first experiment indicated that, while the complex decay of the high K^+-evoked Ca^{2+} transient is due in part to mitochondrial buffering, mitochondria do not appear to influence either the

magnitude or decay of the caffeine evoked Ca^{2+} transient. That is, both the magnitude (32.85 ± 0.8%, $p < 0.05$, $n = 7$) and decay ($p < 0.01$, Table 1) of the high K^+-evoked Ca^{2+} transient were significantly increased in the presence of CCCP. Furthermore, not only was the decay of the high K^+-evoked transient significantly increased, most dramatically during the initial phase of decay (i.e., at T25, Table 1), but the shape of the transient was dramatically altered, with no evidence of a "shoulder" just above the T50 of decay (Figure 8A). In contrast, changes in neither the magnitude (-8.2± 0.04%) nor duration (25.13 ± 0.02%) of the caffeine-evoked transient in the presence of CCCP, were significant ($p > 0.05$, $n = 6$, Figure 8A).

For the second experiment, caffeine was also co-applied with CPA to prevent depletion of the ER that occurs with the pre-treatment protocol used for the high K^+ experiment (Figure 6). Interestingly, the impact of CPA on the caffeine-evoked Ca^{2+} transient was similar to that on the high K^+-evoked Ca^{2+} transient (Figure 6), where there was no influence on the magnitude (-4.59 ± 0.09% of control, $p > 0.05$, $n = 6$) but a significant increase in the duration (210.42 ± 0.57% of control, $p < 0.05$) of the caffeine-evoked Ca^{2+} transient (Figure 8B, Table 1). These results suggest that the magnitude of the caffeine-evoked Ca^{2+} transient, at least in response to a saturating concentration and duration of caffeine, is largely determined by the concentration of Ca^{2+} in the ER and the density and distribution of RyRs, while the duration of the transient is largely determined by SERCA.

Finally, the reproducible response to caffeine even in a Ca^{2+} free bath (Figure 4) suggests that extrusion mechanisms contribute minimally to both the magnitude and duration of the caffeine-evoked transient. In contrast, we have previously demonstrated the Ca^{2+} extrusion via NCX influences the duration of the high K^+-evoked Ca^{2+} transient in putative nociceptive DRG neurons (Lu et al., 2006). Therefore, to confirm that extrusion, at least via NCX, contributes

minimally to the regulation of the caffeine-evoked transient in cutaneous nociceptive neurons, we assessed the response to caffeine before and after block of NCX with zero Na^+ bath (where NaCl was replaced with choline-Cl). The results of this experiment indicated that block of NCX had no significant ($p > 0.05$, $n = 6$) influence on either the magnitude (-6.07 ± 0.04% of control) or duration (-6.4 ± 0.06% of control) of the caffeine-evoked Ca^{2+} transient (Figure 8C, Table 1). In contrast, and consistent with our previous results in unlabeled DRG neurons, inhibition of NCX had no significant influence on the magnitude of the high K^+-evoked transient in cutaneous nociceptive neurons, but was associated with a significant ($p < 0.01$, $n = 12$) increase in the duration (490.54 ± 0.89%) of the high K^+-evoked transient (Figure 8C).

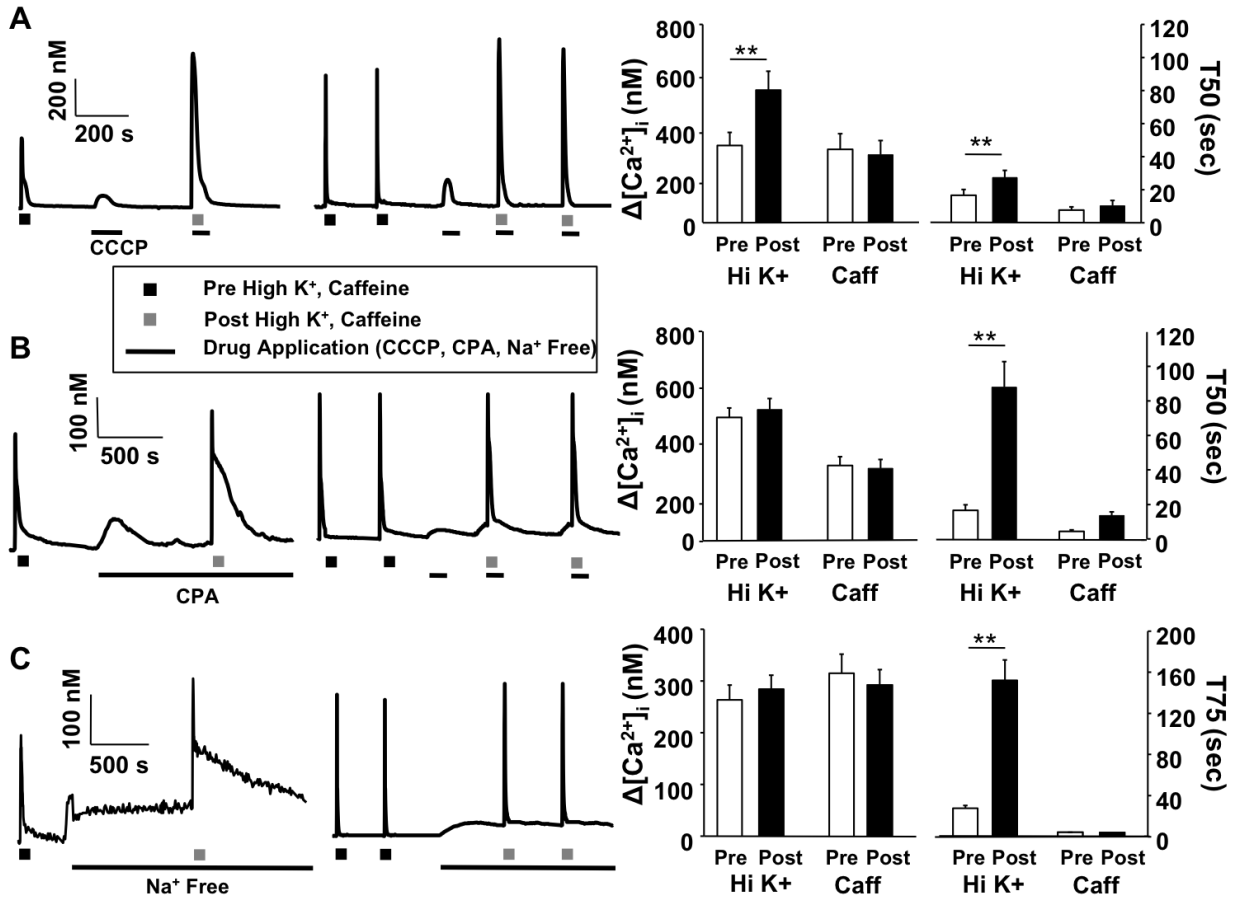

Figure 8: High K^+- and caffeine-evoked Ca^{2+} transients engage distinct Ca^{2+} regulatory machinery.

Putative nociceptive cutaneous DRG neurons from naive rats were challenged with either high K^+ (30 mM, 4s, Left Traces) or caffeine (10 mM, 4s, Right Traces), before and after the application of CCCP (10 μM, A), CPA (10 μM, B), or Na^+ Free bath (C). Pooled magnitude (peak change in concentration of intracellular Ca^{2+} ($[Ca^{2+}]_i$) from baseline) and duration (time of decay) data obtained before and after the application of CCCP, CPA and Na^+ Free bath are plotted. For the high K^+ experiments, the number of neurons studied were 7, 11, and 12, with CCCP, CPA and Na^+ free bath, respectively, while for the caffeine experiments, the number of neurons studied were 6, 6 and 6 for CCP, CPA and Na^+ free bath, respectively. Data were analyzed with a mixed design two-way ANOVA: differences between before and after the application of CCCP, CPA or Na^+ Free bath, as well as between high K^+ and caffeine are indicated. * is $p < 0.05$, and ** is $p < 0.01$.

2.5 DISCUSSION

In the present set of experiments, we sought to determine whether a change in mechanisms underlying CICR and/or the association between influx and release of Ca^{2+} could contribute to the inflammation-induced increase in the high K^+-evoked Ca^{2+} transient. Towards that end, we were able to reproduce our previous results indicating inflammation is associated with an increase in both the magnitude and duration of the high K^+-evoked Ca^{2+} transient. While there was no evidence for an inflammation-induced recruitment of IP3 receptor mediated release, the inflammation-induced increase in duration, but not magnitude of the high K^+-evoked Ca^{2+} transient was at least partially blocked by the RyR blocker, ryanodine. Interestingly, however, there was no influence of inflammation on either the magnitude or duration of transients evoked with a brief (4 second) application of caffeine, or the potency or efficacy of the caffeine-induced release of Ca^{2+} from the ER. There was also no influence of inflammation on the response to repeated caffeine application in Ca^{2+} free bath solution. Furthermore, there was no detectable influence of inflammation on the potency or efficacy of the ryanodine-induced block of the caffeine-evoked Ca^{2+} transients. There was also no evidence that inflammation was associated with a decrease in SERCA activity. Finally, inflammation was associated with a selective increase in the duration of the Ca^{2+} transient in response to prolonged (12 second) caffeine application.

These observations have several interesting implications. Most relevant to the purpose of the present study, these data suggest that mechanism(s) other than a change in CICR or the coupling between Ca^{2+} influx and CICR underlie the inflammation-induced changes in the high K^+-evoked Ca^{2+} transient. This was most readily demonstrated by a lack of evidence for the involvement of CICR in the regulation of the magnitude of the high K^+-evoked Ca^{2+} transient, in

the face of a clear inflammation-induced increase in this parameter. Furthermore, evidence that mechanisms underlying CICR are comparable in neurons from naïve and inflamed animals leaves only a change in coupling between influx and release as a possible mechanism contributing to the inflammation-induced increase in the duration of the high K^+-evoked Ca^{2+} transient. However, while we have not conclusively ruled out a shift in the coupling, which enabled the Ca^{2+} influx via VGCC to engage CICR, the results from the prolonged caffeine application experiment demonstrate that an inflammation-induced change in another Ca^{2+} regulatory mechanism can now be engaged via Ca^{2+} release from the ER. Given our present results with a zero Na^+ bath, our previous results (Lu et al., 2006) as well as those of others (Werth et al., 1996, Pottorf and Thayer, 2002) suggesting that the plasma membrane Ca^{2+}-ATPase (PMCA) and NCX play a greater role in regulating the duration rather than the magnitude of the depolarization-induced Ca^{2+} transient, an inflammation-induced decrease in the rate of Ca^{2+} extrusion could account for increased duration of the Ca^{2+} transient evoked by both depolarization and prolonged release from the ER.

There are distinct Ca^{2+} regulatory machinery engaged by Ca^{2+} entering the cytosol via voltage-gated Ca^{2+} channels versus release from the ER, as suggested by several lines of evidence. These include 1) differences in kinetics of the high K^+ and caffeine-evoked Ca^{2+} transients despite the comparable magnitude of the transients evoked with these two stimuli, 2) the impact of inflammation on the duration (and magnitude) of the high K^+ but not caffeine-evoked transient, 3) the impact of an increase in PKA activity on the duration of the high K^+ but not the caffeine-evoked transient, 4) the contribution of mitochondria to the regulation of both the magnitude and decay of the high K^+-evoked transient, but neither the magnitude nor decay of the caffeine-evoked transient, and 5) the impact of NCX block on the duration of the high K^+ but

not the caffeine-evoked transient. Of note, while the absence of an inflexion on the falling phase of the caffeine-evoked transient, a signature of mitochondria-mediated buffering (Berridge et al., 2003), in combination with the absence of a detectable influence of CCCP on the caffeine-evoked transient in putative nociceptive cutaneous DRG neurons argue strongly against a direct role for mitochondria in the regulation of the caffeine-evoked transient, these observations are in contrast to previous results from unlabeled sensory neurons indicating mitochondria are involved in buffering the Ca^{2+} released from the ER (Friel and Tsien, 1994). Nevertheless, we are not the first to report that mitochondria are differentially engaged by Ca^{2+} influx and release, as comparable results have been previously reported by others in mouse DRG neurons (Svichar et al., 1997). We suggest that heterogeneity among DRG neurons is the most likely explanation for the apparent difference between out results and those in these previous studies.

Evidence that caffeine-evoked transients were stable in the presence of Ca^{2+} free bath solution and unaffected by NCX block suggests that the majority of Ca^{2+} released during caffeine application is pumped back into the ER by SERCA. While we have not collected data on spatial segregation, the results appear to be in support of a tightly regulated microdomains (Berridge, 2006) in putative nociceptive cutaneous neurons through which the magnitude and decay of the caffeine-evoked Ca^{2+} transient are determined by the amount of Ca^{2+} in the ER, the density and distribution of ryanodine receptors, and SERCA activity. Strikingly, even a 12 second application of caffeine to this subpopulation of neurons from naïve rats appeared to be insufficient to engage mitochondrial Ca^{2+} buffering. An additional interesting note is that while Ca^{2+} influx via VGCC was insufficient to activate RyRs in neurons from naïve rats, SERCA still contributes to the regulation of the duration of the high K^+-evoked Ca^{2+} transient as illustrated by the results obtained with CPA. This observation suggests that it is SERCA that largely defines

the barrier separating Ca^{2+} influx from release. Given evidence for the dynamic regulation of SERCA activity in DRG neurons (Usachev et al., 2006), a SERCA-mediated barrier would provide a sensitive mechanism for the modulation of the coupling between Ca^{2+} influx and release in these neurons.

The observation that the inflammation-induced changes in high K^+-evoked transient are manifest despite a decrease in VGCC current density (Lu et al., 2010) argues that regulation of the magnitude and duration of the Ca^{2+} transient is largely independent on the magnitude of the initial Ca^{2+} influx. Furthermore, the observation that inflammation is associated with an increase in both the magnitude and duration of the high K^+-evoked Ca^{2+} transient, in the face of evidence that there are mechanisms such as SERCA and NCX that influence the duration but not the magnitude of the high K^+-evoked Ca^{2+} transient raises the possibility that there are two Ca^{2+} regulatory processes that are altered in the presence of inflammation. Interestingly, despite recent evidence suggesting that Ca^{2+} influx via TRP channels may drive CICR secondary to the activation of IP3 receptor (Rohacs et al., 2008), such a mechanism does not appear to contribute to the high K^+-evoked Ca^{2+} transient. While this may be a unique feature of the subpopulation of neurons studied here, this difference raises the possibility that Ca^{2+} influx via TRP channels engages Ca^{2+} regulatory processes distinct from those engaged by caffeine or high K^+. While future experiments would be needed to address this possibility, the further definition of the microdomain engaged following Ca^{2+} influx through VGCC serves to limit the number of mechanisms that may ultimately be responsible for the inflammation-induced changes in the high K^+-evoked Ca^{2+} transient.

While not the focus of the present study, results obtained with CCCP suggest mitochondria are not a potential mechanisms contributing to the inflammation-induced change in

the high K^+-evoked Ca^{2+} transient. That is, because CCCP results in a significant increase in the duration of the high K^+-evoked Ca^{2+} transient in cutaneous neurons from naïve rats, albeit with altered decay kinetics, one would predict that if a decrease in mitochondrial buffering of the high K^+-evoked transient contributed to the changes observed in the presence of inflammation, the impact of CCCP on the high K^+-evoked Ca^{2+} transient in neurons from inflamed rats should be attenuated. Preliminary results with a pre-application protocol similar to that employed previously (Lu et al., 2006) suggest that this is not the case, as CCCP (10 μM) was associated with an increase in the duration of the high K^+-evoked transient (T50 = 113.2 ± 14.2 s, n = 9) that was, if anything even larger than that observed in neurons from naïve rats (T50 = 72.9 ± 11 s, n = 11). However, given the complex way in which mitochondria contribute to the regulation of $[Ca^{2+}]_i$, this issue may need to be addressed more systematically.

The suggestion that distinct mechanisms underlie the inflammation-induced increase in the magnitude and duration of the high K^+-evoked Ca^{2+} transient raises the possibility that these mechanisms are separable within the neuron. The functional implications of this possibility will depend on where the changes are manifest. For example, activation of a sustained increase in $[Ca^{2+}]_i$ in central or peripheral afferent terminals would facilitate transmitter release, thus augmenting neurogenic inflammation in the periphery or increasing the transmission of nociceptive information at the central terminal. A comparable increase in the duration of the transient at a spike initiation zone or along an axon where Ca^{2+}-dependent K^+ channels may be localized would influence spike pattern or the relative refractory period. In the cell body, the dynamics of the Ca^{2+} transient may lead to very different effects on gene expression (Fields et al., 2005). Conversely, an increase in the magnitude of the Ca^{2+} transient independent of a change in duration may lead to differential activation of regulatory proteins or second messenger

pathways based on Ca^{2+} affinity, alternative gene transcription and translation, and/or excitotoxicity (Carafoli et al., 2001, Berridge et al., 2003, Fields et al., 2005).

In contrast to previous results indicating that 10 μM ryanodine is sufficient to completely block caffeine-evoked Ca^{2+} transients in sensory neurons (Usachev et al., 1993, Shmigol et al., 1995, Solovyova et al., 2002), we only observed a ~60% block of the caffeine-evoked transient at this concentration in cutaneous DRG neurons. We have previously observed that differences in how the neurons were processed and the amount of time in culture prior to study are factors that to influence the properties of Ca^{2+} transients in DRG neurons (data not shown). Nevertheless, we suggest that the most likely explanation for the difference between our results and previous studies is due to heterogeneity among DRG neurons. We have previously reported that there are significant differences between subpopulations of DRG neurons with respect to the relative impact of CICR to the high K^+-evoked Ca^{2+} transient (Lu et al., 2006). Furthermore, the results of the present study indicate that even within a small subpopulation of cutaneous DRG neurons, there is heterogeneity with respect to the impact of ryanodine on the caffeine-evoked Ca^{2+} transient. Indeed, consistent with these previous results, we observed some neurons in which 10 μM ryanodine was sufficient to completely block the caffeine-evoked transient, arguing against a problem with how the compound was prepared or the neurons were challenged. However, this was clearly not the case in all neurons. We also suggest that a differential expression of RyR subtypes within the subpopulation of interest is likely to account for this heterogeneity in the actions of ryanodine. That is, while RyR 3 is similar to RyR 2 in its threshold of Ca^{2+}-induced activation (1μM), the two receptors differ in open channel probability (P_o) in response to comparable levels of Ca^{2+}: RyR 3 has a P_o of ~1 while that of RyR 2 is ~0.6 and RyR 1 is ~0.15 at ~100μM Ca^{2+}. Furthermore, RyR 3 is able to maintain its open state and requires higher Ca^{2+}

concentrations for inactivation compared to RyR1 or RyR 2 (Chen et al., 1997, Jeyakumar et al., 1998, Meissner, 2002). Ryanodine is an open channel blocker, therefore, the difference in P_o would suggest that RyR 1 is the dominant receptor in neurons "resistant" to ryanodine and RyR 3 is the dominant receptor in neurons "highly sensitive" to ryanodine. This would also account for the larger caffeine-evoked transient in "highly sensitive" neurons. Importantly, a differential distribution of RyR subtypes both within and between neurons would result in very different responses to stimuli capable of engaging CICR.

In summary, while our results argue against a change in CICR or the coupling between CICR and Ca^{2+} influx via VGCC as the mechanism underlying the inflammation-induced increase in the high K^+-evoked Ca^{2+} transient, we further characterized the regulation of $[Ca^{2+}]_i$ in putative nociceptive cutaneous neurons, revealing several aspects of the Ca^{2+} regulation that may have a profound impact on the function of this subpopulation of neurons. This includes evidence that mechanisms underlying the inflammation-induced increase in magnitude and duration of the high K^+-evoked transient are distinct, that SERCA serves as a barrier isolating Ca^{2+} regulatory domains accessed by release from the ER and influx via VGCC, and that there is a differential distribution of RyR subtypes among subpopulations of these neurons. Future experiments will be needed to assess the functional consequences of these unique features.

3.0 THE PROPERTIES, DISTRIBUTION, AND FUNCTION OF SODIUM CALCIUM EXCHANGER ISOFORMS IN RAT CUTANEOUS SENSORY NEURONS

3.1 ABSTRACT

The Na^+/Ca^{2+} exchanger (NCX) appears to play an important role in the regulation of the high K^+-evoked Ca^{2+} transient in putative nociceptive dorsal root ganglion (DRG) neurons. The purpose of the present study was to 1) characterize the properties of NCX activity in subpopulations of DRG neurons 2) identify the isoform(s) underlying NCX activity, and 3) begin to assess the function of this isoform *in vivo*. In retrogradely labeled neurons from the glabrous skin of adult male Sprague-Dawley rats, NCX activity, as assessed with fura-2 based microfluorimetry, was only detected in putative nociceptive IB4+ neurons. There appear to be two modes of NCX activity: one evoked in response to relatively large and long lasting (~325 nM for > 12 second) increases in the concentration of intracellular Ca^{2+} ($[Ca^{2+}]_i$), and a second that is active at resting $[Ca^{2+}]_i$ > ~150 nM. There also appeared to be two modes of evoked activity: one that decayed relatively rapidly (< 5 min) and a second that persisted (>10 min). Whereas mRNA encoding all three NCX isoforms (NCX1-3) was detectable in putative nociceptive cutaneous neurons with single cell PCR, pharmacological analysis suggested that NCX3 was responsible for >70% of total activity in cutaneous neurons, and NCX2 was responsible for the remainder. Comparable results were obtained with small interfering RNA

(siRNA) knockdown of each isoform *in vivo*, but with potentially larger role for NCX2 suggested as well. Western blot analyses suggested that NCX isoforms were differentially distributed within sensory neurons. Functional assays of excitability, action potential propagation, and nociceptive behavior suggest NCX activity has little influence on excitability per se, but instead influences axonal conduction velocity, resting membrane potential, and nociceptive threshold. Together these results indicate that the function of NCX in regulation of $[Ca^{2+}]_i$ in putative nociceptive neurons may be unique relative to other cells in which these exchanger isoforms have been characterized and it has the potential to influence sensory neuron properties at multiple levels.

3.2 INTRODUCTION

We have previously demonstrated marked differences among subpopulations of dorsal root ganglia (DRG) neurons defined by cell body size, IB4 binding and capsaicin sensitivity with respect to the magnitude and decay of depolarization-evoked Ca^{2+} transients that were associated with differences in the relative contribution of many of the core components of the Ca^{2+} signaling toolkit (Berridge et al., 2000). These included voltage gated Ca^{2+} channels, ryanodine receptor-mediated Ca^{2+}-induced Ca^{2+} release, internal Ca^{2+} store operation mediated by sarco-endoplasmic reticulum ATPase (SERCA), mitochondria, and store operated Ca^{2+} entry, as well as extrusion mechanisms such as the plasma membrane Ca^{2+} ATPase (PMCA) and the Na^{+}/Ca^{2+} exchanger (NCX) (Lu et al., 2006, Scheff et al., 2013)

There are several reasons to focus on NCX for further analysis in DRG neurons. First, there are conflicting results in the literature regarding the extent to which NCX activity is

detectable in sensory neurons. Whereas our data (Lu et al., 2006) and those of Verdru and colleagues (Verdru et al., 1997), suggest that the duration of depolarization-evoked Ca^{2+} transients in sensory neurons are determined, at least in part, by NCX activity, others have concluded that there is little if any detectable NCX activity in either the sensory neuron cell body (Werth and Thayer, 1994) or central terminals (Wan et al., 2012, Shutov et al., 2013). Second, there has been no systematic analysis of the biophysical properties of NCX in sensory neurons. This is important as available evidence from other systems suggest that while NCX has a higher extrusion rate than the PMCA, it should only be active in the presence of higher concentrations of intracellular $[Ca^{2+}]_i$ due to a lower affinity for Ca^{2+} (Blaustein and Lederer, 1999, DiPolo and Beauge, 2006). This property could account for the apparent absence of NCX activity in sensory neurons, as the Ca^{2+} transients in the "negative" studies were relatively small. Biophysical characterization of NCX activity in sensory neurons is also important in light of recent evidence that NCX can function in "reverse mode" (Kuroda et al., 2013), that has been suggested to contribute to axon injury observed in some forms of peripheral neuropathy (Ma, 2013). Third, there is not only evidence of the differential distribution of NCX activity among subpopulations of sensory neurons (we were only able to detect NCX activity in putative nociceptive DRG neurons (Lu et al., 2006)), there is evidence of the differential distribution of NCX isoforms among sensory neurons, where NCX2, the only isoform detectable in sensory neurons, was restricted to those with a small cell body diameter (Persson et al., 2010). Thus, the selective distribution of NCX isoforms may also contribute to the conflicting results in the literature on NCX activity in sensory neurons. Finally, with the exception of data on the duration of evoked Ca^{2+} transients and recent evidence suggesting that NCX may act in reverse mode to contribute to peripheral nerve injury (Persson et al., 2013), there are no data on how NCX activity

influences the normal function of sensory neurons. Therefore, the present study was designed to begin to address this relative dearth of information concerning the properties, distribution and function of NCX isoforms in sensory neurons.

A combination of approaches ranging from the microfluorometric and PCR analysis of retrogradely labeled isolated sensory neurons *in vitro* to behavioral analysis following targeted knock down of NCX isoforms were employed to address these issues. Our results suggest that NCX, more specifically NCX3, plays a significant role in the regulation of decay of the evoked change in $[Ca^{2+}]_i$ at the level of the cell body. However, functional assays of excitability, action potential propagation, and nociceptive behavior suggest NCX activity influences axonal $[Ca^{2+}]_i$ levels, resting membrane potential, and nociceptive threshold via a mechanisms likely secondary to the regulation of $[Ca^{2+}]_i$ in afferent terminals.

3.3 METHODS

Adult male Sprague-Dawley rats (Harlan, 220-300g) were used for all experiments. Animals were housed two per cage in a temperature and humidity controlled animal facility on a 12:12 light:dark schedule with food and water freely available. All procedures were approved by the University of Pittsburgh Institutional Animal Care and Use Committee and performed in accordance with National Institutes of Health guidelines for the use of laboratory animals in research.

3.3.1 Tissue labeling

Fourteen to 17 days prior to tissue harvest, the retrograde tracer 1,1'-dioctadecyl-3,3,3',3'-tetramethylindocarbo-cyanine perchlorate (DiI, Invitrogen, Carlsbad, CA) was injected into the glabrous skin of the hindpaw to label cutaneous afferents. The tracer was dissolved at 170 mg/mL in dimethylsufoxide (DMSO, diluted 1:10 in 0.9% sterile saline, and injected in 3-5 subcutaneous sites using a 30 g needle for a total volume of 10 μL per hindpaw under isoflurane (Abbott Laboratories, North Chicago, IL, USA) anesthesia.

3.3.2 Tissue collection and isolation

Prior to tissue removal, rats were deeply anesthetized with an intraperitoneal injection of a cocktail containing ketamine (55 mg/kg), xylazine (5.5 mg/kg) and acepromazine (1.1 mg/kg). For studies involving isolated sensory neurons, the L4-L5 DRG were removed ipsilateral to labeling. Ganglia were enzymatically treated, mechanically dissociated, and neurons plated on laminin (Invitrogen, Carlsbad, CA; 1mg/ml) and poly-L-ornithine-coated (Sigma-Aldrich; 1 mg/ml) glass cover slips as previously described (Lu et al., 2006). All subsequent experiments were preformed within 8 h of tissue harvest and only neurons containing the retrograde label DiI were studied. For isolated nerve recordings, rat sciatic nerves were harvested and prepared for compound action potential (CAP) recording as previously described (Yilmaz-Rastoder et al., 2012). Briefly, sciatic nerves (~30 mm) were quickly dissected and transferred to a dish containing ice-cold Locke's solution of the following composition (in mM): 136 NaCl, 5.6 KCl, 14.3 $NaHCO_3$, 1.2 NaH_2PO_4, 2.2 $CaCl_2$, 1.2 $MgCl_2$, 11 glucose, equilibrated continuously with 95% O_2, 5% CO2, pH 7.2–7.4. In ice-cold oxygenated Locke's solution nerves were trimmed of

excess connective under a dissecting microscope. All subsequent experiments were preformed within 24 h of tissue harvest.

3.3.3 Calcium Imaging

Neurons were incubated with 2.5 μM Ca^{2+} indicator fura-2 AM ester with 0.025 % Pluronic F-127 for 20min at room temperature. Neurons were then labeled with FITC-conjugated IB4 (10 μg/ml) for 10 min at room temperature. Labeled neurons were placed in a recording chamber and continuously superfused with normal bath solution (mM: 130 NaCl, 3 KCl, 2.5 $CaCl_2$, 0.6 $MgCl_2$, 10 HEPES, 10 glucose, pH 7.4, osmolality 325 mOsm) or a 'Na^+-free' bath solution (mM: 130 Choline-Cl or LiCl, 3 KCl, 10 $MgCl_2$, 2 EGTA, 10 Hepes, 10 glucose, pH 7.4, osmolality 325 mOsm). A Na^+-free solution was used to block NCX activity by preventing NCX from fulfilling the Na^+ binding requirement for exchange activity (Cook et al., 1998). Fluorescence data were acquired on a PC running Metafluor software (Molecular Devices, Sunnyvale, CA, USA) via a CCD camera (Roper Scientific; model RTE/CCD 1300). The ratio (*R*) of fluorescence emission (510 nm) in response to 340/380nm excitation (controlled by a lambda 10–2 filter changer (Sutter Instrument, Novato, CA)) was acquired at 1 Hz during drug application. All drugs were applied through a computer-controlled peizo driven perfusion system (switching time <20 ms; Warner Instruments, Hamden, CT, USA, Fast-Step Model SF-77B). $[Ca^{2+}]_i$ was determined from fura-2 ratio following in situ calibration experiment as described in detail previously (Grynkiewicz et al., 1985, Kao, 1994, Scheff et al., 2013).

3.3.4 Patch Clamp Electrophysiology

Gramicidin-perforated patch clamp experiments were carried out using a HEKA EPC9 amplifier (HEKA Elektronik, Lambrecht/Rhineland-Pfalz, Germany). Glass electrodes (1–4 MΩ) were filled with (mM) 110 K-methanesulfonate, 30 KCl, 5 NaCl, 1 $CaCl_2$, 2 $MgCl_2$, 10 HEPES, 11 EGTA, 2 Mg-ATP, and 1 Li-GTP for current clamp excitability recordings. The pH was adjusted with Tris-base to 7.2 and osmolality was adjusted with sucrose to 320 mOsm.

To obtain whole cell access for patch clamp experiments, a stock solution of gramicidin (1.5 mg/100 µl, Sigma–Aldrich) was prepared in DMSO. This was diluted with electrode solution at 1:300 to give a final concentration of 50 µg/ml. The gramicidin containing electrode solution was vortexed for > 15 s. No filtering was applied. The tip of the electrode was loaded with a small volume of gramicidin free electrode solution in order to avoid interference of the antibiotic with seal formation. Gramicidin-containing electrode solution was subsequently back loaded. The progress of perforation was monitored from a holding potential of -60 mV with a 10 ms step to -65 mV. Experiments were not started until access resistance was < 7 MΩ.

Neuronal excitability was assessed in current clamp (Scheff and Gold, 2011) before and after a 4 s voltage step from -60 mV to 0 mV to drive an increase in $[Ca^{2+}]_i$, and consequently an increase in NCX activity. Resulting changes in $[Ca^{2+}]_i$ were simultaneously monitored with Fura-2 AM based microfluorimetry. Series resistance compensation (>70%) was employed for all voltage-clamp recordings. Five distinct measures of excitability were used: the emergence of spontaneous activity, action potential (AP) threshold, rheobase, the response to suprathreshold current injection, and following frequency. Spontaneous activity was assessed at resting membrane potential (V_{rest}) for 30 s before and up to 90 s after the application of Na^+ free Bath. The subsequent three measures were determined with a 750 ms depolarizing square-pulse current

injection. AP threshold was defined as the greatest depolarization reached before spike generation in response to depolarizing current injections. Rheobase was defined as the smallest amount of current needed to evoke a single AP. The results to suprathreshold current injection was determined by counting the number of action potentials evoked in response to current 2x and 3x rheobase. As rheobase is positively correlated with cell size, values were normalized with respect to membrane capacitance to facilitate comparisons between neurons. Following frequency was assessed at 10, 20, and 40 Hz with 1 ms pulses 1.5-fold above threshold (determined as with rheobase but with the 1 ms pulse duration).

3.3.5 Single cell polymerase chain reaction (PCR)

Isolated neurons were prepared for single cell RT-PCR experiments in a manner identical to that used for patch clamp and microfluorimetry experiments. Single neurons were collected with large bore (30 μm) glass pipettes and expelled into reaction tube for subsequent cDNA synthesis via methods identical to those described previously (Nealen et al., 2003, Zhang et al., 2012a). The cDNA generated from each neuron was used as a template for subsequent PCR reactions. To confirm successful cell collection and cDNA synthesis, 0.5 μl of the template cDNA was used for the amplification of the housekeeping gene, cyclophilin. Negative controls for each round of cell collection included two neurons in which no reverse transcriptase was added to the reaction mixture and two tubes in which all other procedures were performed as if a neuron was collected, except no neuron was collected. Nested PCR primers (Table 1) were used in two successive rounds of PCR amplification to assess the expression of NCX 1, 2 and 3, as this strategy increases the sensitivity and specificity of the PCR reaction. The “outer” set of primers was used in the first round of amplification and 2 μl of this reaction product was used for a

second round of amplification with the “inner” set of primers. Thirty five cycles were used for both rounds of amplification. Following agarose gel electrophoresis, PCR reaction products were visualized with ethidium bromide.

3.3.6 Western Blot

L4 and L5 DRG were homogenized with Teflon tube and mortar for less than 10 strokes in ice cold radioimmunoprecipitation assay (RIPA) buffer supplied with protease inhibitors (aprotinin, leupeptin, pepstatin, E-64, trypsin inhibitor, and phenylmethanesulfonyl fluoride (PMSF), all at a final concentration of 2 ng/ml except PMSF, which was used at a final concentration of 1 mM). All protease inhibitors were obtained from Sigma–Aldrich. Lysates were collected in 0.5-ml tubes. Teflon tubes were rinsed with RIPA buffer and the solutions were combined with the lysates previously collected. Lysates were centrifuged for 5 min at 10,000 rpm at 4°C. Protein concentration was determined via bicinchoninic acid (BCA) protein assay using a BCA assay kit (Thermo scientific, Rockford, IL, USA). Lysates were then mixed with Laemmli buffer (2×, 400 µl + 100 µL β-mercaptoethanol) and boiled for 5 min before loading. Protein (30 µg) from one animal was then loaded per lane and separated on a 7 % SDS–PAGE gel and transferred to nitrocellulose membrane. Membranes were blocked with 5% milk for 1 hour at room temperature and then incubated with primary antibody at 4°C overnight (1:100 for R3F1 (anti-NCX1),1:200 for W1C3 (anti-NCX2), and 1:100 for anti-NCX3 (cat # LS-B5775, LifeSpan Biosciences, Inc., Seattle WA), diluted with 5% milk/Tris-buffered saline with Tween 20 (TBST, Sigma–Aldrich). The blots were washed and then incubated with peroxidase-conjugated secondary antibody (1:2000 in 5% milk/TBST, Jackson ImmunoResearch Laboratories Inc. West Grove, PA, USA) for an hour at room temperature. An ECL kit (Amersham Biosciences,

Piscataway, NJ, USA) was used for detection of immunoreactivity, luminescence data were collected on an LAS3000 imager (Fujifilm Inc., Japan), and analyzed with ImageJ (NIH). Both antibodies used to detect NCX1 and NCX2 were gifts from Dr. Kenneth Philipson of University of California Los Angeles. Both antibodies have been characterized by Dr. Philipson and colleagues in heterologous expression systems and hippocampal cultures, where R3F1 (anti-NCX1) detects a prominent band at 120 kDa and minor bands at 70 kDa and 60 kDa, and W1C3 (anti-NCX2) detects only one prominent band at 60 kDa. There appears to be no cross reactivity between isoforms (Thurneysen et al., 2002b, Papa et al., 2003). Furthermore, the specificity of the anti-NCX2 antibody was confirmed in NCX2 null mutant mice (Jeon et al., 2003).

3.3.7 Compound Action Potential (CAP) Recordings

Isolated sciatic nerve recording was performed at room temperature. The isolated nerves were mounted in a recording chamber such that the distal end was laid over two platinum stimulating electrodes isolated from the central portion of the nerve with a grease-gap. A glass suction electrode connected to a differential preamplifier (WPI model DAM-80, Sarasota, FL, USA) was used to isolate the central end of the nerve. The remainder of the nerve (~15-20 mm) was superfused continuously (2-5 ml/min) with oxygenated Locke's solution with and without drugs delivered via a gravity driven perfusion system. CAPs were evoked with electrical pulses 0.2 - 0.5 ms in duration applied at 0.1 Hz unless otherwise indicated, where the stimulus amplitude was ~2x that needed to evoke a maximal amplitude C-fiber component of the CAP. CAP data were filtered at 2 kHz and sampled at 20 kHz via a CED 1401 Micro A/D converter, and acquired and analyzed using CED Spike 2 version 5 for MS Windows (CED, Cambridge, England). CAP data were rectified and the average of 6 consecutive CAPs, were integrated to

quantify A- and C-fiber components as area under the curve (AUC). The A-fiber deflection of the CAP (A-wave) was easily distinguished from that associated with the C-fiber deflection (C-wave) because of the time delay between the arrivals of the two waves at the recording electrode.

3.3.8 siRNA and IB4 saporin injections

Slc8a ON-TARGETplus SMARTpool siRNAs (Thermo Scientific, Pittsburgh, PA, USA) were tested for their ability to knock down expression of individual isoforms of NCX in cultured L4-L5 DRG neurons where the extent of knockdown was assessed with PCR. Catalog numbers for each isoform are as follows: NCX1 (LQ-091320-02), NCX2 (LQ-094819-02), NCX3 (LQ-094821-02). The siRNA sequence that produced the largest decrease in the expression of the targeted isoform was chosen for sciatic nerve injection with the transfection agent, lipofectamine (Invitrogen, Carlsbad, CA, USA). At least 7-10 days after DiI injection, rats were deeply anesthetized with isoflurane. The hair over the back of the thigh was shaved and blunt dissection was used to separate the hamstring muscle exposing the sciatic nerve. A subfasicular injection of 4-6 µl 1:1 lipofectamine to NCX-targeted siRNA or control siRNA was made using a 33 g needle. For Ca^{2+} imaging experiments, DRG were isolated as described above 6 days after siRNA injection. The extent of the knockdown was assessed with western blot analysis of the sciatic nerve.

Methodology for the IB4/saporin and siRNA co-injections was adapted from Vulchanova et al (2001) (Vulchanova et al., 2001). Under deep anesthesia, the left sciatic nerve was exposed and a subfasicular injection of 10 µl consisting of either a mixture of 5 µl control or NCX3 siRNA (1:1 lipofectamine to siRNA) and 5 µl IB4 conjugated saporin (400 µg/mL) or unconjugated IB4 and saporin (2.5 µl IB4 (280 µg/ml, 71%) + 2.5 µl saporin (120 µg/mL, 29%)) was slowly infused

using a 33 g needle at a rate of 10 µl/min. IB4+ fiber loss was confirmed using IB4-FITC (Sigma-Aldrich) staining of 25 µm sections of the spinal cord lumbar enlargement.

3.3.9 Nociceptive Behavior

Testing for each group of rats was initiated at the same time of day with no more than two groups (12 rats) being tested on any given day. Rats from each experimental and control group were randomized between testing sessions. Rats were habituated to the testing procedure and experimenter for three days before the collection of baseline data. Habituation consisted of moving the rats from their home room to the testing room, handling the rats, and placing them in the testing apparatus for 30 min. The testing apparatus consisted of a row of six clear acrylic enclosures (4 inches [~10.2 cm] wide, 7–5/8 inches [19.4 cm] long, and 5 inches [12.7 cm] high). Opaque dividers separated the enclosures. On testing days, rats were loaded in their enclosures and given 10 min of habituation before the initiation of data collection.

Von Frey: Acrylic enclosures sat atop anodized aluminum mesh (1/4" [6.4 mm] waffle hole). An electronic von Frey anesthesiometer (IITC Plantar Test Analgesia Meter 2390; IITC Life Sciences Inc., Woodland Hills, CA) fitted with a rigid tip (1.0-mm tip diameter) was used to assess changes in mechanical threshold. The tip was applied to the glabrous skin of the hind paw with steady vertical pressure until the rat withdrew from the stimulus or until the paw was lifted off the mesh floor (at ~ 70 g). The greatest force generated before withdrawal was recorded. This procedure was repeated three times, and the average of the three measures for each paw was considered the withdrawal threshold.

Hargreaves: Thermal withdrawal latency was determined using a plantar analgesia meter (IITC Life Sciences, Woodland Hills, CA). Acrylic enclosures sat atop a glass surface

maintained at 30°C. A light beam was focused onto the middle of the ventral surface of each hind paw and the amount of time lapsed until the animal withdrawals the paw cut-off (20 sec) was reached.

3.3.10 Chemicals and Reagents

DiI 1,1'-dioctadecyl-3,3,3',3'-tetramethylindocarbo-cyanine perchlorate was purchased from Invitrogen (Carlsbad, CA, USA). Fura-2 acetoxymethyl (AM) ester (2.5 mM stock in DMSO) and Pluronic F-127 (0.025 % in water) were purchased from TEF Laboratories (Austin, TX, USA). Isolectin B4 (IB4) was purchased from Sigma (St Louis, MO, USA). KB-R7943 and SN-6 were purchased from R&D Systems, Inc (Minneapolis, MN, USA) and SEA0400 was purchased from ChemScene, LLC (Monmouth Junction, NJ, USA). All NCX inhibitors were dissolved to 100mM stock concentration in DMSO (Sigma-Aldrich, St Louis, MO, USA). Saporin (unconjugated and IB4-conjugated) was purchased from Advanced Targeting Systems (San Diego, CA, USA).

3.3.11 Statistical Analysis

Data are expressed as mean ± s.e.m. Student's *t* test was used for simple comparison between groups. For experiments involving the application of test compounds, vehicle controls were always included. Concentration-response data for NCX blockers were fitted with a modified Hill equation: $E_{max}*D^n/(D^n + EC_{50}{}^n)$, where E_{max} is the maximal increase in the duration of the evoked Ca^{2+} transient, D is the concentration of NCX blocker, EC_{50} is the concentration of NCX blocker producing a response 50% of maximal, and n is the Hill coefficient. One and two-way

ANOVA was used for analysis of more than two groups with the Holm-Sidak test used for post-hoc analysis. Statistical significance was assessed at $p < 0.05$.

3.4 RESULTS

3.4.1 NCX contributes to the decay of the evoked Ca^{2+} transient in IB4+ small diameter cutaneous DRG neurons

We initially screened cutaneous (DiI+) DRG neurons for the presence of NCX activity by comparing high K^+ (30 mM, 4s)-evoked Ca^{2+} transients before and after blocking NCX using Na^+ free bath solution (Figure 9A). A neuron was considered to have NCX activity if application of Na^+ free bath produced an increase in the duration of the evoked Ca^{2+} transient, assessed as time to decay to 50% of the peak, or T50, following, >20%. Consistent with our previous results in unlabeled DRG neurons (Lu *et al.*, 2006), NCX activity was only detected in a subpopulation of the cutaneous neurons: those with a small cell body diameter (≤ 30 μm), that were IB4+, and were, in general (29/34), responsive to 500nM capsaicin. In this subpopulation of IB4+ (n = 34) neurons, blocking NCX activity had no effect on the magnitude of the evoked Ca^{2+} transient, but was associated with a significant increase in duration (529.22 ± 12.68 %, Figure 9B). In contrast, blocking NCX activity in IB4- neurons (n = 15) had no effect on either the magnitude or duration of the evoked Ca^{2+} transient (Figure 9B). Failure to detect NCX activity was not due to differences in the magnitude of Ca^{2+} transient used to assess the presence of activity (Figure 9B). Comparable results were obtained with Na^+ free bath solution in which Na^+ was replaced with Li^+ or choline (Figure 9C), arguing against non-specific effects of Li^+ on the regulation of

$[Ca^{2+}]_i$. Lastly, there was no significant difference between IB4+ and IB4- neurons with respect to resting $[Ca^{2+}]_i$ which was 104.02 ± 4.31 nM and 111.04 ± 3.98 nM, respectively.

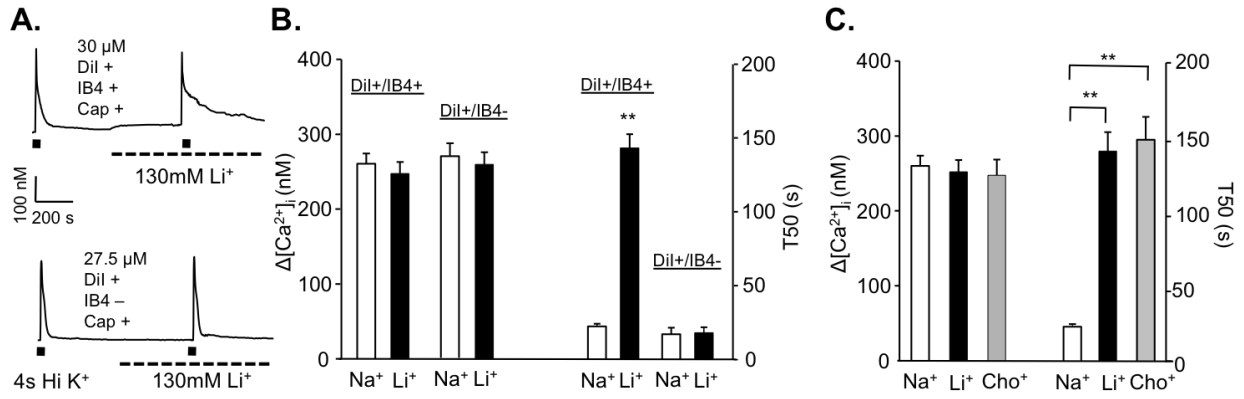

Figure 9: NCX activity in isolated cutaneous DRG neurons

A) High K^+ (30 mM) evoked Ca^{2+} transients in small diameter (≤ 30 µm) retrogradely labeled (DiI+), capsaicin sensitive (Cap+), IB4+ (top trace) and IB4- (bottom trace) DRG neurons before and after NCX block with a bath solution in which Na^+ was replaced with Li^+. **B**) Pooled magnitude ($\Delta[Ca^{2+}]_i$) and decay (time to 50% decay from peak, or T50) of high K^+ evoked Ca^{2+} transient data from the two populations of neurons illustrated in (**A)** (DiI+ small diameter Cap+ neurons that were either IB4+ (n = 34) or IB4- (n = 15)). The increase in the duration of the evoked transient was only observed in IB4+ neurons. **C**) Pooled magnitude and decay of high K^+ evoked Ca^{2+} transient data from DiI+/IB4+ neurons before (Na^+) and after block of NCX with Li^+ (n = 20) or choline (Cho+, n = 14) replacement. ** $p<0.01$

3.4.2 Biophysical properties of NCX in putative nociceptive cutaneous neurons

NCX is described as a low affinity Ca^{2+} extrusion mechanism and evidence from other systems suggest that it is only activated with relatively large increases in $[Ca^{2+}]_i$ (Blaustein and Lederer, 1999, Hilge, 2012). Furthermore, if NCX has a relatively high threshold for activation in sensory neurons, this biophysical property could explain the apparent inconsistencies among previous studies of sensory neurons as to whether NCX contributes to the regulation of evoked Ca^{2+} transients (Verdru et al., 1997, Thayer et al., 2002, Lu et al., 2006, Usachev et al., 2006). We therefore sought to characterize the relationship between $[Ca^{2+}]_i$ and NCX activity in putative nociceptive cutaneous neurons. To address this issue, neurons (n = 20 to 40) were challenged with high K^+ applied at durations increasing from 250 ms to 4 s, before and after Li^+-induced block of NCX (Fig 10A). The stimulus duration-dependent increase in the peak of the evoked Ca^{2+} transient was well described by a single exponential with a time constant of 1.25 ± 0.08 sec, and this was not changed by NCX block (Fig 10B). The stimulus duration-dependent increase in the decay of the evoked transient was more complex, with a marked increase in transient duration detectable as the duration of high K^+ application was increased from 1 to 2 s. This transition was further highlighted by NCX block (Fig 10C), where a Li^+-induced increase in transient duration was readily apparent in response to a 2 s high K^+ application. Consistent with our previous results indicating that there are distinct mechanisms in sensory neurons responsible for the regulation of the magnitude and duration of evoked Ca^{2+} transients, the magnitude of the evoked transient was saturated by a 2 s high K^+ application, at 403.7 ± 20.9 nM, while there was still a ~ 60% increase in duration of the evoked transient between 2 and 4 s of application.

Interestingly, even within the IB4+ subpopulation of small diameter cutaneous neurons, there was heterogeneity with respect to the duration of high K^+ application at which an influence

of Li^+ application was detectable. To illustrate this point, we plotted the percentage of neurons responsive to block of NCX, as determined by an increase in high K^+-evoked transient duration in Na^+ Free bath, as a function of the duration of high K^+ application (Fig 10D). While NCX activity was detectable in all neurons following a 4 s high K^+ application, NCX activity was only detectable in 62% of these with a 2 s high K^+ application. Not surprisingly, there was no difference with respect to the magnitude of the Ca^{2+} transient evoked between neurons in which NCX activity was (2s-responder) or was not (2s-non-responder) detected with a 2 s high K^+ application (Fig 10E; 267.25 ± 15.03 nM and 265.06 ± 17.61 nM, respectively). However, there was a significant difference between 2s-responders and 2s-non-responders with respect to the duration of the 2 s high K^+-evoked transient (Fig 10F; 27.42 ± 2.11 s and 12.39 ± 1.74 s, respectively; $p < 0.05$).

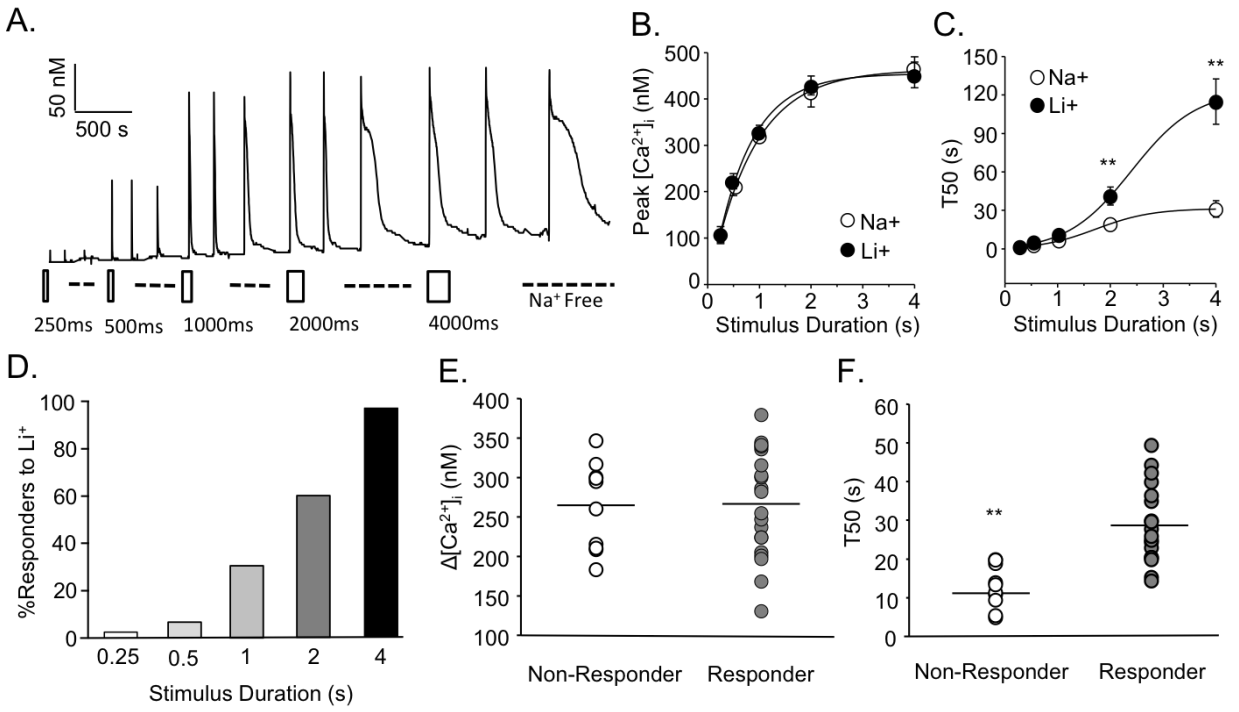

Figure 10: Properties of the Ca^{2+} transient necessary for the detection of NCX activity.

A) High K^+ (30 mM) was applied to a cutaneous putative nociceptive neuron for stimulus durations ranging between 250 ms and 4 s, before and after NCX block with Na^+ free bath solution (dashed line). The open rectangles indicate the first of three fixed-duration pulses of High K^+ (30 mM). **B**) The peak evoked response from neurons (n = 40) stimulated as in (**A**) before (Na^+) and after (Li^+) NCX block, plotted as a function of the high K^+ application duration. **C**) The duration, as assessed with the T50, of the evoked response of the neurons plotted in B, before (Na^+) and after (Li^+) block of NCX. **D**) A cumulative histogram of the neurons illustrated in B and C, analyzed as a percent of neurons studied (n = 32) in which NCX block resulted in an increase in the transient duration (% Responders to Li^+) plotted as a function of the stimulus duration. A neuron was considered a responder if NCX block resulted in a 20% increase in the evoked transient duration (T50) over the baseline response. Because there appeared to be a group of neurons in which application of Li^+ resulted in an increase in baseline $[Ca^{2+}]_i$ and we were originally interested in evoked NCX activity, these neurons were not included in this analysis. Scatter plots of the magnitude (**E**) and decay (**F**) of the evoked Ca^{2+} transient in neurons with (2s-Resp, n = 20) and without (2s-Non-Resp, n = 14) evidence of NCX activity in response to a 2 s application of high K^+.

We performed a more detailed analysis of the evoked Ca^{2+} transient in 2s-responder and 2s-non-responder neurons to determine whether it was possible to define a "threshold" for NCX activation. Because the duration of the Ca^{2+} transient in 2s-responders was so much longer than that in 2s-non-responders (Fig 11A), we analyzed Ca^{2+} transients for each neuron as a function of the duration at which the transient was at or above an $[Ca^{2+}]_i$ ranging from 275 to 400 nM. Increments of 25 nM Ca^{2+} were used, as they appeared to provide sufficient resolution to detect a separation between subpopulations of neurons. For example, there was a separation in the time spent at or above 325 nM Ca^{2+} between 2s-responders and 2s-non-responders as the transient in 2s-responders was at or above 325 nM Ca^{2+} for 13.4 ± 2.5 s (n = 20), compared to 7.00 ± 2.2 s (n = 14) in 2s-non-responders ($p < 0.01$, Fig 11B). This separation was further increased in Na^+ free bath. Since the 2s-non-responders became responders with a 4 s high K^+ application, we repeated this analysis for 2s-non-responder comparing the response to 2 s and 4 s high K^+ applications to determine if the "threshold" of NCX activation was comparable in this group of neurons to that of the 2s responders (Fig 11C). An $[Ca^{2+}]_i$ at or above 325 nM was again the separation point for the amplitude-duration plots (which increased from 4.0 ± 0.9 s to 12.0 ± 2.9 s (n = 10) with 2 and 4 s of high K^+, respectively). This separation was again further augmented in the presence of Na^+ free bath. Both sets of data suggest that NCX activity may be evoked in putative nociceptive cutaneous neurons with Ca^{2+} transients ≥ 325 nM for a duration of ≥ 12 s.

In our initial analysis of the 2 s high K^+ data set, we identified a subset of 2s-responsders (8/20) that had evoked Ca^{2+} transients in normal bath solution with parameters comparable to those of 2s-non-responders (i.e., note the overlap in the scatter plot in Figure 10F). However, the resting $[Ca^{2+}]_i$ appeared to be the unique feature in this group of 2s-responders as it was increased following application of Li^+ bath (Figure 11D). Pooled data indicate that this increase

in resting $[Ca^{2+}]_i$ was significantly ($p < 0.01$) greater than changes observed in the other 2s-responder or 2s-non-responders (Fig 11E). In this "Li^+ recruited" group of neurons, the evoked transient amplitude-duration plot again revealed a significant increase in the duration of the transient at or above 325 nM Ca^{2+} in the presence of Li^+ (Figure 11F). In these Li^+ recruited neurons, the 2 s-evoked Ca^{2+} transient resembled a "non-responder", such that it did not fulfill the amplitude-duration criteria that appears to be necessary to engage NCX activity. However, the Li^+-induced increase in $[Ca^{2+}]_i$ enabled a 2 s depolarization to engage NCX. This group of neurons provided the first evidence of two modes of NCX activity: one evoked in response to relatively large and long-lasting Ca^{2+} transients and a second in which a resting activity contributes to the maintenance of the baseline or resting $[Ca^{2+}]_i$.

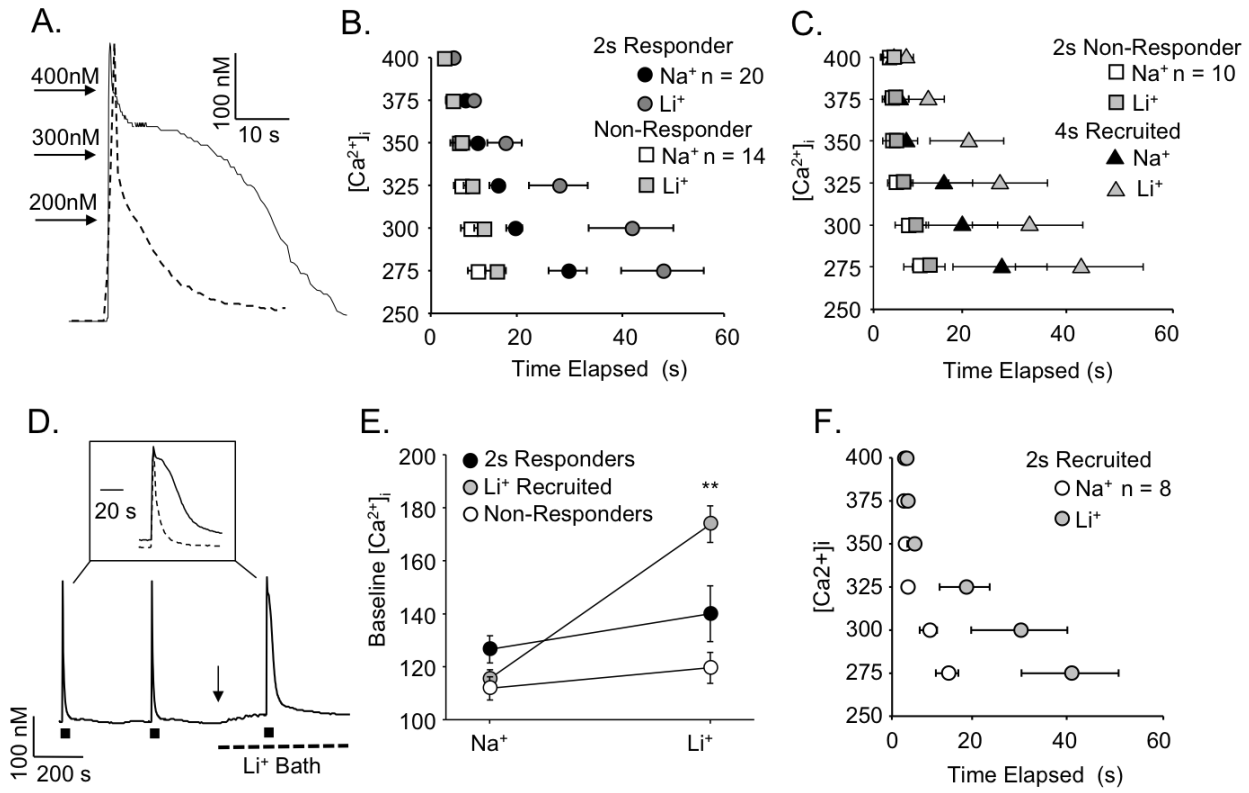

Figure 11: Ca^{2+} transient parameters associated with evoked NCX activity.

A) High K^+ evoked Ca^{2+} transients from an IB4+ (solid trace) and an IB4- (dashed trace) cutaneous DRG neuron, in which bins used to determine the transient amplitude-duration relationship for each neuron are illustrated. **B**) Pooled transient amplitude-duration (time elapsed at or above an $[Ca^{2+}]_i$) data for the 2s-Responders and 2s-Non-Responders analyzed in Figure 2 E and F, where transient duration data before and after Li^+ application are plotted. **C**) Data for the 2s-Non-Responders in B (in response to the 2 s high K^+ application) are replotted along with the average amplitude-duration data for these neurons in response to the 4 s high K^+ application, before (Na^+) and after (Li^+) NCX block. **D**) Evoked NCX activity was detected in a third subset of neurons in which application if Li^+ resulted in an increase in resting $[Ca^{2+}]_i$ (arrow). Inset: Evoked Ca^{2+} transients before (dashed line) and after (solid line) NCX block. **E**) Pooled data demonstrating the significant shift increase in resting $[Ca^{2+}]_i$ with application of Li^+ in a subset of neurons ($p < 0.01$, $n = 8$) in which evoked NCX activity was subsequently detected. **F**) Pooled amplitude-duration data for the subset of neurons in which the Li^+ induced increase in resting $[Ca^{2+}]_i$ resulted in the recruitment of evoked NCX activity.

We next sought to determine whether NCX activity persists once activated, and if so, for how long. We assumed that, as with PMCA, which appears to be constitutively active in sensory neurons to counter what appears to be a persistent Ca^{2+} leak (Rigaud et al., 2009), inhibition of NCX would result in an increase in $[Ca^{2+}]_i$. We could then monitor the duration of NCX activity following high K^+ application with brief (60 sec) applications of Li^+ to temporally inactivate NCX if present (Figure 12A). Li^+ bath was applied before and at 5 min intervals after two consecutive high K^+-induced transients until Li^+ application resulted in no change in $[Ca^{2+}]_i$. This protocol revealed two subsets of neurons: those with a Li^+-induced increase in $[Ca^{2+}]_i$ prior to 4s depolarization (Resting NCX activity n = 14) and those without (n = 24). Furthermore, within the no resting NCX activity subset, there was a group of neurons (14/24) in which the evoked NCX activity recovered relatively rapidly so that Li^+ challenge before and after the high K^+-evoked transient resulted in no change in $[Ca^{2+}]_i$. The remaining neurons in the no resting activity subset (10/24), appeared to have evoked NCX activity that persisted well beyond full recovery to baseline $[Ca^{2+}]_i$ levels so that Li^+-evoked transients were detectable for up to 10 min after the 4 s stimulus (Figure 4A and B). Within the subset of neurons with resting NCX activity, there as a group of neurons (9/14) in which evoked NCX activity appeared to recover rapidly: a Li^+-evoked Ca^{2+} transient was clearly detectable prior to high K^+ challenge, but there was no change in the magnitude of the Li^+-evoked transient after the 4 s stimulus (Figure 12B). Finally, in the remaining neurons in the subset with resting NCX activity (5/14), there was evidence of both resting NCX activity (i.e., a Li^+ transient prior to high K^+ challenge) and persistent evoked activity in which there was an increase in the magnitude of the Li^+-evoked transient after the 4 s stimulus (Figure 12A and B). Analysis of the resting $[Ca^{2+}]_i$ in these four subpopulations of neurons indicated that resting NCX activity was present in neurons with baseline $[Ca^{2+}]_i > 150$

nM (Figure 12C). Interestingly, despite the fact that the Li^+-evoked transients were no longer detectable 15 min after high K^+ challenge in neurons in which evoked NCX activity appeared to persist (Figure 4B), there was no evidence of recovery of resting $[Ca^{2+}]_i$ to baseline levels in this subpopulation (Figure 12C). Similarly, there was no significant increase in resting $[Ca^{2+}]_i$ in neurons with resting NCX activity in which there appeared to be a persistent evoked NCX activity. Taken together, these data lend further support to the suggestion that there are at least two distinct pools of NCX in putative nociceptive sensory neurons.

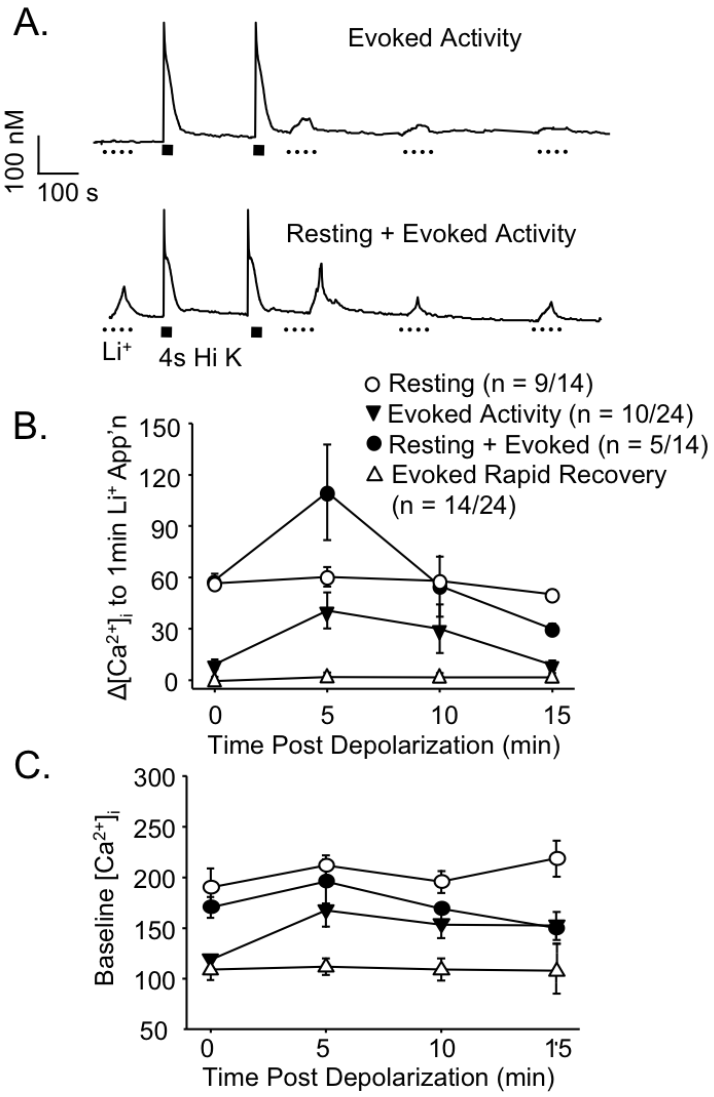

Figure 12: Characterization of "Resting" NCX activity in putative nociceptive cutaneous DRG neurons. **A**) Examples of neurons in which Ca^{2+} transients were evoked with Li^+. In one neuron (Top Trace), Li^+ (1 min) evoked transients were only detected after stimulating the neuron with high K^+ and the amplitude of these transients decayed over time. In the second (Bottom Trace), Li^+ evoked transients were evoked before and after stimulating the neuron with high K^+. In this neuron, the amplitude of the Li^+ evoked transient increased following high K^+ stimulation, but decayed to baseline levels over time. **B**) The amplitude of the Li^+ evoked transient in 4 types of putative nociceptive cutaneous DRG neurons are plotted as a function of time relative to high K^+ stimulation as illustrated in A, where 0 is before and 15 indicates 15 min after high K^+-induced depolarization. **C**) Resting $[Ca^{2+}]_i$ data for the four groups of neurons plotted in B, where resting $[Ca^{2+}]_i$ was determined 10 sec prior to Li^+ application.

3.4.3 NCX expression in isolated cutaneous sensory neurons

The results of our biophysical characterization of NCX activity in putative nociceptive cutaneous neurons suggested that there is considerable heterogeneity in the properties of NCX both within and between putative nociceptive cutaneous neurons. Because of evidence suggesting that NCX isoforms have different properties (Thurneysen et al., 2002b, Jeon et al., 2003, Molinaro et al., 2011), we next sought to determine whether the heterogeneity in functional properties might be due, at least in part, to a differential expression of NCX isoforms. PCR analysis of NCX isoform expression of mRNA extracted for whole DRG indicated that not only are all three isoforms expressed in DRG, but at least two splice variants of NCX1 and NCX3 were detectable as well (Figure 13). To confirm NCX expression in putative nociceptive neurons, single cell PCR analysis was performed. Results of this analysis indicated that mRNA encoding all 3 NCX isoforms is present in the vast majority of DRG neurons from L4/L5 DRG (Figure 13) including two splice variants of NCX1 and two of the three splice variants of NCX3.

Table 2: Fully nested NCX PCR primers for single cell PCR

Target	Gene	Position	Start	Sequence
NCX1	NM_001270778.1	**Outer**	**1771**	F: AGGGGAGGACTTTGAGGACA
			2075	R: TCCTCCTCCTCTTTGCTGGT
		Inner	**1779**	F: GGAGGACTTTGAGGACACCTG
			2068	R: TCCTCTTTGCTGGTCAGTGG
NCX2	NM_078619.1	**Outer**	**1954**	F: TTCTTGGGGAGAACTGTCGC
			2379	R: GCAAACGTGTCAGGGATGGA
		Inner	**2065**	F: CACTCATGGAGGGAGCAGTTT
			2270	R: AGGATGCAGACACCAAAGCA
NCX3	NM_078620.1	**Outer**	**2681**	F: TGCCCTTGGTGAACCGAAAT
			3263	R: CATACACATCCTGCAGGGCA
		Inner	**2763**	F: ATGGAGGAAGAGGAGGCCAA
			3263	R: CATACACATCCTGCAGGGCA

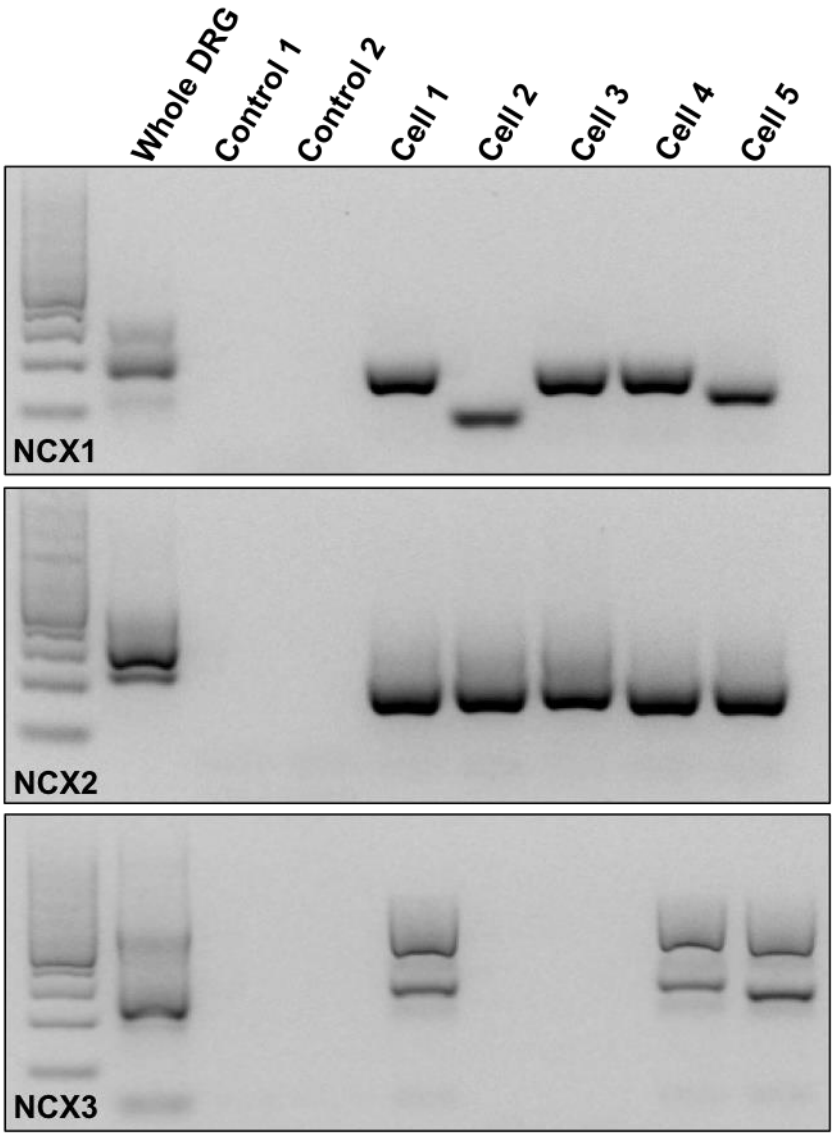

Figure 13: NCX isoform expression in DRG

RT-PCR was used to screen for the presence of NCX1, 2 and 3 in mRNA extracted from whole ganglia and isolated putative nociceptive cutaneous DRG neurons. Images of ethidium bromide stained agarose gel loaded with molecular weight marker (lane 1) and then as indicated where Control 1 is a no-cell control and Control 2 is a single neuron in which no reverse transcriptase was included in the reverse transcriptase reaction prior to PCR amplification, and Cells 1 – 5 are products from single putative nociceptive cutaneous DRG neurons.

Because the presence of mRNA does not necessarily indicate the presence of functional protein, we next sought to determine which isoforms were functional within the isolated cell body. High K^+ was applied for 4 s to putative nociceptive cutaneous neurons before and after application of three different NCX inhibitors, KB-R7943, SEA0400, and SN-6 (Figure 14A). These inhibitors were chosen based on their relative selectivity for individual isoforms. In transfected fibroblasts, when NCX is functioning in the reverse mode, KB-R7943 has shown been to block NCX3 with a higher potency than NCX1 or 2, whereas SEA0400 and SN-6 have been shown to block NCX1 with higher potency than NCX2 and 3 (Iwamoto and Shigekawa, 1998, Watanabe et al., 2006). There is currently no commercially available NCX2 selective blocker. KB-R7943 produced a concentration-dependent increase in the duration of the high K^+-evoked transient (E_{max} = 107.25 ± 20.36 s; EC50 = 0.045 ± 0.01 μM, Figure 14B). The impact of KB-R7943 on the duration of the evoked Ca^{2+} transient appeared to be specific for NCX block as the application of KB-R7943 (100 nM) in the presence of Li^+ bath resulted in no further change in the duration of the evoked transient (-2.26 ± 1.58 %, n = 8). While 100 nM was not quite a saturating concentration of KB-R7943 in cutaneous putative nociceptive neurons, this concentration was used in subsequent experiments for two main reasons. First, because NCX blocker "selectivity" is concentration-dependent, we wanted to use a concentration that was likely to provide the best combination of block and selectivity based on results previously reported by Kuroda and colleagues (Kuroda et al., 2013). Second, we observed what appeared to be non-specific effects of all 3 blockers at concentrations >5 μM, as had been described by others (Iwamoto et al., 1996, Birinyi et al., 2005, Niu et al., 2007). Thus, we also sought to minimize the potential for non-specific actions of the blocker. To estimate the fraction of total NCX activity blocked by KB-R943, we compared the maximal increase in the decay of the

evoked Ca^{2+} transient to that produced by Na^{+} free block. At 100nM, KB-R7943 inhibited 67.4 ± 0.1 % of total NCX (Figure 14C). Neither SEA0400 nor SN-6 produced a detectable change in resting Ca^{2+} (Figure 14A) or the evoked (Figure 14B) Ca^{2+} transient at concentrations between 1 nM and 1 μM, at and above those thought to be specific for NCX1.

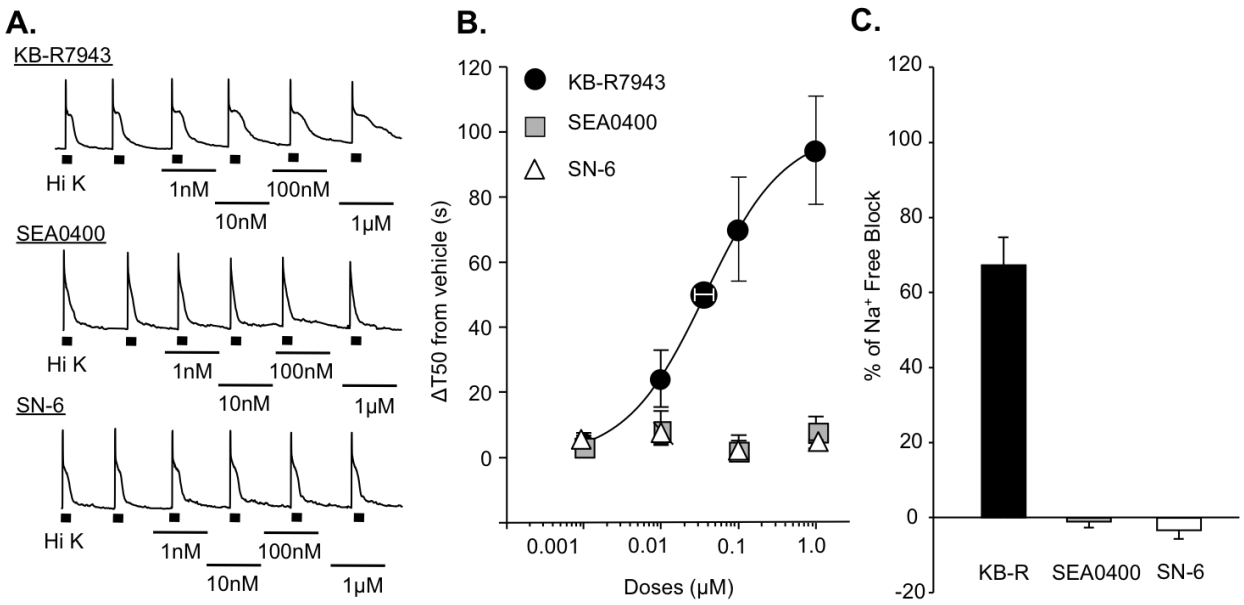

Figure 14: Pharmacological analysis of NCX activity in putative nociceptive cutaneous DRG neurons

A) Hi K^+ evoked Ca^{2+} transients in putative nociceptive cutaneous neurons before and in the presence of increasing concentrations of the NCX3 selective blocker KB-R7943 (Top trace), the NCX1 selective blocker SEA0400 (Middle trace), and a second NCX1 selective blocker SN-6 (Bottom trace). **B**) Pooled concentration-response data from neurons treated with KB-R7943 (n = 25), SEA0400 (n = 11) or SN-6 (n = 10). Data were analyzed as an increase in transient duration (T50) relative to the transient duration in the presence of vehicle. KB-R7943 data were well fitted with a Hill equation, yielding an Emax = 107.25 ± 20.36 s and EC50 = 0.045 ± 0.01 μM. **C**) The maximal change in transient duration in the presence of blocker was analyzed as a % of the total block of NCX activity represented by the maximal change in duration observed in Na^+ free bath, Data for each blocker was pooled and plotted.

Previous studies suggest that Li^+ bath activates NCX in the reverse mode (Annunziato et al., 2004). However, as suggested earlier, we attributed the change in baseline resting $[Ca^{2+}]_i$ with application of Li^+ bath (Figure 11D) to inhibition of resting NCX activity and a subsequent build-up of Ca^{2+} from a persistent Ca^{2+} leak. In support of this hypothesis, application of 100 nM KB-R7943 also resulted in a $\geq$ 20 % increase in baseline resting $[Ca^{2+}]_i$ ($\Delta[Ca^{2+}]_i$ = 31.16 ± 4.8 nM) in 15 of the 29 neurons tested (Figure 15).

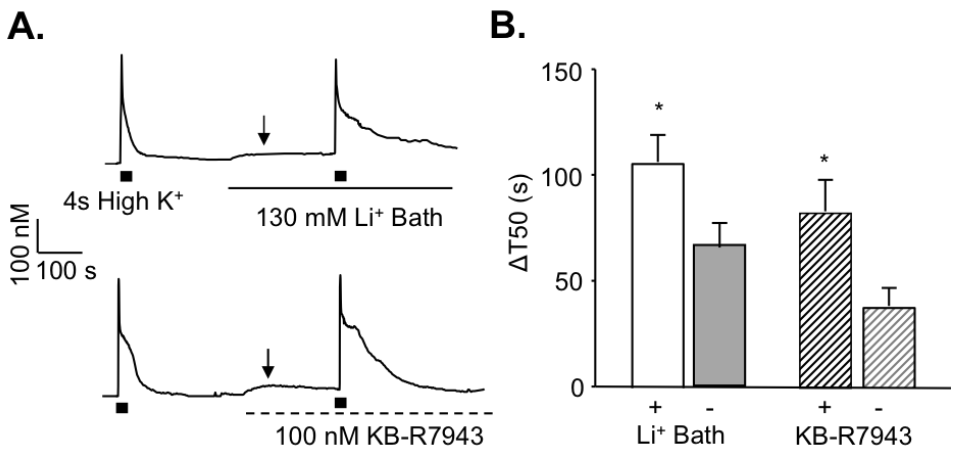

Figure 15: NCX contributes to the regulation of resting $[Ca^{2+}]_i$ in a subpopulation of putative nociceptive cutaneous neurons.

A. Examples of neurons in which application of Li^+ Bath (Top Trace) or KB-R7943 (Bottom Trace) resulted in an increase in resting $[Ca^{2+}]_i$ (Indicated by arrow). **B**. Pooled change in T50 (ΔT50) data, calculated as the difference between the T50 in the presence of NCX block and the baseline response, for neurons in which NCX was blocked with Li^+ bath (Li^+ Bath) or KB-R7943 (100 nM). Data for each group of neurons was separated according to whether NCX block was associated with an increase in resting $[Ca^{2+}]_i$ (+, n = 14 and 15 for Li^+ and KB-R7943 groups, respectively), relative to those in which there was no detectable change in resting $[Ca^{2+}]_i$ associated with NCX block (-, n = 24 and 14 for Li^+ and KB-R7943 groups, respectively) following NCX block. * is $p < 0.05$.

To further assess the relative contribution of NCX isoforms to resting and evoked NCX activity, we used siRNA to selectively knock down expression of each isoform. Targeted or control siRNA was injected into the sciatic nerve 6 days prior to the harvest and dissociation of DRG neurons for assessment of NCX activity. The extent of the knockdown was estimated using western blot analysis of the sciatic nerve (Figure 16A). A single intraneural injection of targeted siRNA resulted in a decrease in NCX protein of 57.44 ± 3.36%. Importantly, Western blot analysis confirmed the specificity of each siRNA construct, where the only significant change in each isoform was in response to the appropriately targeted siRNA (Figure 16A). Consistent with results obtained with SEA0400 and SN-6, NCX1 knockdown was associated with no detectable changes in resting or evoked Ca^{2+} transients, or in the changes observed in response to Na^{+} free bath or 100nM KB-R7943 application (T50 = 100.55 ± 11.8 s and 65.9 ± 12.1 s respectively) compared to the effect of NCX inhibition in neurons from naïve or control-targeted siRNA-treated rats (Figure 16B). Results with NCX3 knockdown were also consistent with pharmacological results, where, in contrast to NCX1 siRNA-treated rats, evidence of evoked NCX activity in putative nociceptive cutaneous neurons was significantly attenuated (Figure 16B). NCX3 knockdown was also associated with a significant suppression of the effects of 100nM KB-R7943 (Figure 16B). Strikingly, in contrast to assumptions made about the concentration-dependent specificity of inhibitors, there was a significant suppression of the increase in T50 associated with both Li^{+} bath and KB-R7943 in neurons from NCX2 siRNA-treated rats (Figure 16B).

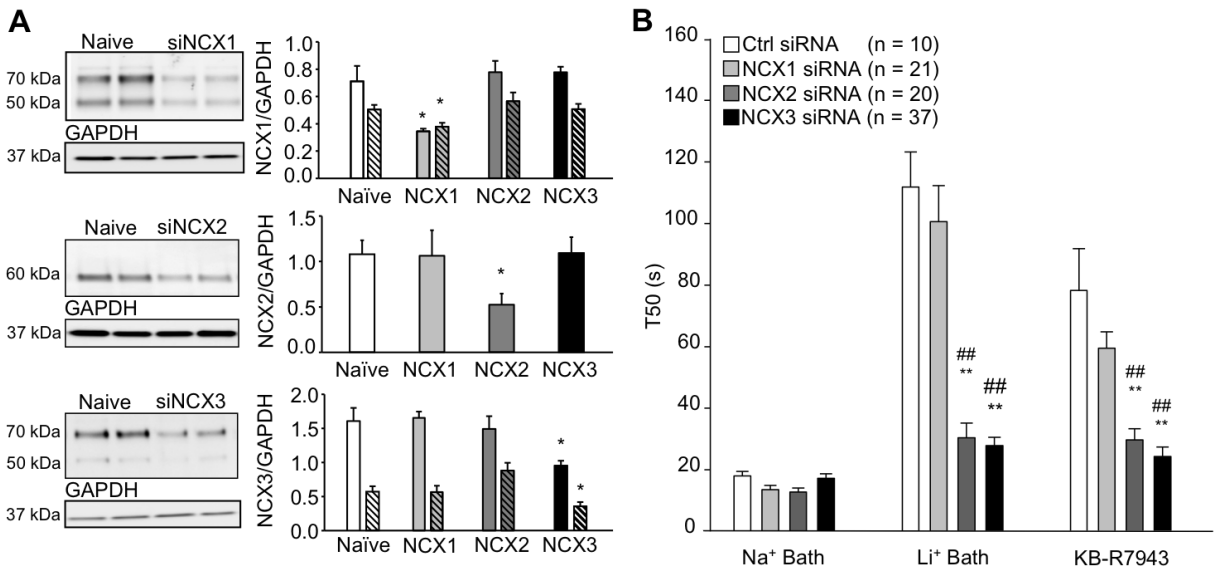

Figure 16: Targeted siRNA knockdown of NCX isoforms on high K^+-evoked Ca^{2+}-transients in cutaneous neurons. **A**) Western blot analysis of protein extracted from the sciatic nerve proximal to the site of siRNA injection was used to quantify the extent of the knock down 6 days after siRNA treatment. Typical blots from animals treated with siRNA targeted to NCX1, 2 and 3. Pooled data from 4 animals per condition demonstrate specificity of siRNA sequences, where relative density of each isoform is plotted for tissue obtained under 4 conditions: naïve, NCX1-siRNA, NCX2-siRNA, and NCX3-siRNA treated. Antibodies for NCX1 and NCX3 detected multiple bands and all were quantified. Solid bars represent pooled data for higher molecular weight (70kDa) band and hatched bars represent pooled data for lower molecular weight (50 kDa) band. Data were normalized with respect to GAPDH and plotted. **B**) Pooled high K^+-evoked transient duration (T50) data for neurons from control and NCX isoform targeted siRNA treated rats, before (Na^+ bath) and after block of NCX with Na^+ free (Li+ Bath) or KB-R7943 (100 nM). ** $p < 0.01$ relative to control siRNA treated and ## $p < 0.01$ relative to NCX1 siRNA treated.

3.4.4 Differential distribution of NCX isoforms within sensory tissues

The presence of mRNA encoding all three NCX isoforms in sensory neurons and in the face of evidence that only NCX3 and/or both NCX2 and NCX3 are functional in the sensory neuron cell body raises the possibility that NCX isoforms are differentially distributed within sensory neurons. To begin to address this possibility, we assessed the relative protein density of NCX isoforms in the spinal cord, dorsal root, DRG, and sciatic nerve (Figure 17). Consistent with the literature (Schulze et al., 2002, Quednau et al., 2004), antibodies for NCX1 (Figure 17A) and NCX3 (Figure 17C) detected multiple bands. Only the most robust bands were quantified across tissues. Consistent with the functional data showing dominant activity from NCX3, NCX3-like immunreactivity (LI) was greatest in the DRG and sciatic nerve relative to the spinal cord suggesting trafficking of NCX3 towards the periphery. In contrast, there was substantially more NCX1-LI in the spinal cord (n = 4) compared to peripheral tissues. NCX2 (Figure 17B) appeared to be equally distributed among peripheral tissues, but only weakly expressed in the spinal cord.

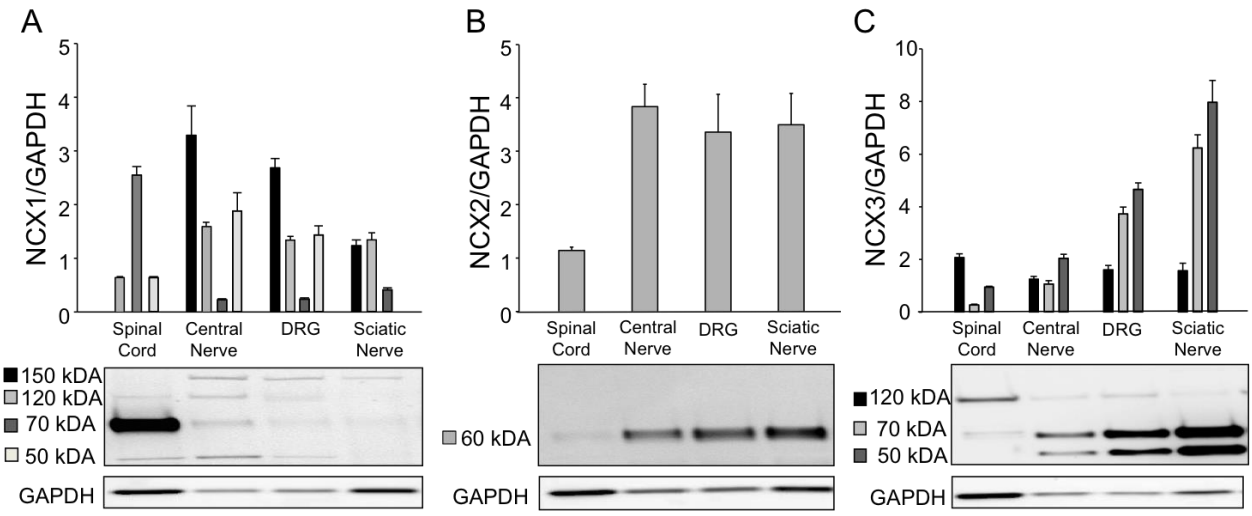

Figure 17: Distribution of NCX isoform-like immunoreactivity (LI)

Protein extracted from spinal cord, central segment of the sensory nerve, DRG and sciatic nerve. Pooled data (n = 4) and representative blots demonstrating the relative density of expression of NCX1 (A), NCX2 (B), and NCX3 (C) in spinal cord, central nerve, DRG, and sciatic nerve tissues. Band intensity at each molecular weight was normalized to that for GAPDH. For the representative blots different protein amounts were loaded in each lane to facilitate visualization of the bands in each tissue type.

3.4.5 NCX plays a limited role in the regulation of primary afferent excitability

NCX activity may influence excitability directly and/or indirectly. Because the exchanger is electrogenic, a direct influence of NCX on excitability would be through depolarizing inward Na^+ current associated with exchanger activity in forward mode. The most proximal indirect influence of NCX activity on excitability would be via an influence on $[Ca^{2+}]_i$, which may influence the activity of other ion channels. We therefore sought to assess the impact of NCX activity on the excitability of putative nociceptive cutaneous DRG neurons. To minimize the impact of recording on the regulation of intracellular Ca^{2+} and consequently, NCX activity, we used gramicidin perforated-patch to obtain whole cell access for current clamp recording. Neurons were first loaded with Fura-2 AM to enable simultaneous recording of membrane potential and $[Ca^{2+}]_i$. The impact of NCX on the excitability was assessed with direct current injection protocols designed to enable determination of AP threshold, rheobase, and the response to suprathreshold stimuli (2x and 3x rheobase) in which each parameter was assessed under 4 different conditions: in the absence and presence of Li^+ bath, and before and after activating NCX with a 4 s voltage-step to 0 mV to drive an increase in $[Ca^{2+}]_i$. The Ca^{2+} transient evoked with a voltage step was comparable to that evoked with a 4 s application of high K^+ (the peak magnitude was 467.77 ± 23.3 nM and T50 of decay was 24.57 ± 6.5 s (n = 9)). Furthermore, as evidence that this Ca^{2+} transient was sufficient to activate NCX, block of NCX with Li^+ resulted in a 276.96 ± 75% increase in T50 of the depolarization-evoked transient. Excitability data under each of these four experimental conditions are summarized in Table 2 and Figure 18 (A-C). Analyzing excitability data with a two-way ANOVA revealed a main effect associated with NCX activation (depolarization) on rheobase ($p < 0.05$; Figure 18A) and the response to

suprathreshold stimulation ($p < 0.05$; Figure 18C). However, there was no significant effect of NCX block (Li^+ bath) on these parameters, nor was there an interaction between depolarization and Li^+ bath ($p > 0.05$). There was, however, a significant ($p < 0.05$) main effect of Li^+ bath on action potential threshold (Figure 18B), but no significant influence of depolarization, or an interaction between depolarization and Li^+ bath, on this parameter. Comparable analysis of passive and active electrophysiological properties (Table 2) revealed a main effect of Li^+ bath on resting membrane potential (RMP), and AP overshoot. Additionally there was a main effect of depolarization on afterhyperpolarization (AHP) and AP overshoot (Table 2). However, there was no interaction between depolarization and Li^+ bath on any parameter assessed.

Table 3: Changes in passive and active electrophysiological properties with NCX inhibition

	Baseline		Depolarization-induced Activity	
	Na^+ Bath	Li^+ Bath	Na^+ Bath	Li^+ Bath
Diameter (μM)	23.74 ± 1.3			
RMP (mV)	-67.47 ± 2.0	-61.67 ± 1.6	-70.14 ± 2.5	-63.50 ± 3.0
Rin (mΩ)	1143.06 ± 179.2	1050.40 ± 333.6	603.70 ± 180.4	445.08 ± 42.6
AP Overshoot	50.54 ± 1.6	47.11 ± 2.1	42.18 ± 1.6	35.35 ± 2.5
AP Duration (ms)	3.02 ± 0.3	2.72 ± 0.03	2.61 ± 0.2	2.67 ± 0.2
AHP Magnitude (mV)	21.56 ± 0.7	20.47 ± 1.9	18.74 ± 1.1	15.97 ± 2.1
AHP τ Decay (ms)	70.90 ± 7.4	54.40 ± 8.5	48.90 ± 6.5	38.24 ± 9.5

Values are expressed as means ± SE. Depolarization consisted of a 4 s voltage step from -60 mV to 0 mV. Na^+ Bath values were collected in the presence of Na^+ in the bath solution. Li^+ Bath values were collected in the absence of Na^+ and presence of Li^+ in the bath solution. RMP, resting membrane potential; Rin, input resistance; AP, action potential; AHP, afterhyperpolarization; τ, time constant. Data were analyzed with a two-way ANOVA to assess the impact of NCX block (with Li^+ Bath) and depolarization-induced activation of NCX (Depolarization), or the interaction between the two. Results revealed a significant influence of Li^+ Bath on both RMP ($p < 0.05$) and AP overshoot ($p < 0.05$), but no significant influence of Depolarization ($p > 0.05$) or a significant interaction between Li^+ Bath and Depolarization ($p > 0.05$). There was a main effect of Depolarization on AHP and AP overshoot ($p < 0.05$) but no significant impact of Li^+ Bath on these parameters ($p > 0.05$), or a significant interaction between Depolarization and Li^+ Bath ($p > 0.05$).

As a second measure of excitability, we assessed following frequency of neurons in the presence or absence of Li^+ bath. Following frequency was assessed with a train of 20 depolarizing current injections (1 ms at 1.5 x current threshold) delivered at 10, 20 and 40 Hz. It was not necessary to use the 4 s depolarization protocol for this measure, as a 20 Hz stimulus was able to evoke a Ca^{2+} transient (Figure 18D (peak magnitude was 412.66 ± 23.1 nM and T50 of decay was 22.33 ± 5.5 s)) similar to a 4 s high-K^+-evoked transient ($p > 0.05$). Furthermore, a 20 Hz stimulus was sufficient to evoke NCX activity as indicated by the impact of Li^+ which resulted in a significant 254.30 ± 84.3 % increase in the T50 of decay (Figure 18E).

Current threshold was determined for each neuron in the presence and absence of Li^+ for a 1 ms depolarizing current step in a manner identical to that used for determination of rheobase. Li^+ bath was associated with a 16.59 ± 4.7 % increase in the amount of current necessary to evoke an AP relative to that in Na+ bath ($p < 0.05$, data not shown). Nevertheless, there was no detectable influence of Li^+ on the following frequency at 10 and 20 Hz stimulation. However, at 40Hz, there was a significant increase in the failure rate following NCX block from 5.0 ± 2.5% to 38.1 ± 6.0% (Figure 18F, $p < 0.01$, paired t-test).

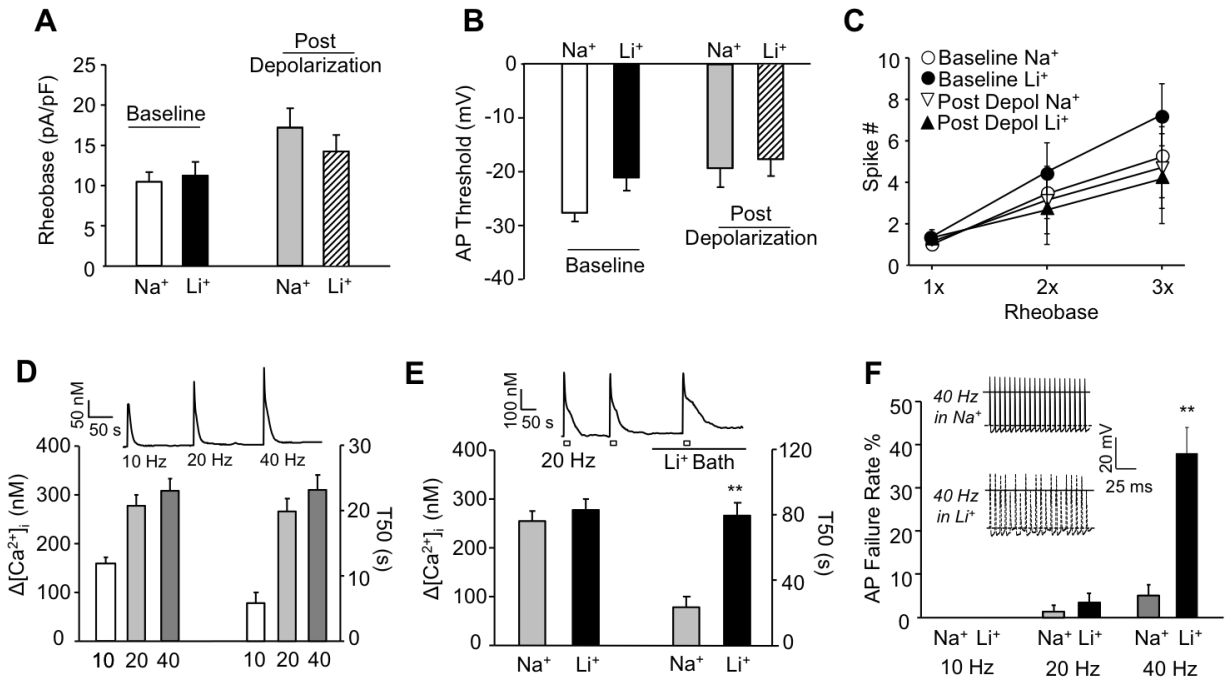

Figure 18: The impact of NCX on the excitability of putative nociceptive cutaneous DRG neurons

Using gramicidin-perforated patch configuration, excitability was assessed with a square-wave current injection as described in methods to enable determination of rheobase (**A**), action potential threshold (**B**), and the response to suprathreshold current injection (at 2 and 3x rheobase) (**C**). Excitability was assessed for each neuron (n = 6) before (Na^+) and after (Li^+) NCX block under resting $[Ca^{2+}]_i$ (Baseline) and after a depolarization (4 s to 0 mV)-induced increase in $[Ca^{2+}]_i$. The impact of depolarization was significant ($p < 0.05$, two-way ANOVA) on both rheobase and AP threshold (i.e., decrease in excitability). However, there was no significant ($p > 0.05$) effect of NCX block on these parameters, nor was there a significant ($p > 0.05$) interaction between depolarization and NCX block. **D**) Representative Ca^{2+} trace (inset) and pooled data showing average magnitude ($[Ca^{2+}]_i$) and decay (T50) of Ca^{2+} transients evoked with 20 pulses of depolarizing current injection delivered at 10, 20, 40 Hz. **E**) Representative Ca^{2+} trace (inset) and pooled data (n = 8) for the change in the magnitude ($\Delta[Ca^{2+}]_i$) and duration of the Ca^{2+} transient evoked with 20 pulses of depolarizing current injection delivered at 20 Hz before (Na^+) and after (Li^+) block of NCX. There was a significant ($p < 0.01$) interaction between stimulation frequency and NCX block on the duration of the evoked transient, where post-hoc analysis indicated that the increase in duration for both the 20 Hz and 40 Hz (not shown), but not the 10 Hz stimulation frequency (not shown), were significant. **F**) The 20 pulse current injection protocol was used to assess following frequency. Inset: Typical voltage traces of a neuron stimulated at 40

Hz before (in Na^+) and after (in Li^+) block of NCX. Pooled following frequency data (n = 8), where the failure rate (# of failed action potentials/train of 20 stimuli) before (Na^+) and after (Li^+) block of NCX is plotted for stimulation frequencies of at 10, 20, and 40 Hz. There was a significant ($p < 0.01$, two-way ANOVA) interaction between stimulation frequency and NCX block on the failure rate, where post-hoc analysis confirmed the increase in failure rate observed at 40 Hz was significant. ** is $p < 0.01$.

3.4.6 Compound action potentials and NCX activity

Given recent evidence suggesting that NCX functioning in reverse-mode contributes to axon damage in small fiber peripheral neuropathy (Persson *et al.*, 2013), we next sought to determine whether the NCX protein observed in the peripheral nerve might be functional in the absence of tissue injury. To do this, compound action potential (CAP) recording was performed on isolated sciatic nerves in the presence and absence of Li^+ or 100 nM KB-R7943. The CAP was evoked at 0.1 Hz to assess "resting" NCX activity and following 100 pulses at 5 Hz and 2x the intensity required to evoke a maximal C-wave, to assess "evoked" NCX activity (Figure 19A). Li^+ bath had no significant effect on the AUC (a measure of the number of fibers contributing to the CAP) or conduction velocity (CV) of the CAP A-wave (0.36 ± 1.6% and 1.91 ± 0.8 % of baseline, respectively). Similarly, at 0.1 Hz stimulation, neither Li^+ nor KB-R7943 had a significant influence on the AUC of the CAP C-wave. However, the application of KB-R7942 (Figure 11A), but not Li^+, resulted in a significant increase (20.31 ± 5.3 %, $p < 0.05$, n = 7) in the CV of the C-wave (C-CAP) (Figure 19B). Five Hz stimulation, used to assess "evoked activity," resulted in a decrease in CV in the CAP C-wave. This decrease was significantly ($p < 0.05$)

attenuated in Li^+ bath (Figure 19C). KB-R7943 further reduced the activity-dependent decrease in CV such that there was no net change in CV in the presence of KB-R7943 at 5Hz stimulation. Control nerves sampled every 10 min for 1 hour (Na^+ bar, Figure 19B) showed very little change in CV with time (0.78 + 4.25 %). Because the impact of KB-R7943 on CV was roughly comparable at 0.1 and 5 Hz, we performed an additional experiment to determine whether the NCX contribution to the regulation of CV was already saturated at 0.1 Hz stimulation. Two nerves were stimulated at 0.017 Hz before and after Li^+ application. With this frequency of stimulation, Li^+ bath resulted in a 24.88% decrease in CV (data not shown).

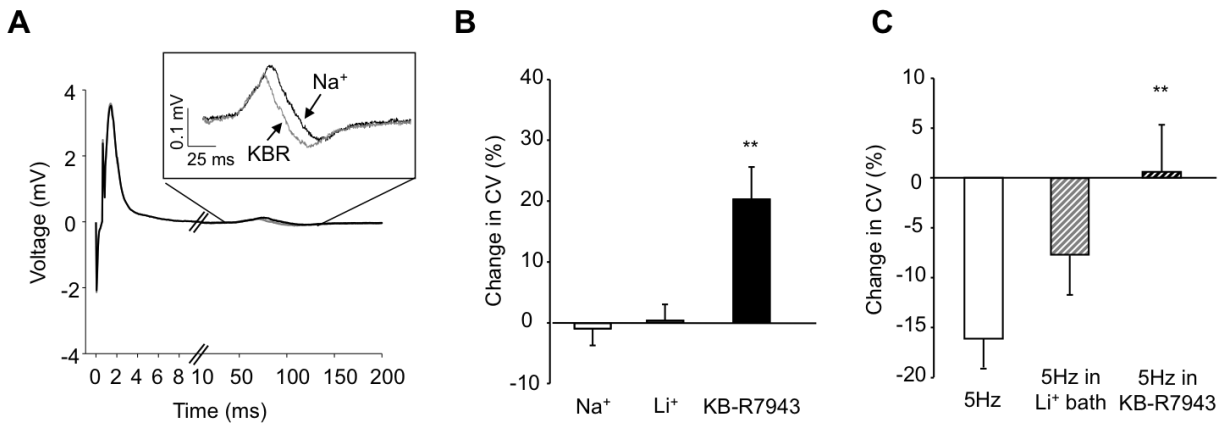

Figure 19: Impact of NCX on the compound action potential (CAP) in the sciatic nerve

A) Compound action potentials were evoked in the sciatic nerve before (black trace) and after (grey trace) block of NCX with Li^+. The sciatic nerve is long enough that the A- and C-waves are easily distinguished. Inset: C-wave re-plotted on a more appropriate scale. **B**) No changes in the A-wave or the area of the C-wave were detected. However, there appeared to be an increase in the conduction velocity of the C-wave following block of NCX. Pooled data analyzed as a percent change from baseline were analyzed over time (Na^+) relative to that associated with NCX block with Li^+ bath (Li^+) or KB-R79423 (100 nM). Control nerves were sampled every 10 min for 1 hour (Na^+ bar). **C**) Pooled data indicating that 5 Hz stimulation resulted in activity-dependent slowing of the nerve, which was significantly attenuated in the presence of Li^+ (n = 6) and 100 nM KB-R7943 (n = 6). * is $p<0.05$ and ** is $p < 0.01$.

3.4.7 Loss of NCX3 in IB4+ fibers decreases nociceptive thresholds

The restricted distribution of NCX activity in putative nociceptive cutaneous afferents suggests that this exchanger may play a particularly important role in nociceptive processing. Therefore, as a final test of NCX function, we assessed the impact of targeted siRNA knock down of NCX isoforms on nociceptive threshold. A single intrasciatic nerve injection of targeted or control siRNA was used to knock down NCX in the afferents innervating the glabrous skin of the hindpaw. Changes in mechanical nociceptive threshold were assessed with an electronic von Frey and changes in thermal nociceptive threshold were assessed with a Hargreaves apparatus. The extent of NCX knockdown was assessed with Western blot as shown in Figure 15. Interestingly, knockdown of NCX3, but not NCX1 of NCX2 resulted in a significant reduction in both mechanical (Figure 20A) and thermal (Figure 20B) threshold. Changes in threshold were detectable at 5 days and returned to baseline levels by 10 days post siRNA injection. Western blot analysis at day 10 shows no change in protein compared to baseline levels (data not shown, $p > 0.05$) suggesting natural recovery from siRNA.

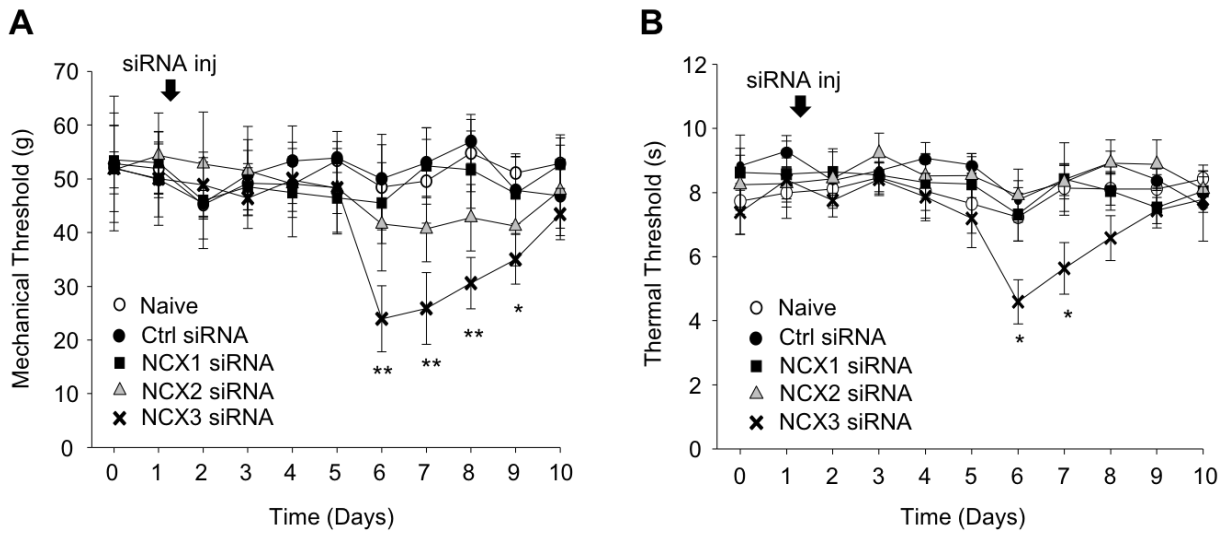

Figure 20: Nociceptive threshold changes in response to knockdown of NCX isoforms

A) Mechanical nociceptive threshold as determined with an electronic von Frey, was assessed once daily in naïve animals (n = 6) and in animals before and after a single sciatic nerve injection with control (n = 6) or targeted siRNA against NCX1 (n = 12), 2 (n = 12) or 3 (n = 18). B) Thermal nociceptive threshold was determined with a Hargreaves device in the same groups of animals. Knockdown was confirmed using Western blot analysis as indicated in Figure 7. (* $p < 0.05$ ** $p < 0.01$).

Lastly, we sought to determine if the significant reduction in both mechanical and thermal thresholds were due to loss of NCX3 in IB4+ fibers, based on our in vitro results indicating that NCX activity is only present IB4+ neurons. Using the cytotoxin, saporin, conjugated to IB4 (IB4/SAP) to specifically ablate the IB4+ fiber population (Vulchanova et al., 2001, Tarpley et al., 2004). We injected the sciatic nerve with a combination of the unconjugated or conjugated form of saporin (IB4/SAP) with either NCX3-targeted or control non-targeted siRNA. The co-injection of IB4/SAP and control-siRNA (IB4/SAP + Ctrl-siRNA) or NCX3-siRNA (IB4/SAP + NCX3-siRNA) significantly elevated mechanical (Figure 21A) and thermal

(Figure 21B) thresholds ($p < 0.05$, $n = 6$). Unconjugated saporin with control-siRNA (Unconj + Ctrl-siRNA) had no significant effect on nociceptive behavior compared to naïve animals ($p > 0.05$, $n = 6$). Unconjugated saporin co-injected with NCX3-siRNA (Unconj + NCX3-siRNA) resulted in decrease in both mechanical (Figure 21A) and thermal (Figure 21B) thresholds, consistent with NCX3-siRNA alone ($n = 6$). The change in nociceptive threshold over time was analyzed as an area under the curve (AUC) where data on day 0 was used to assess the change in threshold for each animal on days 0 through 10. The results confirms that there was no significant difference between IB4/SAP + Ctrl-siRNA and IB4/SAP + NCX3-siRNA (Figure 21C) suggesting that loss of IB4+ fibers attenuates the siRNA-induced hypersensitivity seen in the Unconj + NCX3-siRNA treated group. To confirm the loss of IB4 fibers following IB4/SAP treatment, we analyzed the pattern of IB4 staining in the spinal cord of IB4/SAP and control treated rats. Consistent with previous studies using IB4/SAP (Vulchanova et al., 2001, Tarpley et al., 2004), there was a dramatic decrease in IB4+ staining in the superficial dorsal horn of L4 and L5 spinal segments in rats treated with the conjugated saporin (IB4/SAP + Ctrl-siRNA and IB4/SAP + NCX3-siRNA) (Figure 21D). The loss of IB4 staining was restricted to the medial portion of the dorsal horn thought to be the zone of innervation of the sciatic nerve. No significant loss of IB4 staining was detected in those rats treated with the unconjugated saporin (Figure 21D).

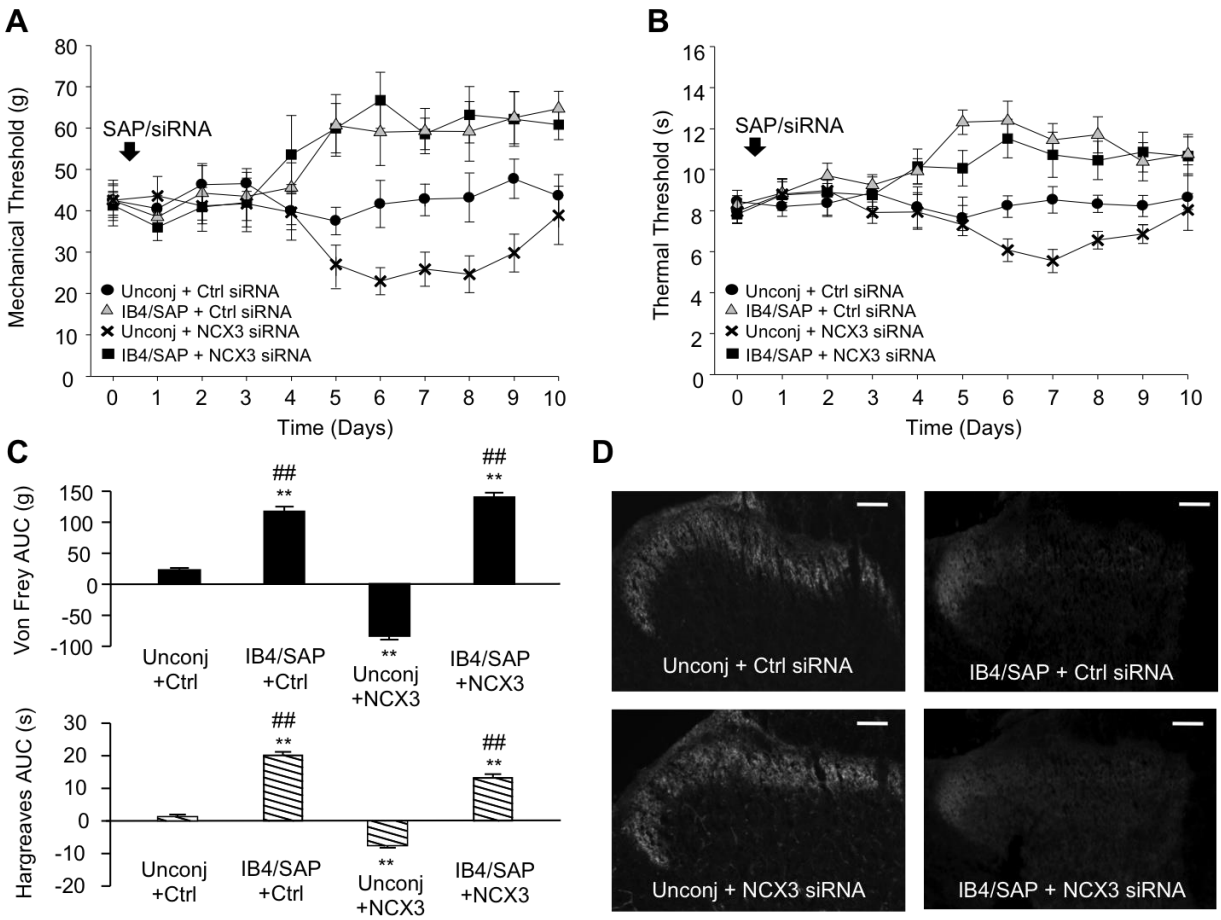

Figure 21: Assessment of the relative contribution of IB4+ fibers to the changes in nociceptive behavior associated with NCX3-targeted knockdown

The IB4+ population of sensory neurons in the sciatic nerve was ablated with an intra-sciatic injection of IB4 conjugated to the toxin, saporin (IB4/SAP). The control for this was an injection of unconjugated IB4 and saporin (Unconj). Groups of rats (n = 6 per group) received injections of either IB4/SAP or Unconj with either control siRNA (Ctrl) or NCX3-siRNA (NCX3). Mechanical (**A**) and thermal (**B**) nociceptive thresholds were determined as in Figure 11 before and after sciatic nerve injections. **C**) The change from baseline over time in each group was analyzed as an area under the curve (AUC) for both mechanical (top graph) and thermal (bottom graph) data. **D**) The extent of IB4 fiber ablation was assessed in spinal cord sections stained with IB4-FITC as described in Methods. Consistent with the termination pattern of afferents in the sciatic nerve, there is almost a complete loss of IB4 binding in the medial superficial dorsal horn of IB4/SAP treated animals. ** $p < 0.01$ relative to unconj + Ctrl and ## $p < 0.01$ relative to unconj + NCX3.

3.5 DISCUSSION

The purpose of this study was to characterize the biophysical properties of NCX among subpopulations of sensory neurons, identify the NCX isoform(s) underlying NCX activity, and to begin to determine the function of this exchanger in sensory neurons. We have confirmed our previous results indicating NCX activity is restricted to a subpopulation of putative nociceptive neurons, which extends to cutaneous neurons innervating the glabrous skin of the hindpaw. There appear to be two modes of NCX activity: one evoked in response to relatively large and long lasting (~325 nM for > 12 second) increases in $[Ca^{2+}]_i$, and a second that is active at resting $[Ca^{2+}]_i$ > ~150 nM. There also appeared to be two modes of evoked activity: one that decayed relatively rapidly (< 5 min) and a second that persisted (>10 min). While NCX activity was detected in all IB4+ small diameter cutaneous neurons, there was heterogeneity in this subpopulation of neurons with respect to the different modes of NCX activity present. Pharmacological data suggest that NCX3 accounts for ~70% of the NCX activity in sensory neurons with NCX2 accounting for the remaining 30%. Knockdown using targeted siRNA of NCX isoforms yielded results consistent with the pharmacological data, but suggested a larger role of NCX2. Additionally, mRNA encoding all three isoforms was detectable in putative nociceptive cutaneous neurons, with evidence for the differential distribution of splice variants of NCX1 and 3. Western blot analysis confirmed the presence of all three isoforms in sensory neuron and spinal cord tissue and they appeared to be differentially distributed among these tissues. While NCX appears to contribute to the regulation of resting $[Ca^{2+}]_i$ in a small subpopulation of neurons, it appears to play a much more dominant role in regulating the decay rate of evoked Ca^{2+} transients. Additionally, NCX appears to have a minor role in the regulation of neuronal excitability, where the only detectable influence was on the following frequency of

neurons at relatively high (40 Hz) rates of stimulation. We also obtained evidence of NCX activity in C-fiber axons, where block of the exchanger resulted in a small increase in conduction velocity. Furthermore, knockdown of NCX3 but not NCX1 or 2 resulted in a significant decrease in nociceptive threshold. Using IB4 conjugated to the toxin saporin, we obtained evidence consistent with the suggestion that the shift in nociceptive thresholds is due to the loss of NCX3 in the IB4+ fiber population. Together, these data show that NCX, most likely NCX3, plays an important role in the regulation of $[Ca^{2+}]_i$ within the primary sensory neurons.

3.5.1 Biophysical properties: Evoked activity

The primary approaches used to assess the presence of NCX activity in the first half of this study were largely indirect, inferred from changes in $[Ca^{2+}]_i$ secondary to the removal of extracellular Na^+ needed for exchange activity (Cook et al., 1998) or the application of NCX inhibitors. Li^+ was used in the majority of experiments as the replacement for Na^+ because it is voltage-gated Na^+ channel permeable (Hille, 1972, Gold and Thut, 2001b), and does not block the mitochondrial Na^+/Ca^{2+} exchanger (Palty et al., 2010). We acknowledge, however, that the use of Li^+ is potentially problematic for the assessment of NCX activity, particularly with the indirect approach used due to the variety of other proteins that may be affected and result in a secondary influence on $[Ca^{2+}]_i$ including other pumps (Tolkovsky and Richards, 1987, Hermans et al., 1997), exchangers (Herbert et al., 2004, Palty et al., 2010), and ion channels (Vaughn and Gold, 2010, Zhang et al., 2010b). Nevertheless, while there may have been off-target effects of Li^+ in these experiments, we propose that the Li^+-induced changes in resting and evoked Ca^{2+} transients were due predominantly to block of NCX, and therefore reflect NCX activity for two reasons. First, comparable changes in resting and evoked Ca^{2+} transients were observed with Li^+,

choline, and the relatively NCX-specific blocker, KB-R7943. Second, siRNA-induced knockdown of NCX occluded the Li^+-induced changes to the evoked Ca^{2+} transient.

In most tissues, NCX is considered a low affinity exchanger requiring a high $[Ca^{2+}]_i$ for activation. The present results were generally consistent with this model, where in putative nociceptive neurons, an increase in $[Ca^{2+}]_i$ to ~325 nM for at least 12 seconds was required to evoke NCX activity. That is, despite evidence that NCX was present and functional in all putative nociceptive neurons, NCX activity was only detected in these neurons if the evoked transient met this threshold. At first pass, it appeared paradoxical that the evoked transient in neurons, such as the 2s-responders, in which NCX had been activated, decayed more slowly than the 2s-non-responders in which NCX had not been activated. The implication of this observation is that 2s-responders are less able to handle large Ca^{2+} loads with other Ca^{2+} regulatory mechanisms, such that Ca^{2+} influx associated with the 2 s high K^+ application overwhelms the available buffering capacity, and NCX is engaged.

3.5.2 Biophysical properties: Resting activity

We were also able to detect resting NCX activity in 35% of the putative nociceptive neurons tested. There are at least two likely explanations for the presence of resting NCX activity in a subpopulation of sensory neurons. First, as suggested above for the persistent evoked activity, microdomains of elevated $[Ca^{2+}]_i$ above the threshold of activation could account for the presence of resting NCX activity in a subpopulation of neurons. Second, there is evidence that the Ca^{2+} affinity for NCX activation depends on splice variants within the intracellular loop that makes up two distinct Ca^{2+} binding domains (CBD1 and 2). The primary Ca^{2+} sensor responsible for Ca^{2+} activation, CBD1, has a higher affinity for binding (~ Kd = 100 – 600 nM) (Hilgemann

et al., 1992), whereas CBD2 has a low affinity for Ca^{2+} (~ Kd = 250 nM – 20 μM). Thus, a splice variant with only CBD1 may have activity at an $[Ca^{2+}]_i$ comparable to that observed in the present study. Similarly, a combination of CBD1 and CBD2 in some neurons may result in a pattern of NCX activity that requires a high $[Ca^{2+}]_i$ for full activity, as well as partial activity at considerably lower $[Ca^{2+}]_i$. Consistent with this suggestion, data from cardiomyocytes indicates that ~5% of the maximal NCX current is detected at resting $[Ca^{2+}]_i$ levels, whereas full activity requires a the rise of $[Ca^{2+}]_i$ to 1-2 μM (Boyman et al., 2011).

Our biophysical characterization of NCX as a low affinity exchanger is consistent with Verdru et al (1997) who found that removal of external Na^+ dramatically slowed the $[Ca^{2+}]_i$ decay in a subpopulation of DRG neurons in which the average peak was > 400 nM. Furthermore, they also detected a shift in baseline $[Ca^{2+}]_i$ with the block of NCX activity in 85% of the DRG neurons tested (Verdru et al., 1997). Shutov and colleagues found that inhibition of NCX in synaptic terminals resulted in a small but significant increase in $[Ca^{2+}]_i$ (Shutov et al., 2013) suggesting there is some resting NCX activity in the central terminals as well as the cell body. In contrast, others have failed to detect a significant contribution of NCX to the regulation of either resting or evoked Ca^{2+} (Thayer and Miller, 1990, Usachev et al., 2006, Gemes et al., 2012) leading the authors of these studies to conclude that NCX does not contribute to the regulation $[Ca^{2+}]_i$ in sensory neurons. We suggest, however, that the presence of NCX was likely missed in these previous studies because of the relatively small Ca^{2+} transients evoked (all less than 300 nM) and/or because of the relatively limited number of neurons in which NCX appears to function.

Another possible explanation for the presence of "resting" NCX activity is that it is actually NCX working in "reverse" mode where the exchanger is thought to extrude Na^+ in

exchange for an increase in $[Ca^{2+}]_i$. This was the suggested explanation for the small increase in resting $[Ca^{2+}]_i$ observed after removal of extracellular Na^+ in rat and mouse DRG (Duchen, 1990, Verdru et al., 1997). NCX exchange depends on the driving force on the exchanged ions defined as the difference between the membrane potential and the "equilibrium potential" for Na^+ and Ca^{2+} across the exchanger ($E_{Na/Ca}$). $E_{Na/Ca}$ is estimated by the Nernst potentials for the Na^+ and Ca^{2+} and the net flux of ions by the exchanger: three Na^+ in one direction for every one Ca^{2+} in the other (Fang et al., 1998). Under physiological conditions $E_{Na/Ca}$ is ~ -26 mV, resulting in a driving force that enables the exchanger to function in forward mode at membrane potentials more negative than -26 mV. Theoretically, with increases in intracellular Na^+, as may occur with high levels of neural activity, $E_{Na/Ca}$ may hyperpolarize to a potential less than the resting membrane potential. As a result, the driving force on the exchanger would enable it to function in reverse mode. By this reasoning, the Na^+ free bath used to assess the presence of resting NCX activity should result in an $E_{Na/Ca}$ that is very negative to the resting membrane potential, generating a tremendous driving force on the exchanger to work in reverse mode. However, there are at least three observations that argue against the possibility that NCX functioning in reverse mode accounts for the increase in $[Ca^{2+}]_i$ observed following application of Na^+ free bath. First, we failed to detect the evidence of resting NCX activity in the majority of putative nociceptive neurons tested despite evidence of functional NCX in all of these neurons. Second, we observed "resting activity" that was not only activated, but resolved in neurons with evidence of persistent evoked activity. Third, as shown in Figure 7, we detected an increase in $[Ca^{2+}]_i$ NCX specific blocker, KB-R7943 comparable to that observed in Na+ free bath. Thus, rather than NCX acting in reverse mode, we would suggest that the increase in $[Ca^{2+}]_i$ observed in the presence of 0 Na^+ bath or KB-R7943 is due to Ca^{2+} leak that is no longer being attenuated by the NCX activity in

forward mode. Nevertheless, conclusively ruling out the possibility of NCX functioning in reverse mode in sensory neurons will require more direct measurements of NCX function under conditions in which the concentrations of Na^+ and Ca^{2+} on either side of the membrane are better controlled.

3.5.3 Isoform(s) underlying NCX activity in the isolated neuron

We used complementary strategies to determine which isoforms contribute to resting and evoked NCX activity in sensory neurons. Consistent with the suggestion that differential expression of the three NCX isoforms accounts for the heterogeneity in the biophysical properties of NCX in sensory neurons, pharmacological analysis of NCX suggested that NCX2 and 3 contributed to both resting and evoked NCX activity. Also consistent with this finding, PCR analysis indicated the presence of mRNA encoding both NCX2 and NCX3 in putative nociceptive sensory neurons and our siRNA data indicating that knock down of NCX2 or 3 was sufficient to occlude the actions of 0 Na^+ bath.

Contrary to our PCR analysis suggesting NCX1 mRNA is expressed in putative nociceptive neurons, we failed to detect evidence of NCX1 activity in the isolated sensory neuron cell body with the relatively selective NCX1 selective blocker SEA0400 (Iwamoto and Shigekawa, 1998) or with siRNA-induced knockdown of NCX1. This was even more surprising in light of evidence that NCX1 appears to be ubiquitous with splice variants found in brain, heart, kidney, and pancreas (Philipson et al., 1993). And while incomplete knockdown could explain the negative results with NCX1 targeted siRNA, inhibition of $[Na^+]_i$-dependent $^{45}Ca^{2+}$ uptake (i.e. reverse mode) in fibroblasts (Iwamoto and Shigekawa, 1998) suggests that the concentration of SEA0400 used here should have been sufficient to enable detection of NCX1

activity in sensory neurons. We therefore suggest that the failure to detect evidence of functional NCX1 activity in sensory neurons is due to one of three likely possibilities: 1) the $[Ca^{2+}]_i$ generated in response to high K^+ was insufficient to activate NCX1 in the cell body, 2) the protein is synthesized and trafficked out of the cell body consistent with the Western blot data discussed below and/or 3) the mRNA does not result in functional protein, although this is least likely given our western blot analysis. Additional experiments will be needed to distinguish between these possibilities.

There was also an apparent discrepancy between results obtained with the relatively selective NCX3 blocker, KB-R7943 and siRNA-induced knockdown of NCX2 and NCX3. While there is evidence to suggest that the potency of KB-R7943-induced block of NCX is comparable when the exchanger is functioning in forward or reverse mode under conditions enabling bi-directional exchanger activity (Watanabe et al., 2006), the relative potency of these compounds was determined in reverse mode (Iwamoto and Shigekawa, 1998). Thus, it is possible even the limited selectivity for NCX3 over NCX1 or NCX2 reported for KB-R7943 in reverse mode, is lost in forward mode. Furthermore, with only three times higher potency for NCX3 over NCX1 and 2, there should be at least some block of NCX2 at all concentrations of KB-R7943. Therefore, we have likely underestimated the relative contribution of NCX2 with the combination of blockers employed. More perplexing however, was the observation that knocking down either NCX2 or NCX3 rendered the T50 insensitive to KB-R7943. This observation raises the possibility that full NCX activity requires the interaction of both NCX2 and NCX3 isoforms. It is also possible that there are compensatory changes associated with siRNA knockdown of a protein such as NCX that is critical for cell homeostasis which masked our ability to fully characterize relative contribution of NCX isoforms. Consistent with this last possibility, was the

observation that following siRNA knockdown of NCX2 or 3, there was no increase in the duration of the evoked transient as is observed following acute block of NCX activity. This suggests an increase in other Ca^{2+} regulatory mechanisms such as PMCA or SERCA may have been recruited to compensate for the loss of NCX activity.

3.5.4 Identification of NCX isoforms within sensory tissues

The results of our PCR experiments are consistent with the presence of splice variants for both NCX1 and NCX3 in sensory neurons. In contrast, there was no evidence of NCX2 splice variants at either the mRNA or protein level, consistent with previous results (Kofuji et al., 1994, Quednau et al., 2004). The PCR analysis focused on exons A and B, which have previously been shown to be mutually exclusive, whereas the four other exons (C, D, E, and F) in the splicing region are thought to be cassette exons (Kofuji et al., 1994). The present data are consistent with the expression of at least six out of the 17 possible variants that have been identified for NCX1. Three of the possible five NCX3 variants identified in brain are denoted NCX3-AC, NCX3-B, and NCX3-BC. The PCR product sizes we detected at the single cell level are consistent with the presence of NCX3-AC and NCX3-B splice variants (Quednau et al., 1997, Michel et al., 2014).

The size of the splicing region within the intracellular loop is relatively small consisting of ~ 250 amino acids and the mutually exclusive exons A and B do not differ much in the relative number of base pairs. Therefore, it would be very difficult to differentiate between isoform splice variants at the protein level. Nevertheless, multiple NCX1- and NCX3-, but not NCX2-LI bands were detected with western blot analysis of peripheral neural tissue. The additional bands larger than the predicted molecular weight of NCX1 suggest the possibility of tissue-dependent post-translational modifications, as a number of putative glycosylation sites are

present on putative extracellular regions of all three isoforms. The bands below the predicted NCX molecular weight are likely cleavage products as the bands appear to be the size of the large intracellular loop, a region particularly prone to proteolytic cleavage by endogenous proteases (Linck et al., 1998, Thurneysen et al., 2002b). While confirmation that these additional bands are in fact NCX protein will ultimately be necessary, it is important to note that the bands detected in the present study are comparable to those previously reported with the antibodies used for all three isoforms and at least NCX2 and NCX3 specificity has been confirmed in knockout mice (Jeon et al., 2003, Molinaro et al., 2011). Thus, if reflective of differential processing and/or protein cleavage, results from the present analysis of tissue from the dorsal horn to the peripheral nerve suggest that there is a differential distribution of NCX isoforms.

The expression and distribution of NCX has yet to be extensively characterized in the peripheral nervous system. Consistent with the results of the present study, previous expression analysis indicates mRNA for all three NCX isoforms is detectable in sensory neurons (Kuroda et al., 2013, Shutov et al., 2013). Other immunohistochemical (IHC) data indicating that NCX1-LI protein is only detectable in satellite cells within the DRG are also consistent with the results of the present study (Persson et al., 2010). In contrast, however, previous IHC data on the distribution of NCX2 and 3 suggests that NCX2 is the dominant isoform in putative nociceptive neurons and NCX3 is more widely distributed but at much lower levels (Persson et al., 2010). To begin to explore the basis for the apparent difference between these previous results and those of the present study, we probed protein from DRG, sciatic nerve and skin with the anti-NCX2 antibody used in this previous study. However, we were only able to detect a band at 36 kDa (not shown), suggestive of an NCX ancillary protein (Michaelis et al., 1992) as the estimated size of NCX2 protein is 102 kDa. However, the present results with an antibody obtained from Dr.

Philipson at UCLA were consistent with previous results in brain tissue (Thurneysen et al., 2002a, Papa et al., 2003).

3.5.5 Functional Implications: Somal Excitability, CAP, and Nociceptive Behavior

The results of our functional analysis of NCX suggests that beyond the regulation of the Ca^{2+} transient and possibly resting Ca^{2+} in the soma of a small subpopulation of neurons, NCX contributes minimally to the regulation of excitability. As noted above, there are two primary ways NCX is likely to influence neuronal excitability. We have previously demonstrated that Ca^{2+}-dependent K^+ currents are present at relatively high density in putative nociceptive cutaneous neurons (Zhang et al., 2010a), suggesting that, as with the direct influence of NCX activity in forward mode, an indirect influence would also be excitatory, secondary to the net suppression of these K^+ channels. Consistent with the suggestion that Ca^{2+}-dependent K^+ channels have a dominant influence on the excitability of putative nociceptive neurons following an increase in $[Ca^{2+}]_i$, the depolarization-induced increase in $[Ca^{2+}]_i$ was associated with a decrease in excitability. Our largely negative results in the cell body excitability experiments suggest that mechanisms other than those influenced by NCX play a much more dominant role in the regulation of the excitability of the isolated cell body. Consistent with this suggestion, it was only under relatively extreme conditions (40 Hz stimulation), that a weak excitatory influence of NCX could be detected.

The impact of NCX on action potential propagation in the isolated sciatic nerve was consistent with the mechanisms described in the cell body, but suggested that NCX is active even at relatively low levels of activity. That is, if both direct and indirect actions of NCX activity are associated with membrane depolarization, this depolarization would lead to the inactivation of

voltage-gated Na^+ channels, and a concomitant decrease in CV. Conversely, block of NCX should result in membrane hyperpolarization, the relief of Na^+ channel inactivation and an increase in CV. Li^+ bath was associated with a relatively large (~24%) decrease in the C-wave CV when the CAP was evoked at a very low frequency (i.e., 0.017 Hz). We suggest that this decrease in CV is not due to NCX block, but instead due to what is equivalent to a partial block of voltage-gated Na^+ channels that reflects the slightly lower permeability (85%) of Li^+ compared to Na^+ through voltage-gated Na^+ channels (Gold and Thut, 2001a). There is also evidence that there may be CV slowing due to a block of the Na^+/K^+ ATPase (De Col et al., 2008), resulting in further membrane depolarization and a further reduction in Na^+ channel density due to Na^+ channel inactivation. Thus, in the face of Li^+-induced CV slowing via mechanisms independent of an action on NCX, we suggest that absence of a change in CV with Li^+ at 0.1 Hz stimulation, actually reflects a significant increase in CV due to NCX block. That this effect appears to be attenuated at 5 Hz stimulation, would suggest that NCX activity is close to maximal even at 0.1 Hz stimulation. Consistent with this suggestion, KB-R7943 produced a significant increase in CV at 0.1 Hz but only reversed the activity-dependent slowing observed at 5 Hz.

Lastly, given evidence in support of a contribution of both NCX2 and 3 to the regulation of $[Ca^{2+}]_i$ in putative nociceptive cutaneous neurons, it was surprising that hypersensitivity to mechanical and thermal stimuli was only observed following knockdown of NCX3. While this observation is consistent with our pharmacological data implicating a dominant role for NCX3 in putative nociceptive neurons, this result may also suggest that the functional role of these isoforms in sensory neurons may be dissociable. Importantly, the timing of the changes observed is consistent with previous studies using similar siRNA based strategies (Xie et al., 2013, Acosta

et al., 2014), and recovery of the behavior corresponded with recovery of NCX3 protein in the ganglia.

The decrease in nociceptive threshold observed following NCX3 knockdown was larger than expected given the relatively small number of fibers in which our results suggested NCX3 should be functional. However, the observation that nociceptive behavior of rats treated with both NCX3 siRNA and IB4 conjugated to saporin (IB4/SAP) resembled the rats treated with control siRNA and IB4/SAP, suggests that the loss of IB4 fibers attenuated the NCX3 siRNA-induced hypersensitivity. If the hypersensitivity had been due to dysregulation of fibers in addition to the IB4+ population, one would have expected an additive effect in which the increase in nociceptive threshold observed with IB4/SAP would have been significantly attenuated by the NCX3 siRNA. Nevertheless, it is possible that the antinociception associated with the loss of IB4+ fibers caused a ceiling effect, masking the NCX3 siRNA-induced hypersensitivity. We consider this possibility unlikely, however, as the IB4/SAP-induced thermal antinociception detected was far from 20 s cut off employed.

There are several possible explanations for the hypersensitivity observed following knockdown of NCX3. However, we suggest the simplest explanation is a loss of NCX-mediated regulation of $[Ca^{2+}]_i$ in the central terminals. This would result in an increase in the duration of evoked Ca^{2+} transients and, consequently, an increase in transmitter release, and thus hypersensitivity. While such a mechanism is often proposed in the literature (Maggi et al., 1990, Evans et al., 1996, Neher and Sakaba, 2008, Xie et al., 2013, Acosta et al., 2014), there is, unfortunately little direct evidence for a role of NCX in synaptic transmission. However, in the only study of which we are aware addressing a role of NCX in the central terminals of putative nociceptive afferents, it was demonstrated that mitochondria and PMCA, but not NCX, are

involved in presynaptic Ca^{2+} regulation; NCX appeared to contribute to the regulation of resting Ca^{2+} levels and only 12% of the decay of evoked transients (Shutov et al., 2013). Unfortunately, the impact of NCX block on post-synaptic responses was not determined in this study, so the contribution of NCX to transmitter release from central terminals of nociceptive afferents has yet to be determined.

In summary, the results of the present study indicate that NCX isoforms contribute to the regulation of the duration of the evoked Ca^{2+} transient in putative nociceptive neurons from naïve animals, and in a subpopulation of these neurons NCX contributes to the regulation of resting $[Ca^{2+}]_i$. In the absence of tissue injury, NCX appears to have little influence on excitability per se, but contributes to both determination of the action potential conduction velocity in C-fiber axons as well as the establishment of nociceptive threshold. Our characterization of this protein in tissue from naïve animals suggests that it is poised to play an important role in tissue injury and repair. Indeed, it has been suggested the NCX contributes to nerve injury observed in small fiber polyneuropathies (Ma, 2013) and there is evidence to suggest it is important for neurite outgrowth during regeneration (Persson et al., 2013). Now, with a better mechanistic understanding of NCX in sensory neurons, there is a framework with which to interpret changes observed following injury. Future experiments will need to assess the function of NCX in the presence of injury and/or chronic pain states.

4.0 PERSISTENT INFLAMMATION-INDUCED INCREASE IN THE TRAFFICKING OF SODIUM CALCIUM EXCHANGER TO PERIPHERAL TERMINALS IN A SUBPOPULATION OF CUTANEOUS RAT DRG NEURONS

4.1 ABSTRACT

We have previously reported that persistent inflammation results in an increase in the magnitude and duration of depolarization-evoked Ca^{2+} transients in putative nociceptive afferents. These changes were neither the result of increased neuronal excitability nor an increase in the magnitude of depolarization driven by a high K^+ application. Subsequent data also ruled out an increase in Ca^{2+} influx via voltage-gated Ca^{2+} currents and recruitment of Ca^{2+}-induced Ca^{2+} release. Parametric studies indicated that the inflammation-induced increase in the duration of the evoked Ca^{2+} transient required a relatively large and long lasting increase in the concentration of intracellular Ca^{2+} ($[Ca^{2+}]_i$) implicating the Na^+/Ca^{2+} exchanger (NCX), a major Ca^{2+} extrusion mechanism activated with high intracellular Ca^{2+} loads. The functional contribution of NCX was tested using fura-2AM imaging and electrophysiological recordings. Changes in NCX expression and protein were assessed with real-time PCR and western blot analysis respectively. Results indicated a significant inflammation-induced decrease in NCX activity in a subpopulation of putative nociceptive neurons innervating the site of inflammation. The time-course of the decrease in NCX activity paralleled that of the inflammation-induced

changes in nociceptive behavior. While there were no detectable changes in NCX mRNA at the whole ganglia level, there was a decrease in NCX3 protein detectable in the DRG by 3 days after the CFA injection. The change in NCX3 in the cell body was associated with a significant decrease in NCX3 protein in the ganglia, a significant increase in the peripheral nerve (sciatic), yet no change in the central nerve root. These data suggest altered trafficking of NCX3 that may serve as a compensatory mechanism to attenuate pro-nociceptive processes associated with inflammation.

4.2 INTRODUCTION

Tissue inflammation is associated with an increase in the magnitude and duration of the evoked Ca^{2+} transient in a subpopulation of putative nociceptive cutaneous DRG neurons (Lu and Gold, 2008). Alterations in intracellular Ca^{2+} ($[Ca^{2+}]_i$) signaling can increase afferent excitability (Zhang et al., 2012a), facilitate transmitter release (Flake and Gold, 2005), and/or lead to changes in gene expression (Fields et al., 2005), all functions that may contribute to the pain and hypersensitivity of persistent inflammation.

The magnitude and duration of evoked Ca^{2+} transients are determined by the combined action of channels, buffers, pumps and exchangers (Berridge et al., 2000). Therefore, there are a number of mechanisms that could contribute to the inflammation-induced increase in the depolarization-induced Ca^{2+} transient. We have previously ruled out many mechanisms, including an increase in the magnitude of depolarization (Lu and Gold, 2008) and density of voltage-gated Ca^{2+} channels (Lu et al., 2010), the recruitment of Ca^{2+}-induced Ca^{2+} release, a change in sarco-endoplasmic reticulum ATPase (SERCA) function, and mitochondrial-

dependent Ca^{2+} buffering (Scheff et al., 2013). Furthermore, because the inflammation-induced change in Ca^{2+} signaling is not associated with an increase in resting Ca^{2+} (Lu and Gold, 2008), and the available evidence suggests that the plasma-membrane Ca^{2+} ATPase contributes to resting Ca^{2+} levels (Wanaverbecq et al., 2003, Gemes et al., 2012), we predicted that the inflammation-induced changes in the evoked Ca^{2+} transient were not due to a decrease in PMCA activity. However, as we have described previously (Scheff et al., 2014), the Na^{+}/Ca^{2+} exchanger (NCX), a relatively low affinity Ca^{2+} extrusion mechanism, is only active in the IB4-binding (IB4+) subset of small diameter capsaicin-responsive cutaneous neurons; the same population in which the inflammation-induced increase in the duration of the evoked transient is manifest (Lu and Gold, 2008). We have also recently demonstrated that NCX activity in this population of putative nociceptive cutaneous neurons influences the duration of the evoked Ca^{2+} transient, but not the magnitude (Lu et al., 2006). Therefore, we hypothesized that NCX contributes, at least in part, to the inflammation-induced increase in the duration of the depolarization-evoked Ca^{2+} transient.

To test this hypothesis, retrogradely labeled small diameter IB4+ DRG neurons from naïve and complete Freund's adjuvant (CFA)-inflamed rats were studied with ratiometric Ca^{2+} imaging and voltage clamp electrophysiology in combination with a variety of pharmacological manipulations. The potential mechanisms underlying an inflammation-induced decrease in NCX activity were assessed with sqRT-PCR, western blot analysis and immunohistochemistry. Our results suggest that the inflammation-induced increase in the duration of the evoked Ca^{2+} transient is due to a decrease in NCX activity. This appears to be due to an increase in trafficking of the exchanger to the peripheral, but not central terminals of these putative nociceptors. Experiments to determine the functional implications of this finding are currently underway.

4.3 METHODS

Adult male Sprague-Dawley rats (Harlan, 220-300g) were used for all experiments. Animals were housed two per cage in a temperature and humidity controlled animal facility on a 12:12 light:dark schedule with food and water freely available. All procedures were approved by the University of Pittsburgh Institutional Animal Care and Use Committee and performed in accordance with National Institutes of Health guidelines for the use of laboratory animals in research.

Fourteen to 17 days prior to tissue harvest, the retrograde tracer 1,1'-dioctadecyl-3,3,3',3'-tetramethylindocarbo-cyanine perchlorate (DiI, Invitrogen, Carlsbad, CA)) was injected into the glabrous skin of the hindpaw to label cutaneous afferents. The tracer was dissolved at 170 mg/mL in dimethylsufoxide (DMSO, diluted 1:10 in 0.9% sterile saline, and injected in 3-5 subcutaneous sites using a 30 g needle for a total volume of 10 μL per hindpaw under isoflurane (Abbott Laboratories, North Chicago, IL, USA) anesthesia. Three days prior to tissue harvest, rats were again anesthetized with isoflurane and inflammation was induced at the site of tracer injection in the left hindpaw with a 100 μL subcutaneous injection of complete Freud's adjuvant (CFA, (Sigma-Aldrich, St Louis MO), diluted 1:1 in 0.9 % sterile saline). Prior to tissue removal, animals were deeply anesthetized with an intraperitoneal injection of rat cocktail containing ketamine (55 mg/kg), xylazine (5.5 mg/kg) and acepromazine (1.1 mg/kg) and the L4-L5 DRG were removed ipsilateral to labeling and CFA-induced inflammation. Ganglia were enzymatically treated, mechanically dissociated, and plated on laminin (Invitrogen, Carlsbad, CA; 1mg/ml) and poly-L-ornithine-coated (Sigma-Aldrich; 1 mg/ml) glass cover slips as previously described (Lu et al., 2006). All subsequent experiments were preformed within 8 h of tissue harvest.

4.3.1 Ca^{2+} Imaging

Neurons were incubated with 2.5 μM Ca^{2+} indicator fura-2 AM ester with 0.025 % Pluronic F-127 for 20min at room temperature. Neurons were then labeled with FITC-conjugated IB4 (10 μg/ml) for 10 min at room temperature. Labeled neurons were placed in a recording chamber and continuously superfused with normal bath solution (mM: 130 NaCl, 3 KCl, 2.5 $CaCl_2$, 0.6 $MgCl_2$, 10 HEPES, 10 glucose, pH 7.4, osmolality 325 mOsm) or a 'Na^+-free' bath solution (mM: 130 Choline-Cl or LiCl, 3 KCl, 10 $MgCl_2$, 2 EGTA, 10 Hepes, 10 glucose, pH 7.4, osmolality 325 mOsm). A Na^+-free solution was used to block NCX activity by preventing NCX from fulfilling the Na^+ binding requirement for exchange activity (Cook et al., 1998). Fluorescence data were acquired on a PC running Metafluor software (Molecular Devices, Sunnyvale, CA, USA) via a CCD camera (Roper Scientific; model RTE/CCD 1300). The ratio (R) of fluorescence emission (510 nm) in response to 340/380nm excitation (controlled by a lambda 10–2 filter changer (Sutter Instrument, Novato, CA)) was acquired at 1 Hz during drug application. All drugs were applied through a computer-controlled peizo driven perfusion system (switching time <20 ms; Warner Instruments, Hamden, CT, USA, Fast-Step Model SF-77B). $[Ca^{2+}]_i$ was determined from fura-2 ratio following in situ calibration experiment as described in detail previously (Grynkiewicz et al., 1985, Scheff et al., 2013).

4.3.2 Voltage Clamp Electrophysiology

Perforated patch clamp experiments were carried out using a HEKA EPC9 amplifier (HEKA Elektronik, Lambrecht/Rhineland-Pfalz, Germany). Glass electrodes (1–4 MΩ) were filled with (mM) 100 Cesium-methanesulfonate, 5 NaCl, 40 TEA-Cl, 0.1 $CaCl_2$, 2 $MgCl_2$ 1 EGTA and the

pH adjusted with Tris-base to 7.2. Osmolality was adjusted to 320 mOsm with sucrose. A normal bath solution or "Na^+-Free" bath solution were used as mentioned in microfluorimetry experiments. The pH was adjusted with Tris-base to 7.4 and osmolality was adjusted with sucrose to 320 mOsm.

Gramicidin (Sigma–Aldrich)-perforated patch was used for all voltage clamp recordings. A stock solution of gramicidin (1.5 mg/100 μl) was prepared in DMSO. This was diluted with electrode solution in a 1:300 ratio to give a final concentration of 50 μg/ml. The gramicidin containing electrode solution was vortexed for 15 s. No filtering was applied. The tip of the electrode was loaded with a small volume of gramicidin-free electrode solution in order to avoid interference of the antibiotic with seal formation. Gramicidin-containing electrode solution was back loaded. The progress of perforation was monitored with the capacitative transient to a 5 mV step. Experiments were not started until access resistance was less than 7 MΩ.

Series resistance compensation (>70%) was employed for all voltage-clamp recording. A 4s voltage step from -60mV to 0mV was used to evoked a Ca^{2+} transient. Fura-2AM based microfluorimetry was used in succession with all experiments in order to track the decay rate of the voltage step-evoked Ca^{2+} transient. A computer-controlled perfusion fast-step system was used to apply a Na^+ free bath solution while clamping the membrane at -60 mV to measure the amount of Na^+-sensitive current throughout the decay period.

4.3.3 Polymerase chain reaction (PCR)

DRG from anesthetized rats were harvested in a manner identical to that used for neuron isolation and plating. PCR was used to amplify specific sequences within the cDNA generated from mRNA extracted from selected cutaneous afferents. Single neurons were collected with

large bore (30 μm) glass pipettes and expelled into reaction tube for subsequent cDNA synthesis via an anchored oligo-dT primed reverse transcription reaction with Superscript II, as previously described (Nealen et al., 2003). The cDNA generated from each neuron was used as a template for subsequent PCR reactions. To confirm successful cell collection and cDNA synthesis, 0.5 μl of the template cDNA was used for the amplification of cyclophilin. Negative controls for each round of cell collection included two neurons in which no reverse transcriptase was added to the reaction mixture and two tubes in which all other procedures were performed as if a neuron was collected, except no neuron was collected. Nested PCR was used to assess the expression of NCX 1, 2 and 3, as this strategy increases the sensitivity and specificity of the PCR reaction. Two sets of primers specific for each target were used, where 30 cycles were used for the first round of amplification with the "outer" set of primers (Table 1), and 2 μl of this reaction product was used for a second round of amplification for 30 more cycles with the "inner" set of primers (Table 1). Following agarose gel electrophoresis, PCR reaction products were visualized with ethidium bromide.

4.3.4 Western Blot

L4 and L5 DRG were homogenized with Teflon tube and mortar for less than 10 strokes in ice cold radioimmunoprecipitation assay (RIPA) buffer supplied with protease inhibitors (aprotinin, leupeptin, pepstatin, E-64, trypsin inhibitor, and phenylmethanesulfonyl fluoride (PMSF), all at a final concentration of 2 ng/ml except PMSF, which was used at a final concentration of 1 mM). All protease inhibitors were obtained from Sigma–Aldrich. Lysates were collected in 0.5-ml tubes. Teflon tubes were rinsed with RIPA buffer and the solutions were combined with the lysates previously collected. Lysates were centrifuged for 5 min at 10,000 rpm at 4°C. Protein

concentration was determined via bicinchoninic acid (BCA) protein assay using a BCA assay kit (Thermo scientific, Rockford, IL, USA). Lysates were then mixed with Laemmli buffer (2×, 400 µl + 100 µL β-mercaptoethanol) and boiled for 5 min before loading. Protein (30 µg) from one animal was then loaded per lane and separated on a 7 % SDS–PAGE gel and transferred to nitrocellulose membrane. Membranes were blocked with 5% milk for 1 hour at room temperature and then incubated with primary antibody at 4°C overnight (1:100 for R3F1 (anti-NCX1),1:200 for W1C3 (anti-NCX2), and 1:100 for anti-NCX3 (cat # LS-B5775, LifeSpan Biosciences, Inc., Seattle WA), diluted with 5% milk/Tris-buffered saline with Tween 20 (TBST, Sigma–Aldrich). The blots were washed and then incubated with peroxidase-conjugated secondary antibody (1:2000 in 5% milk/TBST, Jackson ImmunoResearch Laboratories Inc. West Grove, PA, USA) for an hour at room temperature. An ECL kit (Amersham Biosciences, Piscataway, NJ, USA) was used for detection of immunoreactivity, luminescence data were collected on an LAS3000 imager (Fujifilm Inc., Japan), and analyzed with ImageJ (NIH). Both antibodies used to detect NCX1 and NCX2 were gifts from Dr. Kenneth Philipson of University of California Los Angeles. Both antibodies have been characterized by Dr. Philipson and colleagues in heterologous expression systems and hippocampal cultures, where R3F1 (anti-NCX1) detects a prominent band at 120 kDa and minor bands at 70 kDa and 60 kDa, and W1C3 (anti-NCX2) detects only one prominent band at 60 kDa. There appears to be no cross reactivity between isoforms (Thurneysen et al., 2002b, Papa et al., 2003). Furthermore, the specificity of the anti-NCX2 antibody was confirmed in NCX2 null mutant mice (Jeon et al., 2003).

4.3.5 Immunohistochemistry

Animals were deeply anesthetized with an intraperitoneal injection of anesthetic cocktail

(55 mg/kg ketamine, 5.5 mg/kg xylazine, and 1.1 mg/kg acepromazine), and transcardially perfused with ice cold 1× phosphate-buffered saline (PBS; pH 7.2). Sciatic nerves were dissected and cryoprotected with 30% sucrose for 48 hr at 4^{o}C, embedded in OCT (Tissue Tek, Torrance, CA, USA), cryostat sectioned at 16 μm and thaw-mounted on SuperFrost plus slides (Fisher Scientific) prior to staining. Slides were heated to 50°C on a hot-plate, for 1 hr, rehydrated with PBS, and post-fixed for 10 min with ice cold 4% paraformaldehyde. Slides were extensively washed in PBS and blocked with PBS containing 3% normal donkey serum, 0.03% Triton X-100, and 1% BSA for 1 hr at room temperature. Subsequently slides were incubated in rabbit anti-NCX3 (1:500, Lifespan Biosciences, Seattle, WA) in PBS containing 1% BSA overnight at 4°C. Slides were extensively washed in PBS and incubated in donkey anti-rabbit secondary antibodies conjugated to cyanine 3 (Jackson ImmunoResearch, West Grove, PA, USA) in blocking solution at 1:500 for 2.5 hours, extensively washed, and coverslipped with Fluoromount-G (Southern Biotech, Birmingham, AL). Slides were photographed under epifluorescence with a Leica DM4000B upright (Leica, Wetzlar, Germany). Images were captured using a Leica DFC300FX camera and processed for brightness and contrast with ImageJ (NIH).

4.3.6 Sciatic Nerve Ligations

Two days after induction of inflammation in the hindpaw, rats were deeply anesthetized with isoflurane. The hair over the back of the thigh was shaved and blunt dissection was used to separate the hamstring muscle exposing the sciatic nerve. Two tight ligatures were placed around the exposed nerve ~ 1 cm apart using sterile 6.0 silk sutures. Subsequently, 24 hr after ligation, animals were deeply anesthetized with anesthetic cocktail and sciatic nerves were removed and

processed for immunohistochemistry as described above. Quantification of protein trafficking was done using Image J software (NIH). Regions of interest (ROIs) were selected as a square area as close the top of the first ligature as possible. ROI area was kept consistent across images and pixel density within the ROI was quantified. To quantify the increase in NCX3-LI, nerves from naïve and inflamed rats were processed in parallel and images were acquired under identical conditions. The density of staining was then assessed in a 4 mm^2 region centered over the middle of the nerve 1 mm from the middle of the center of the constriction left by the ligature. The mean pixel density over the region was measured. Three sections per nerve were averaged to obtain a value per rat and the average value from naïve and inflamed rats were compared.

4.3.7 Chemicals and Reagents

DiI 1,1'-dioctadecyl-3,3,3',3'-tetramethylindocarbo-cyanine perchlorate was purchased from Invitrogen (Carlsbad, CA, USA). Fura-2 acetoxymethyl (AM) ester (2.5 mM stock in DMSO) and Pluronic F-127 (0.025 % in water) were purchased from TEF Laboratories (Austin, TX, USA). KB-R7943 was purchased from R&D Systems, Inc (Minneapolis, MN, USA) and was dissolved to 100mM stock concentration in DMSO (Sigma-Aldrich, St Louis, MO, USA).

4.3.8 Statistical Analysis

Data are expressed as mean ± s.e.m. Student's *t* test was used for simple comparison between groups two groups. For experiments involving the application of test compounds, vehicle controls were always included. A two-way ANOVA was used for analysis of more than two

groups with the Holm-Sidak test used for post-hoc analysis. $p < 0.05$ was considered statistically significant.

4.4 RESULTS

Ca^{2+} imaging data were collected from 367 cutaneous DRG neurons acutely dissociated from 32 male Sprague Dawley rats, of which 18 were control and 30 were inflamed. Based on previous results indicating that the inflammation-induced increase in the 4 s 30 mM KCl (high K^+)-evoked Ca^{2+} transient was primarily manifest in small (< 30 μm) diameter, cutaneous, IB4+, capsaicin-sensitive DRG neurons, this subpopulation was the focus of the present study and is subsequently referred to as a subpopulation of putative nociceptive cutaneous neurons. Consistent with our previous results (Lu and Gold, 2008, Scheff et al., 2013), inflammation was associated with a significant increase in the magnitude (as measured by a change from baseline) and duration (as measured by the time to a 50 % decrease from peak (T50)) of the high K^+-evoked Ca^{2+} transient (Figure 22A). These changes were not associated with a change in resting Ca^{2+}, 120.47 ± 4.09 nM (n = 39) and 125.74 ± 5.88 nM (n = 49) in neurons from naïve and inflamed rats, respectively ($p > 0.05$).

A parametric experiment using DiI+ neurons was used to determine the stimulus duration at which it was possible to detect an inflammation-induced increase in the duration of the evoked transient. Neurons from naïve (n = 24) and inflamed (n = 43) rats were stimulated with high K^+, applied for durations ranging between 250 ms and 4 s (Figure 22A). Analysis of the magnitude (Figure 22B) and T50 (Figure 22C) of decay versus the stimulus duration indicates that a

significant difference between naïve and inflamed neurons emerges with a stimulus duration ≥ 4s.

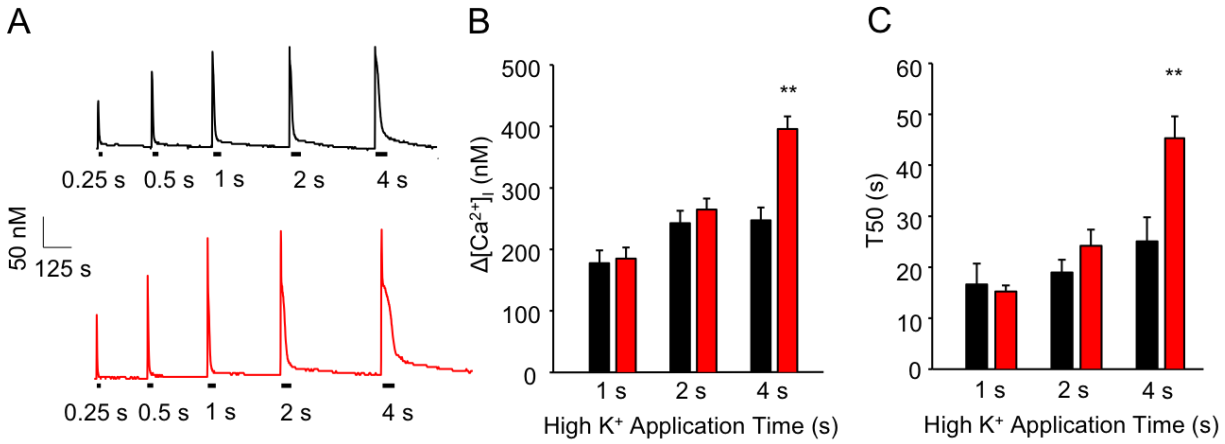

Figure 22: The inflammation-induced increase in the magnitude and duration of the evoked Ca2+ transient are only manifest with long duration stimuli

A) Putative nociceptive cutaneous neurons from naïve (black trace) and inflamed (3 days post CFA injection, red trace) rats were stimulated with 30 mM KCl (high K^+), applied for durations ranging between 250 ms and 4 s. Pooled data indicate that in neurons from both naïve (black bars, n = 24) and inflamed (red bars, n = 43) rats are similar in both magnitude (**B**), as measured by a change from baseline ($\Delta[Ca^{2+}]_i$), and duration (**C**), as measured by the time to 50 % decrease from peak magnitude (T50), with a 1 and 2 s stimuli but the inflammation-induced changes in both parameters are revealed with a 4 s stimulus of high K^+. ** $p < 0.01$

4.4.1 Inflammation is associated with a decrease in NCX activity

To determine whether an inflammation-induced decrease in NCX activity may contribute to the increase in the duration of the evoked Ca^{2+} transient, we measured the transient duration in response to a 4 sec application of high K^+ before and after inhibition of NCX activity using a Na^+ free bath in which Na^+ was replaced with Li^+ or choline (Figure 23A). Consistent with our previous results in unlabeled DRG neurons (Lu et al., 2006) and cutaneous neurons (Scheff et al., 2014), block of NCX resulted in no change in the magnitude (260.3 ± 13.29 and 250.2 ± 16.17 nM respectively), but was associated with a significant increase in duration (529.22 ± 12.68% increase in T50, Figure 23B) of the evoked transient in neurons from naïve rats. In neurons from inflamed rats, however, there was no change in either the magnitude (387.8 ± 29.6 n = 35, and 389.3 ± 37.2, respectively, $p < 0.05$) or duration (42.5 ± 4.9, n = 35 and 57.7 ± 8.5 s, respectively, $p > 0.05$) of the evoked Ca^{2+} transient associated with NCX block (Figure 23B). The absence of an increase in the duration of the evoked Ca^{2+} transient in the presence of 0 mM Na^+ in the bath, is consistent with a loss of NCX activity in neurons from inflamed rats. To confirm the apparent loss of NCX activity with inflammation, two additional experiments were performed. In the first, we tested the efficacy of NCX3-selective blocker, KB-R7943, in the presence of inflammation, based on previous data suggesting that NCX3 underlies the majority of NCX activity in this subpopulation of sensory neurons (Scheff et al., 2014). In neurons from naïve animals, 100nM KB-R7943 significantly prolonged the duration of the transient 237.2 ± 46.7 % ($p < 0.05$, Figure 22). However, consistent with results using 0 mM Na^+ bath, the NCX3-selective blocker had no detectable influence on the duration of the evoked Ca^{2+} transient (5.1 ± 0.23%, $p > 0.05$) in neurons from CFA-treated rats.

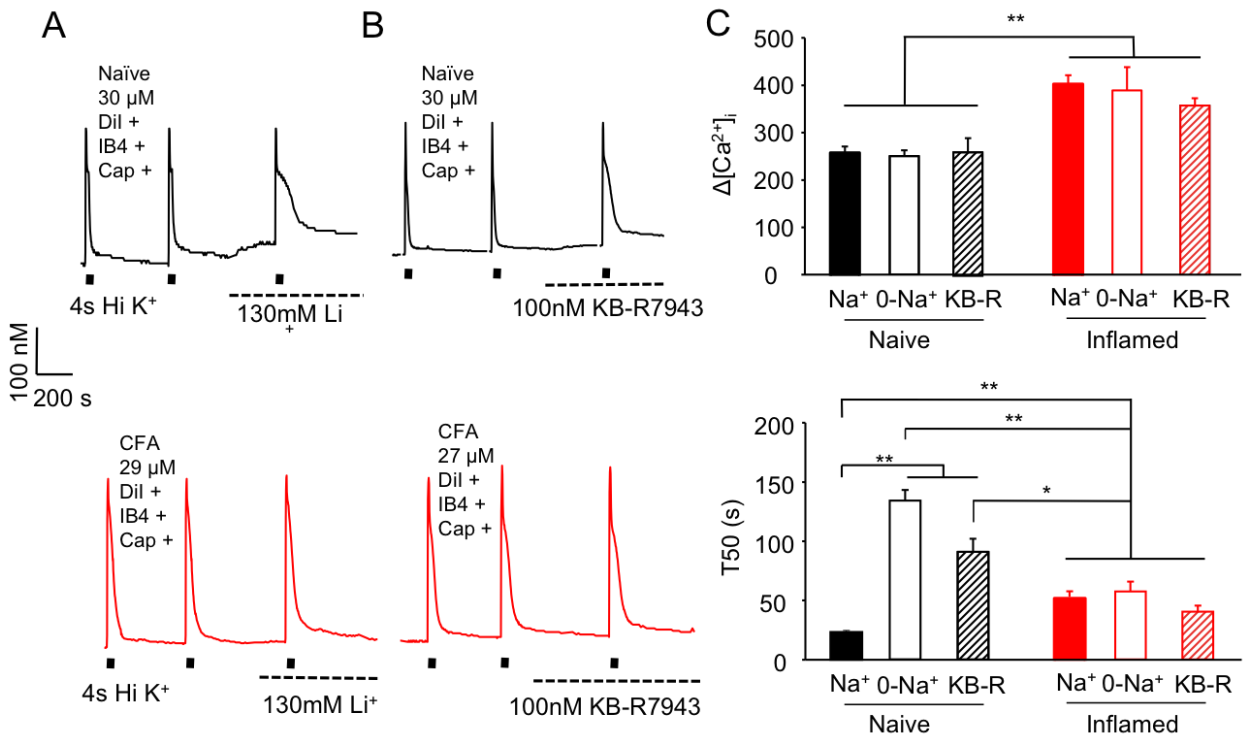

Figure 23: Inflammation is associated with loss of NCX activity in putative nociceptive cutaneous neurons

High K^+ (30 mM) evoked Ca^{2+} transients in small diameter (≤ 30 µm) retrogradely labeled (DiI+), capsaicin sensitive (Cap+), IB4+ neurons from naïve (black top traces) and inflamed (red bottom traces) rats before and after NCX block with a bath solution in which Na^+ was replaced with Li^+ (**A**) or 100nM KB-R7943 (**B**). **C**) Pooled magnitude (top) and duration (bottom) transient data from DiI+/IB4+ neurons from naïve and inflamed rats, before (Na^+) and after block of NCX with 0 mM Na^+ bath in which Na^+ was replaced with Li^+ or choline, or KB-R7943 (KB-R) replacement. 36 and 34 neurons were studied with 0 mM Na^+ from naïve and inflamed rats respectively, while 21 and 23 neurons from naïve and inflamed rats were studied with KB-R7943, respectively. ** $p<0.01$

In the second set of experiments, we sought to directly measure the inward current generated from NCX activity in neurons from naïve and CFA-treated animals. The gramicidin-perforated patch configuration was used for whole cell voltage clamp recording in order to simultaneously assess changes in membrane current and $[Ca^{2+}]_i$ with fura-2 AM imaging. A 4 s depolarization to 0 mV was used to evoke Ca^{2+} influx and consequently, a Ca^{2+} transient. We have demonstrated previously that the transient evoked with this stimulus is similar in magnitude and duration to that evoked with 4s application of high K^+ (Scheff et al., 2014). In the presence of 130 mM $[Na^+]_o$ and $\geq$ 350 nM $[Ca^{2+}]_i$, the exchanger is in Ca^{2+} efflux mode transporting 3 Na^+ in for each Ca^{2+} extruded out at a rate thought to be roughly 5000 sec^{-1} (DiPolo and Beauge, 2006). Therefore, inhibition of exchange activity with the application of 0 mM Na^+ bath, should result in the block of the NCX mediated inward current. There was no detectable change in membrane current or $[Ca^{2+}]_i$ in response to a 4 s application of 0 mM Na^+ bath prior to evoking a Ca^{2+} transient in any of the 12 putative nociceptive cutaneous neurons tested (data not shown). However, following the voltage step to 0 mV, 4s application of 0 mM Na^+ bath resulted in a decrease in inward current, the magnitude of which decreased in association with the decay of the evoked Ca^{2+} transient (Figure 24A). Pooled data from 6 neurons from naïve rats indicated that just after the peak of the evoked Ca^{2+} transient, associated with a $[Ca^{2+}]_i$ of 223.61 ± 9.5 nM, the 0 mM Na^+ bath-sensitive current was 28.73 ± 1.8 pA (Figure 24B). Despite the fact that the depolarization-evoked transient in neurons from inflamed rats (352.72 ± 27.9 nM, n = 6) was significantly ($p < 0.01$) larger than that of neurons from naïve rats, the 0 mM Na^+- bath sensitive current was significantly smaller in these neurons (5.10 ± 1.88 pA, $p < 0.05$, Figure 24B), consistent with an inflammation-induced loss in NCX activity in the isolated cell body.

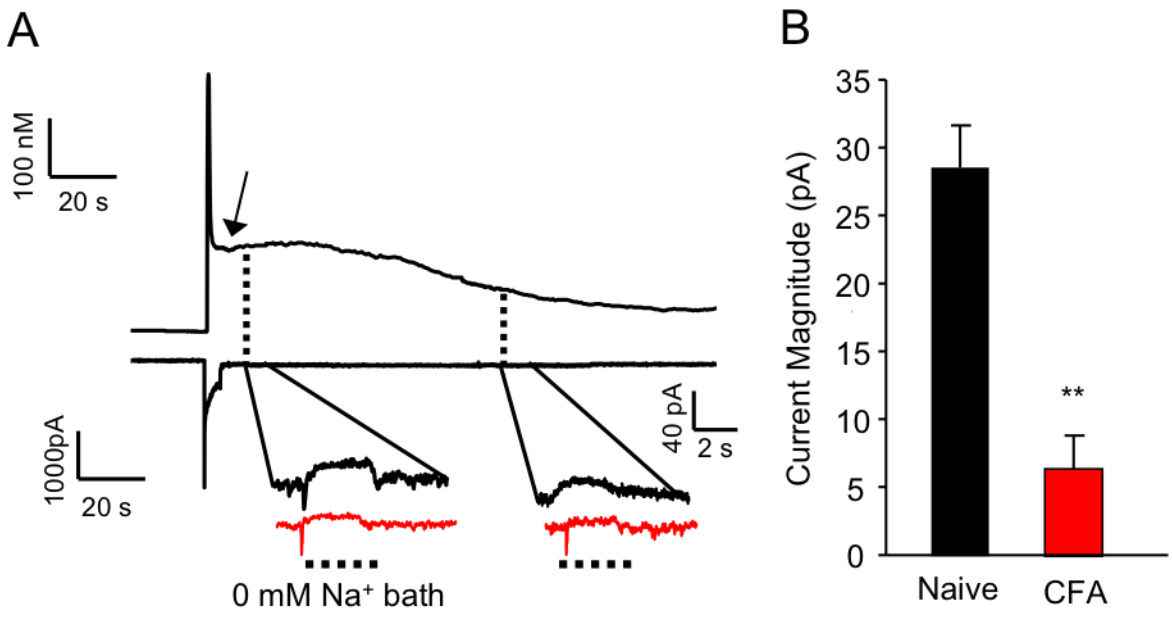

Figure 24: Inflammation-induced decrease in NCX current

A) A combination of perforated patch recording and Ca^{2+} imaging was used to assess the Ca^{2+} transient (top trace) evoked in response to a 4 s voltage step to 0 mV. The Ca^{2+} current (bottom trace), resulted in an increase in 0 mM Na^{+} sensitive current (inset), which decayed in association with the decay of the Ca^{2+} transient. Typical 0 mM Na^{+} sensitive current traces from a neuron from inflamed rats are shown in red. B) Pooled peak 0 mM Na^{+} sensitive current data from neurons (n = 6 in each group) from naïve and inflamed rats. ** $p < 0.01$.

4.4.2 Time course of inflammation-induced changes in NCX activity

To begin to explore both the basis for the inflammation-induced decrease in NCX activity in putative nociceptive neurons and whether these changes might contribute to the onset or resolution of the inflammatory response, we assessed the time course of the inflammation-induced changes in NCX activity. In order to correlate changes in Ca^{2+} regulation with changes the inflammation-induced thermal and mechanical sensitivity, we first assessed the time course of inflammation-induced changes in nociceptive behavior. A significant decrease in both mechanical ($p < 0.01$, Figure 25A) and thermal ($p < 0.01$, Figure 25B) threshold was fully manifest by 24 hrs after the injection of CFA, was relatively stable for up to 72 hrs post CFA, and then returned to baseline over the subsequent 4 – 10 days.

Our initial assessment of the inflammation-induced changes in the evoked Ca^{2+} transient and NCX activity utilized neurons harvested 72 hrs after the injection of CFA. We therefore, assessed the onset of changes in neurons harvested 24 and 48 hrs after the induction of inflammation, and resolution at 7 and 14 days after the induction of inflammation. Results of this analysis indicate that a significant increase in the magnitude of the evoked transient was detectable at 48 hrs, that the increase peaked at 72 hrs post CFA, and was still significantly elevated at 7 days post CFA (Figure 25C). In contrast, the inflammation-induced increase in evoked Ca^{2+} transient duration peaked at 48 hrs post CFA and had resolved by 7 days post CFA (Figure 25D). The inflammation-induced loss of NCX activity followed this same trajectory with a significant decrease in the impact of Li^{+} bath on the Ca^{2+} transient duration that peaked at 48 hours. However, there was still a significant decrease in the impact of Li^{+} bath on day 7 (Figure 25D), suggesting other mechanisms contribute to the normalization of the evoked Ca^{2+} transient.

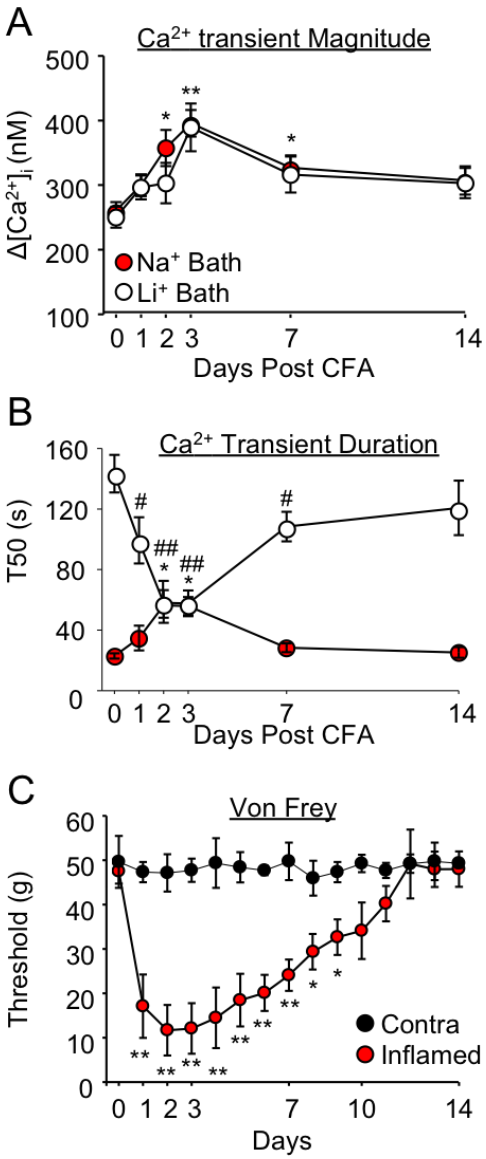

Figure 25: Time-dependent changes in the evoked Ca^{2+} transient and nociceptive behavior

The time course for the inflammation-induced changes in the magnitude (**A**) and duration (**B**) of the evoked Ca^{2+} transient, closely parallel that of the inflammation-induced changes in nociceptive threshold (**C**). The change in nociceptive threshold was manifest in the paw ipsilateral (inflamed) but not contralateral (Contra) to the CFA injection. Block of NCX with 0 mM Na^+ bath (Li^+ Bath), had no influence on the magnitude of the evoked transient, but increased the duration, a change that was completely occluded 2 and 3 days post-CFA. * $p < 0.05$ ** $p < 0.01$ for Na^+-containing bath and # $p < 0.05$ ## $p < 0.01$ for Li^+-containing bath.

4.4.3 The inflammation-induced decrease in NCX activity is due to an increase in trafficking of NCX3 toward peripheral terminals

To explore the basis for the inflammation-induced decrease in NCX activity, we first assessed the impact of inflammation on the expression levels of NCX isoforms in DRG (Table 4). Negative results from this experiment should be viewed with caution because the inflammation-induced change in NCX activity is only present in a subset of neurons that innervate the site of inflammation, which are a subpopulation of the total cells in the L4 and L5 DRG (that give rise to the innervation of the hindpaw). Nevertheless, because others have detected inflammation-induced increases (Lu et al., 2010, DeBerry et al., 2014) and decreases (Zhang et al., 1998, Marsh et al., 2012) in the expression of a number of different molecules, we felt it was still worth assessing changes in NCX expression. However, despite a significant decrease in NCX activity, mRNA extracted from L4 - L5 DRG harvested from naïve (n = 8) and 3 day CFA-treated (n = 7) rats revealed no detectable change any of the isoforms tested (Figure 26A). Next, because mRNA levels do not directly reflect density of protein, we assessed the impact of inflammation on NCX isoform protein levels. Results of this analysis revealed a significant decrease in the relative density of NCX3, but not NCX1 or NCX2 (Figure 26B) in DRG 72 hrs after the induction of inflammation. We have recently demonstrated that NCX3 is the isoform primarily responsible for NCX activity in putative nociceptive DRG neurons (Scheff et al., 2014). Furthermore, pharmacological results of the present study suggesting that a decrease in NCX3 accounts for the inflammation-induced decrease in NCX activity.

Table 4: Fully nested NCX SqRT-PCR primers

Target	Gene	Position	Start	Sequence
NCX1	NM_001270778.1	**Outer**	**2372** **2620**	F: TTTGCCTTCGTCCCACCTACAGAA R: AAGACATTCACAGCGTTGCTTCCG
		Inner	**2515** **2588**	F: TGCAGTTGTGTTTGTCGCTCTTGG R: TGCCTATGGACGCATCTGCATACT
NCX2	NM_078619.1	**Outer**	**2266** **2569**	F: ATCCTGGTCATTGGTCTGCTCACT R: ACGGTGAACAGTGTGACCGAGAA
		Inner	**2382** **2461**	F: CATCCCTGACACGTTTGCCA R: TCCAATGCGGTGAACGTGTT
NCX3	NM_078620.1	**Outer**	**2343** **2890**	F: AATAGTCTTCCTTTGCCACGGGCT R: CCACAACCAATGCCAGGTTTGTCT
		Inner	**2553** **2679**	F: AAGGGTGGTGGTGAGGACTTTGAA R: ATTGCCCTTGGTGAACCGAAATGG

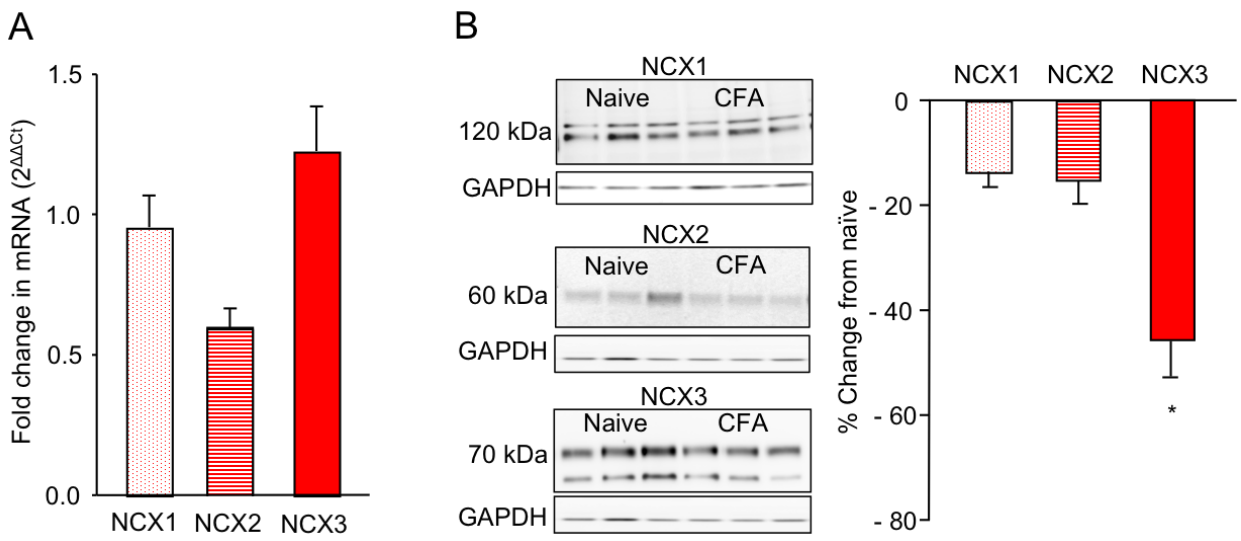

Figure 26: Inflammation was associated with a decrease in NCX protein but not mRNA

A) SqRT-PCR was used to screen for changes in NCX1, 2 and 3 mRNA extracted from whole L4 and L5 DRG. The fold change in NCX isoform in inflamed rats (n = 4) relative to that in naïve (n = 4) was assessed relative to that of GAPDH. B) Western blot analysis of inflammation (CFA)-induced changes in NCX isoforms in total protein extracted from L4 and L5 DRG. Pooled data for inflamed rats (n = 6) are plotted as a percent change from the average band intensity in naïve rats (n = 3), where only the 120 kDa and 70 kDa band for NCX1 and 3 respectively were included in the analysis. * $p < 0.05$.

Therefore, we focused on NCX3 in an expanded analysis of the inflammation-induced changes in NCX protein in which we included both the time course of the changes and whether the decrease was uniform throughout the sensory neuron. Protein was extracted from central nerve, DRG, and sciatic nerve, and analyzed for the relative density of NCX3 at 1, 3, 7 and 14 days after the induction of inflammation. Results of this analysis indicated that changes over time in NCX3 protein in the DRG mirror that of the inflammation-induced decrease in NCX activity observed in isolated putative nociceptive DRG neurons with a decrease that peaks at day 3 post CFA and that rebounded significantly above baseline levels ($n = 4$, $p < 0.05$) by day 7 post CFA treatment (Figure 27A). In contrast, however, there was a robust inflammation-induced increase in NCX3 protein in the sciatic nerve that peaked at day 3 post CFA and resolved by day 7 post CFA ($p < 0.01$ Figure 27B). Interestingly, there was no inflammation-induced change in NCX3 in the central nerve ($p > 0.05$ Figure 27C). This loss of protein in the ganglia and an increase in the peripheral nerve only, near the peak of inflammation-induced loss of NCX activity, is suggestive of differential trafficking.

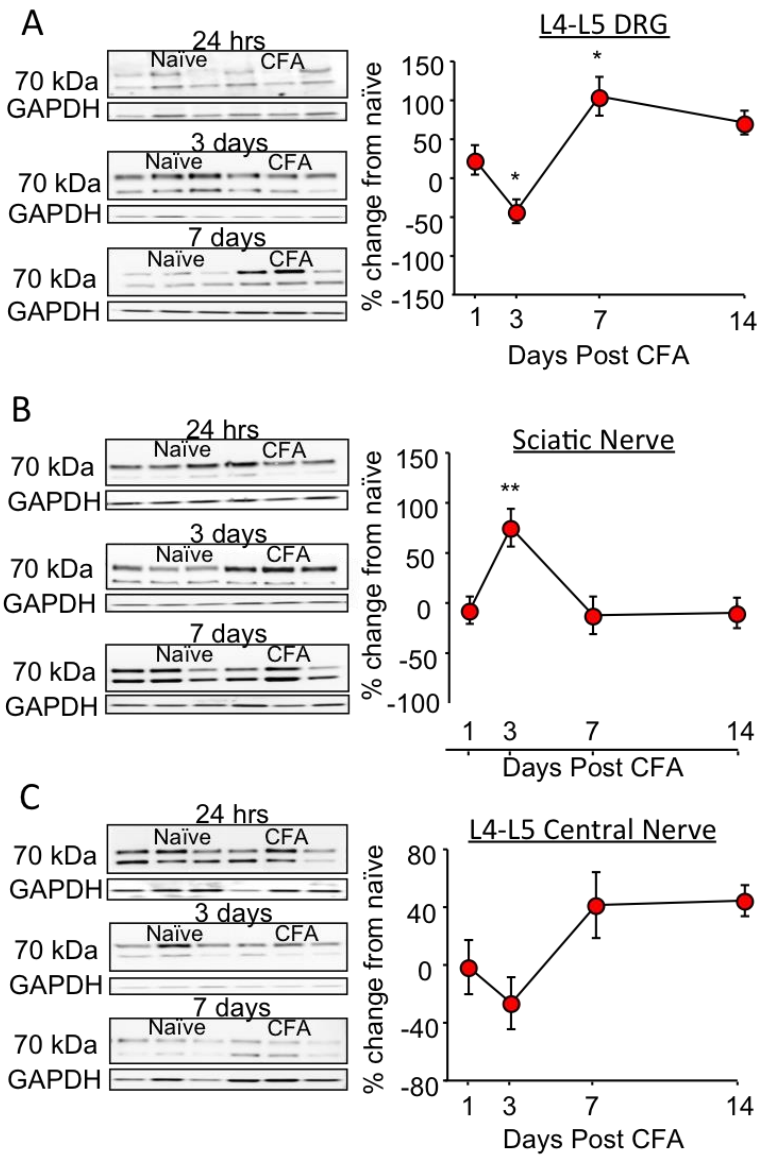

Figure 27: Time-dependent changes in NCX3 protein at three major sites in the nerve

Western blot analysis of total protein extracted from the L4 – L5 DRG (**A**), sciatic nerve (**B**), and central nerve (**C**) at 1, 3, 7, and 14 days the induction of inflammation with subcutaneous injection of CFA. Data were first normalized with respect to GAPDH, and then plotted as a percent change from naïve. Typical blots from animals treated with CFA after 1, 3 and 7 are shown. Pooled data are from 3 rats per time point. * $p < 0.05$, ** $p < 0.01$

To further test the hypothesis that the changes in NCX3 in the DRG and sciatic nerve were due to a change in trafficking of the exchanger, we employed a dual ligation of the sciatic nerve ipsilateral to the site of CFA injection in order to clearly differentiate trafficked protein from that synthesized locally. Ligatures were placed on the sciatic nerve of naïve rats ($n = 4$), or on that of rats ($n = 4$) 48 hrs after the induction of inflammation. The nerves were removed 24 hours after ligation and processed for immunohistochemical analysis. The ligation alone did not produce any detectable changes in NCX3-like immunoreactivity (LI) (Figure 28A). However, in the presence of inflammation, there was a robust increase in NCX3-LI proximal to the first ligature (Figure 28B). Pooled data confirm that the NCX3-LI proximal to the ligature was significantly greater in nerves from inflamed rats than that in nerves from naïve controls (Figure 28C, $p < 0.01$).

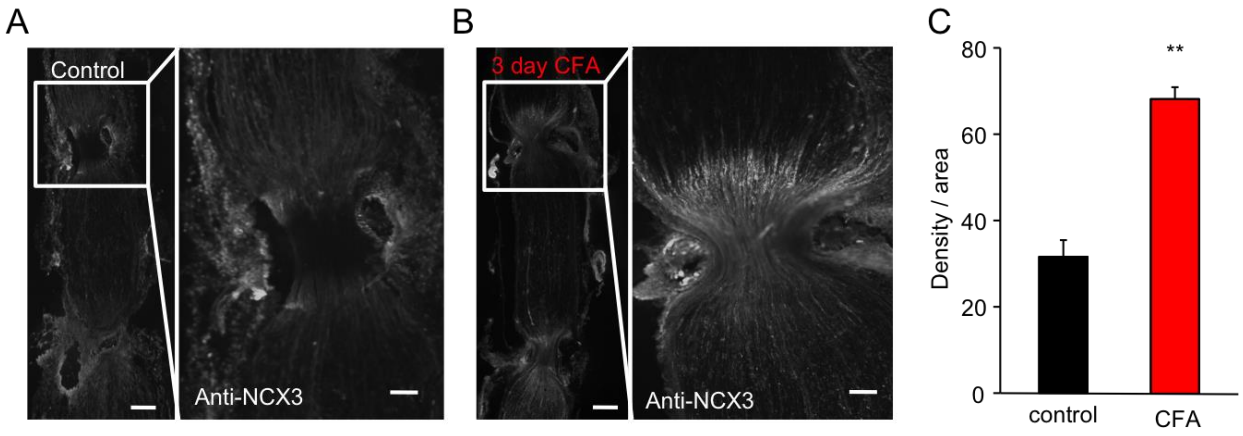

Figure 28: Inflammation-induced increase in NCX3 trafficking to the periphery

Immunohistochemical analysis of NCX3 like-immunreactivity (LI) in the sciatic nerve from a naïve rat (**A**), or from a rat three days after the induction of inflammation with CFA (**B**). Low powered micrographs (4x magnification, left) illustrate the double ligature sites. Higher powered micrographs (10x magnification, right) are of the proximal ligature site. Ligatures were placed 24 hr prior to tissue harvest. Scale bars in both 4x and 10x images are 200 μm **C**) Pooled densitometry data of nerve from control (black, n = 4) and inflamed (red, n = 4) rats. ** $p < 0.01$.

Finally, in order to determine if NCX3 protein was shipped to the terminals innervating the site of injury, western blot analysis was done to assess changes in NCX3 protein in the glabrous skin ipsilateral to CFA injection (n = 8). Results showed a significant increase in NCX3 in the skin from rats 3 days after CFA injection ($p < 0.01$ Figure 29).

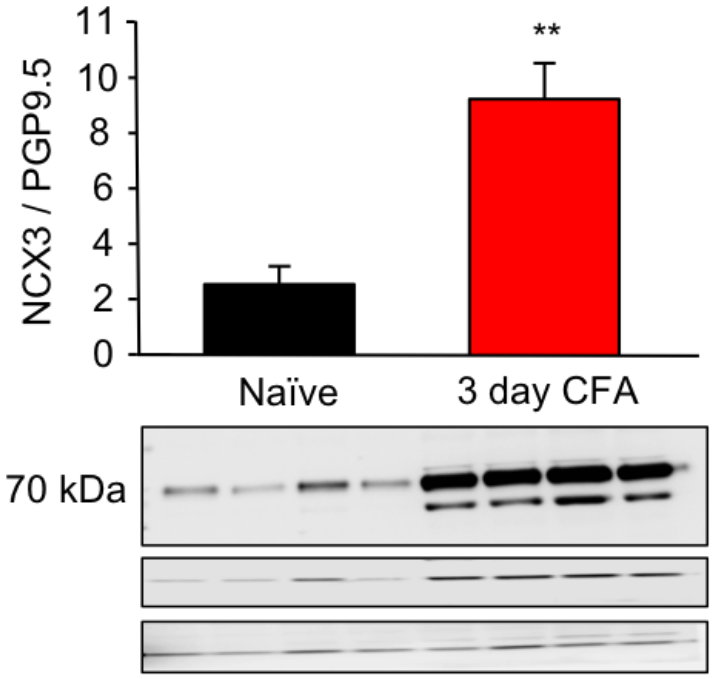

Figure 29: Inflammation-induced increase in NCX3 at the site of inflammation

The glabrous skin of naïve (n = 8) and inflamed (n = 8) rats 3 days after CFA injection was harvested and total protein was processed for western blot analysis of NCX3 content. Both GAPDH and the neural marker PGP9.5 were used as loading controls. To control for inflammation-induced increase in sprouting, pooled data were normalized to PGP9.5. A typical block is shown below the pooled data. ** $p < 0.01$

4.5 DISCUSSION

In the present study, we sought to test the hypothesis that a decrease in NCX activity contributes to the inflammation-induced increase in the duration of the depolarization-evoked Ca^{2+} transient in putative nociceptive cutaneous DRG neurons. Consistent with our previous results (Lu and Gold, 2008), inflammation was associated with an increase in both the magnitude and duration of the depolarization-evoked Ca^{2+} transient in the IB4+ subset of putative nociceptive cutaneous neurons. Also consistent with previous results, block of NCX in the IB4+ subset of putative nociceptive neurons from naïve rats by replacing Na^{+} in the bath with either Li^{+} or choline, or with the NCX3 blocker, KB-R7943, resulted in a significant increase in the duration of the evoked Ca^{2+} transient (Scheff et al., 2014). However, in neurons harvested from rats three days after the induction of inflammation, these manipulations had no detectable influence on the transient duration. Comparable data were obtained with electrophysiological analysis of the 0 mM Na^{+} bath-sensitive current in this population of neurons. Analysis of the time course of these changes indicated that they developed over the first three days after the induction of inflammation and resolved over the subsequent four to ten days. This trajectory mirrored the changes in CFA-induced nociceptive behavior. These changes in NCX activity in the isolated cell body were not associated with a detectable change in NCX expression. They were, however, associated with a significant decrease in NCX3, but not NCX1 or NCX2 protein in the cell body and an increase in NCX3 protein in the sciatic nerve. Sciatic nerve ligation at 48 hours after induction of inflammation resulted in a buildup of NCX3-LI proximal to the ligation site. Finally, there was a significant increase in NCX3-LI in the glabrous skin ipsilateral to CFA

injection. These results are consistent with our initial hypothesis and suggest that the decrease in NCX activity observed in the cell body is due to an increase in the trafficking of NCX3 to the site of inflammation.

The initial parametric experiment designed to establish the relationship between stimulus duration and the manifestation of the inflammation-induced changes in the evoked transient, indicated that mechanisms underlying the increase in both the magnitude and duration of the evoked transient had a high threshold for activation, requiring at least 4 s of depolarization. With respect to the duration of the evoked transient, these results were the first that were consistent with the hypothesis, that the inflammation-induced increase in transient duration is due to a decrease in NCX activity as NCX has been shown to be a low affinity mechanism requiring large $[Ca^{2+}]_i$ for activation. Furthermore, these results argue against a role of PMCA, a higher affinity protein thought to mediate Ca^{2+} homeostasis that should be revealed, if not at rest, than with a much shorter stimulus duration.

It is clear that there are Ca^{2+} regulatory mechanisms that can influence the magnitude, duration and/or both aspects of the evoked Ca^{2+} transient (Lu et al., 2006). Nevertheless, results of the present study indicate that the inflammation-induced increase in the evoked Ca^{2+} transient reflect changes in at least two Ca^{2+} distinct regulatory processes. That is, the increase in transient duration reflects a decrease in NCX activity. However, because NCX activity has no detectable influence on the magnitude of the evoked Ca^{2+} transient, the increase in magnitude must reflect another mechanism. Interestingly, this mechanism must account for the increase in the magnitude of the evoked transient in addition to a decrease in voltage-gated Ca^{2+} channel (VGCC) current density (Lu et al., 2010). This implies a shift in coupling between the initial Ca^{2+} influx via VGCCs, and an amplification system that ultimately influences the transient

magnitude. While ryanodine receptor mediated Ca^{2+}-induced Ca^{2+} release is a well described transient amplification system (Berridge, 2006), we were unable to implicate this system as a potential underlying mechanism of the inflammation-induced increase in the magnitude (Scheff et al., 2013). Furthermore, with evidence against a change in mitochondrial Ca^{2+} buffering as a potential mechanism of the increase in magnitude (Scheff et al., 2013), we are left suggesting far less conventional mechanisms may ultimately be responsible for this change. One such mechanism includes the sensitization of channels typically activated by exogenous stimuli such as ligand-gated transient receptor potential vanilloid 1 (TRPV1) or ankyrin 1 (TRPA1) receptors. TRPV1 in particular demonstrates some voltage-dependence (Matta and Ahern, 2007), and is not only upregulated in the presence of inflammation, but is sensitized (Julius, 2013). Thus, a depolarization-induced recruitment of TRPV1 could contribute to the inflammation-induced increase in the magnitude of the evoked transient.

It was striking that despite a relatively complete loss of NCX activity in neurons from CFA-treated rats, the duration of the evoked Ca^{2+} transient in the presence of inflammation was smaller than that observed following complete block of NCX activity in neurons from naïve rats with either 0 mM Na^{+} bath or the almost complete block of NCX with KB-R7943. While one might have predicted that a complete loss of NCX activity in the presence of inflammation would have resulted in a transient duration comparable to that observed in neurons from naïve animals following NCX block. This mismatch underscores the complex nature of Ca^{2+} regulatory processes. Even a small shift in the relative distribution of Ca^{2+} regulatory mechanisms can have a profound influence on the properties of the evoked transient, and as noted above, inflammation is associated with marked changes in at least three distinct Ca^{2+} regulatory processes. In previous studies we have attempted to rule out additional Ca^{2+} regulatory mechanisms through individual

assessment of different components of the Ca^{2+} signaling toolkit. It is possible, however, that the inflammation-induced increase in the duration of the transient due to the loss of NCX, or the mechanisms underlying the increase in magnitude or both could result in changes in the relative balance of other Ca^{2+} regulatory processes and thus the engagement of other proteins not normally involved in depolarization-evoked Ca^{2+} regulation. This concept has been demonstrated previously, in which a prolonged release of Ca^{2+} from ryanodine receptors normally buffered by the ER ATPase (SERCA) was shown to engage NCX-mediated extrusion in the presence of inflammation but not in the naïve state (Scheff et al., 2014). Thus, it is possible that the increase in the magnitude and duration of the evoked transient has activated additional processes such as a SERCA-uptake into the ER or additional mitochondrial buffering resulting in the attenuation of the evoked transient in the presence of a significant loss in NCX activity.

With several notable exceptions, the time course of the inflammation-induced changes in the evoked Ca^{2+} transient mirrors that of the inflammation-induced hypersensitivity. The observation that the time course of the increase in magnitude of the transient is not identical to that of the increase in duration (the former is still significantly elevated at 7 days post CFA, while the latter has fully recovered) lends further support to the suggestion that distinct mechanisms underlie these two changes. More interestingly, however, is that the significant increase in duration of the evoked transient fully recovered at a time point at which animals are still quite hypersensitive. This separation is also reflected in protein content, where there is a significant decrease in NCX3 protein in the DRG on day 3 post-CFA, which is not detectable at later time points. This suggests that the change in NCX might be more relevant for the initiation and maintenance but not the resolution of inflammation.

While the negative expression data should be interpreted with caution, the initial decrease in NCX activity and protein in the cell body could simply be due to protein turnover. However, the most likely explanation is protein trafficking. This is well supported by the increase in protein in the sciatic nerve at 3 days post-CFA and the increase in NCX-LI in the ligation experiment demonstrating that the increase in NCX3 is in the nerve and that the increase observed with western blot is not due to an infiltration of immune cells, previously shown to express NCX3 (Boscia et al., 2013, Staiano et al., 2013). The increase in NCX3 protein detected in the cell body at 7 days post-CFA injection in the absence of a detectable change in NCX activity in the isolated cell body suggests the increase in protein does not reflect functional protein. Instead, we propose that NCX activity in the cell body is relatively tightly regulated, with spare protein ready to be trafficked if needed. Furthermore, the normalization of NCX in the sciatic nerve lends additional support to the suggestion that NCX only contributes to the earlier stages of the inflammatory response.

While available evidence indicates that both the 70 kDa and 60 kDa bands detected by the NCX3 antibody reflect proteolytic cleavage products of NCX3 (Linck et al., 1998, Thurneysen et al., 2002b), it is interesting to note that the inflammation-induced changes in protein density were restricted to the 70 kDa band. The basis for this distinction is unclear, but may reflect differences in the relative stability of the two cleavage products thought to be the intracellular loop (60 kDa) cleaved from the remainder of the protein. It is possible that the inflammation-induced change in excitability (Zhang et al., 2012a) results in an activity-dependent increase in NCX turnover rate reflected as an CFA-induced increase cleavage products. We suggest this possibility, is unlikely, however, in the absence of a detectable change in NCX mRNA, and a decrease in NCX activity in the cell body that parallels the loss of NCX-

LI. Thus, a more likely possibility is that the trafficked NCX is processed differently that the NCX remaining in the cell body, resulting in the differential pattern of NCX3-LI.

Axonal transport of receptors has historically been found to be bidirectional and microtubule dependent: receptors are associated with vesicles that are externalized and internalized at the nerve terminals, and possibly recycled in the cell body (Laduron and Castel, 1990). Altered trafficking in response to paw inflammation has also been shown to occur with both receptors (Hassan et al., 1993) and peptides (Donnerer et al., 1992). The redistribution of NCX3 out of the DRG and toward the peripheral terminals but not the central terminals resembles the alterations reported with TRPV1 in the presence of inflammation (Ji et al., 2002) and the voltage gated sodium channel 1.8 (NaV1.8) after peripheral nerve injury (Novakovic et al., 1998) suggesting some sorting mechanism must be present within the primary afferent to achieve such directed traffic. Furthermore, there was no detection of significant change in retrograde transport of NCX back to the ganglia suggesting unidirectional transport to the site of inflammation.

Ultimately, the physiological impact of inflammation-induced trafficking depends on NCX function in the terminals and cell body. A decrease in exchanger activity at the cell body results in a change in the duration of the evoked transient. Given evidence that Ca^{2+} is the integrator underlying activity-dependent changes in gene expression (Fields et al., 2005), a change in the properties of the evoked Ca^{2+} transient should result in a change in gene expression. The trend toward the decrease in NCX3 in the central terminals, should, if anything, result in an increase in transmitter release from the central terminals. While there is no direct evidence of NCX-mediated regulation of neurotransmitter release to date, although many have speculated (Blaustein and Lederer, 1999, Jeon et al., 2003, Khananshvili, 2013), we hypothesize

that this was the most likely explanation for the hyperalgesia observed following siRNA-induced knock down of NCX3 (Scheff et al., 2014). In contrast, the increase in NCX in peripheral terminals should result in a decrease in transmitter release. While peptidergic fibers are generally considered in the context of peripheral transmitter release and neurogenic inflammation, there is growing evidence for functional glutamate receptors in the periphery, which may be either pro- or anti-nociceptive (Miller et al., 2011). Alternatively, a decrease in the duration of evoked Ca^{2+} transients in the periphery as a result of the increase in NCX activity may influence the excitability of the peripheral endings if the Ca^{2+} transient is coupled to a Ca^{2+}-dependent ion channel. For example, a decrease in Ca^{2+}-dependent K^+ channel activity should result in an increase in excitability, while a decrease in Ca^{2+}-dependent Cl^- channel activity should result in a decrease in excitability. Because trafficking of NCX3 occurs between days 4 and 7 in the time course of inflammation, one might speculate that this is an anti-nociceptive mechanism in which NCX is sent to the terminals to aid in the regulation of the inflammation-induced increase in activity where it may also limit Ca^{2+}-induced excitotoxicity that could result from ongoing activity in a subpopulation of afferents that are normally inactive. Thus, the impact of the change in NCX3 in the peripheral terminals will be highly context-dependent and likely to be highly dynamic.

5.0 DISCUSSION

5.1 INFLAMMATION-INDUCED DYSREGULATION OF INTRACELLULAR CALCIUM

I set out with the goal to determine the underlying mechanisms of the inflammation-induced changes in the magnitude and duration of the depolarization-evoked Ca^{2+} transient. I have made significant progress towards achieving this goal with the identification of machinery underlying, at least in part, the inflammation-induced increase in the duration of the evoked transient. Furthermore, while the Ca^{2+} regulatory system underlying the inflammation-induced increase in magnitude is still at large, I was able to rule out important additional mechanisms.

In the work described in Chapter 2, I hypothesized that inflammation-induced coupling of influx and release from intracellular stores would engage CICR and subsequently increase the magnitude of the evoked Ca^{2+} signal. However, results from these studies demonstrate that CICR does not appear to be engaged in the subpopulation of cutaneous putative nociceptive neurons with the largest inflammation-induced change in the evoked Ca^{2+} transient. Furthermore, there does not appear to be any inflammation-induced changes in SERCA function or mitochondrial buffering. I did, however, discover what appears to be the presence of tightly segregated Ca^{2+} regulatory domains that isolate cytosolic Ca^{2+} increased via influx from release. Furthermore, there appeared to be an inflammation-induced shift in the regulatory domains so

that prolonged Ca^{2+} release from ryanodine receptors engaged an additional extrusion mechanism, thought to be the Na^{+}/Ca^{2+} exchanger (NCX).

In Chapter 3, an extensive characterization of NCX in cutaneous putative nociceptive neurons from naïve rats was completed, encompassing biophysical properties, isoforms present, location within the neuron, and functional implications of NCX activity. In putative nonpeptidergic neurons only, there appear to be two modes of NCX activity: one evoked in response to relatively large and long lasting increases in the concentration of intracellular Ca^{2+} ($[Ca^{2+}]_i$), and a second that is active at resting $[Ca^{2+}]_i$. While mRNA encoding all three NCX isoforms (NCX1-3) was detectable with single cell PCR, pharmacological analysis suggested that NCX3 was responsible for the majority of activity in cutaneous neurons. Functional assays of excitability, action potential propagation, and nociceptive behavior suggest NCX activity has little influence on excitability, but instead influences axonal conduction velocity, resting membrane potential, and nociceptive threshold.

The last set of analyses focused on the impact of inflammation on NCX activity. Results indicated a significant inflammation-induced decrease in NCX activity in a subpopulation of putative nociceptive neurons innervating the site of inflammation. A time course of NCX activity in the isolated cell body and protein levels throughout the primary afferent suggested altered unidirectional trafficking of NCX3 to the peripheral terminals only. While the impact of an increase in NCX activity in the terminals at the site of injury is currently unknown, the inflammation-induced decrease in NCX activity at the level of cell body accounts for, at least in part, the inflammation-induced increase in the duration of the evoked Ca^{2+} transient in cutaneous putative nociceptive neurons.

The mechanism underlying the increase in magnitude is still unknown in this subpopulation of nociceptors. Previous work by Lu and colleagues demonstrate that the two mechanisms are most likely dissociable so that it is likely that whatever the mechanism turn out to be, it only influence the magnitude but not the duration of the evoked transient (Lu et al., 2006). As discussed in the Introduction, there are a number of influx and release mechanisms that add to the magnitude of the evoked Ca^{2+} transient. A decrease in VGCC current has been identified, and furthermore, it appears that neither release from ER through ryanodine receptors (Scheff et al., 2013) nor IP3 receptors (Lu et al., 2006) influence the depolarization-induced transient. While inflammation-induced changes in several potential ligand gated Ca^{2+} influx pathways (e.g. TRPV1 and TRPA1) have been identified (Ji et al., 2002, Shimosato et al., 2005, DeBerry et al., 2014), it is unlikely that these other influx pathways contribute to the increase in the depolarization-induced Ca^{2+} transient in sensory neurons which largely depends on the activation of VGCC. Although CICR does not appear to be engaged, preliminary data suggests that the increase in the magnitude of the evoked transient might be due to the recruitment of a pharmacologically distinct channel to store-operated Ca^{2+} entry (SOCE), thought to normally function as a mechanism for refilling intracellular Ca^{2+} stores. This is suggested by the observation that SOCE, as assessed with a brief application of extracellular Ca^{2+} following depletion of intracellular stores, is significantly increased in cutaneous putative nociceptive neurons from inflamed rats. Additional experiments will need to be done to understand how this mechanism contributes to the depolarization-induced Ca^{2+} transient in the absence of CICR.

The approach to study the different Ca^{2+} regulatory mechanisms has been to assess the function of each component individually. Furthermore, data presented here suggest that in the presence of inflammation there is a potential shift in the organization of cytosolic

microdomains such that mechanisms underlying influx and release can now interact. Without a good understanding of the spatial orientation or all of the components involved in these microdomains at the level of the cell body, it is possible that I may have missed inflammation-induced changes in regulatory components with this experimental approach. Therefore, to better understand the underlying mechanism of intracellular Ca^{2+} regulation both in the naïve state and in the presence of injury, it might be useful to study the interaction of Ca^{2+} machinery or mechanisms in combination, instead of the how the system functions in the absence of a single mechanism.

5.2 A ROLE FOR NCX IN INFLAMMATORY PAIN SIGNALING

Tissue inflammation is associated with ongoing pain and hyperalgesia that is reflected in three major components: 1) an increase in primary afferent excitability resulting in an increase in input to the central nervous system 2) a change in gene expression secondary to altered Ca^{2+} signaling in the cell body, and 3) an increase in neurotransmitter release in the periphery resulting in a neurogenic inflammatory response. I hypothesize that the inflammation-induced trafficking of NCX3 to the periphery plays a role in all three of these mechanisms.

A lack of inflammation-induced trafficking of NCX3 to the central terminals during the initiation of the inflammation suggests an undeterred increase in neurotransmitter release into the dorsal horn. Previous data from this lab has demonstrated that inflammation is associated with a significant decrease in VGCC current density at the level of the cell body, and furthermore, this loss of VGCC current is thought to result in a decrease Ca^{2+}-dependent K^{+} (BK) currents, which normally serve to repolarize the membrane potential following an action

potential (AP) and to mediate adaptation in response to sustained membrane depolarization (Zhang et al., 2012a). A loss of BK current in response to a decrease in VGCC current is thought to contribute to the inflammation-induced afferent sensitization and subsequently an increase in excitability. The loss in VGCC current is, at least in part, due to trafficking of α2δ1 and CaV2.2 protein to the central terminal. Inflammation-induced increase in excitability in the presence of an increase in VGCC current in the central terminals, but without a subsequent increase in the major Ca^{2+} extrusion protein, NCX, will most likely result in an increase in neurotransmitter release into the central nervous system and ultimately more pain.

Adaptive responses of neurons often require changes in gene expression and there have been numerous accounts of differential changes in gene expression in response to tissue inflammation (Qiu et al., 2012, Schwartz et al., 2013). Because information in the environment is coded in the patterns of AP firing, adaptive changes in gene expression must be regulated by the pattern of APs. Furthermore, studies have shown that AP-mediated Ca^{2+} mobilization, when delivered at an appropriate temporal interval, can be effective in regulating the transcription of genes (Fields et al., 2005). The temporal dynamics of $[Ca^{2+}]_i$ can be more important than the magnitude of the Ca^{2+} change in decoding AP firing, therefore, a loss of NCX activity at the level of the cell body resulting in an increase in the duration of the Ca^{2+} signal should result in changes in gene transcription in the presence of inflammation.

Lastly, tissue inflammation is associated with an increase in the release of neuropeptides and glutamate into the periphery to cause neurogenic inflammation and sensitization of surrounding afferent terminals respectively (Skerry and Genever, 2001, Carozzi et al., 2008). Glutamate has been demonstrated to produce nociceptive effects in animals and humans when injected directly (Miller et al., 2011) and indirectly influencing efferent release of

CGRP, ATP and nitric oxide as well through glutamate receptors expressed on peptidergic fibers and resident microglia (Jackson and Hargreaves, 1999, Beirith et al., 2002). Inflammation-induced trafficking of NCX3 to the peripheral terminals will aid in the control of activity-induced increase $[Ca^{2+}]_i$ at the terminals. The trafficking of NCX only appears to occur in IB4+, putative nonpeptidergic fibers, thus an increase in NCX activity will result in a decrease in efferent glutamate release.

All together, these data suggest a mechanism in which NCX is trafficked to the peripheral terminals to regulate activity and in response, there is an increase in Ca^{2+} transient duration in the cell body, most likely an increase in neurotransmitter release into the central nervous system, although this has not been tested directly. The time course of this mechanism appears to normalize as nociceptive sensitivity resolves suggesting that prolonged peripheral activity in the absence of NCX transport to the terminals to regulate $[Ca^{2+}]_i$ might result in extended neurogenic inflammation and immune response, and excitotoxic levels of glutamate resulting in a persistent inflammatory state.

5.3 IMPLICATIONS FOR DIFFERENT MODELS OF INFLAMMATION

There is an inflammatory component associated with many different pain types, such as nerve injury, cancer pain, pancreatitis, and migraine. Furthermore, the degree of inflammation and the underlying mechanisms responsible for the inflammation vary. It is possible that the mechanism underlying the initiation of inflammation dictates the signaling cascade (e.g. TLR4, NGF, MCP-1) and subsequently the changes in $[Ca^{2+}]_i$. Complete freud's adjuvant (CFA) is the model used to drive persistent peripheral inflammation resulting in the inflammation-induced

changes in the depolarization-evoked Ca^{2+} transient. However, it is unclear whether the underlying signaling initiating the changes in Ca^{2+} regulation and subsequently NCX trafficking will occur with lesser stimuli, across species, or with other types of peripheral inflammation. The peripheral CFA-induced inflammation model is an effective means for stimulation of a local innate immune response through heat shock protein-induced activation of the toll-like receptor 4 (TLR4) signaling cascades (Billiau and Matthys, 2001) similar to the action of lipopolysaccharides (LPS) released from gram-negative bacteria. It is important to note that the CFA model resembles more closely a model for bacterial infection than other models of inflammation such as intra-dermal injection of individual endogenous algogens such as bradykinin (Rang et al., 1991), models of autoimmune inflammation (Tian et al., 2013), inflammation associated with tissue damage (osteoarthritis model with tendon cut) (Fernihough et al., 2004), or even other forms of infection (yeast vs bacteria) (Watkins et al., 2007). Therefore, it is likely that the changes seen with CFA-induced inflammation will not apply to all types of inflammation. For example, despite the inflammatory component to peripheral nerve injury, the dysregulation in $[Ca^{2+}]_i$ in the presence of nerve injury does not share many similarities with those seen in the presence of inflammation. The spinal nerve ligation model of painful nerve injury results in a decrease in resting $[Ca^{2+}]_i$, depleted intracellular Ca^{2+} stores and an increase in PMCA activity in small and medium diameter neurons (Rigaud et al., 2009). However, the inflammation-increase in the magnitude and duration of the depolarization-evoked Ca^{2+} transient appeared to be a common response to persistent inflammation across specifics, as similar changes were observed in retrogradely labeled neurons from mice in association caerulein-induced inflammation of the pancreas (Schwartz et al., 2013), and cyclophosphamide-induced inflammation of the bladder (DeBerry et al., 2014).

A common quality of most inflammatory models is the interaction with the immune system, recruitment of immune cells and subsequent release of both pro- and anti-inflammatory mediators. While I have focused on persistent inflammation-induced regulation of NCX, there is evidence that NCX isoforms are regulated by second messenger cascades activated by a variety of inflammatory mediators. In non-neuronal cell systems, exposure to pro-inflammatory cytokines, TNFα and IL-13, resulted in an increase in NCX expression, protein, and function, whereas inhibition of NCX function occurred following histamine stimulation (Sathish et al., 2011). Nerve growth factor (NGF), a prototypical inflammatory mediator (Bennett, 2001), has been shown to regulate of NCX expression and activity PC12 cells (Sirabella et al., 2012), increase NCX activity in forward mode via p38 activation. NCX activity may also be increased via activation of PKC (Iwamoto et al., 1996) or PI3K/AkT signaling (Sisalli 2014), all activated by an array of inflammatory mediators. Because NCX is not only present but also functional in the cell body (Verdru et al., 1997, Lu et al., 2006, Scheff et al., 2014), peripheral (Scheff et al., 2014) and central (Shutov et al., 2013) axons of primary afferent C fibers, these data suggest that there is potential for acute differential modulation of NCX activity by inflammatory mediators on top of the persistent inflammation-induced changes occurring at all levels of the afferent. The functional implications of acute modulation of NCX activity would depend on where it was manifest. With evidence of inflammation-induced changes second messenger signaling cascades (Hucho and Levine, 2007) and increase NCX protein in the terminals, it is possible that NCX may be dynamically regulated by the actions of inflammatory mediators, thereby implying a more complex role for NCX in the inflammatory response than originally hypothesized.

Hypersensitivity resulting from subcutaneous CFA appears to last roughly two weeks and the time course of NCX trafficking within putative nonpeptidergic fibers mostly mirrors this

trajectory. This begs the question of what is the underlying mechanism in the presence of chronic inflammation lasting months to years. There is a substantial amount of literature implicating increased glutamate release as an underlying cause for pain associated with a chronic arthritis-like inflammatory conditions in both rodent models and in humans (Leem et al., 2001, Walker et al., 2001, Du et al., 2003). Inflammatory animal models demonstrate increased levels of glutamate in peripheral tissues and that peripheral glutamate, interacting with numerous excitatory amino acid receptors (EAARs), produces nociceptive behavior (Miller et al., 2011). Administration of glutaminase inhibitors blocking the synthesis of glutamate in arthritis-like inflammatory animal models produces long lasting analgesia (Miller et al., 2011). Inflammation-induced glutamate elevation has also been confirmed in humans with chronic arthritis as well, such that synovial glutamate concentrations are over fifty times the concentration from non-arthritic controls (McNearney et al., 2000, McNearney et al., 2004). Lidocaine injection in the knee joint prevented the glutamate elevation implicating joint nerve terminals as the source of the inflammation-induced increase (Lawand et al., 2000). With evidence that peptidegeric fibers do not contain adequent machinery for glutametergic signaling, these data implicated hyperactivity of the putative nonpeptidergic fiber population as playing a major role in hyperaglesia associated with arthritis-like inflammatory. Based on the hypothesis that NCX plays a pivotal role in primary afferent signaling in the presence of inflammation, it is possible that in these more chronic inflammatory states, a failure to continually transport NCX to the terminals might result in the failure of acute inflammation to fully resolve. A potential therapeutic approach to increase NCX activity at the peripheral terminal in the presence of persistent inflammation might aid in the reduction in nonpeptidergic fiber activity specifically and reduce primary afferent activity devoid of any major side effects.

5.4 LIMITATIONS OF EXPERIMENTAL APPROACH: LOOKING BEYOND THE CELL BODY

The heterogeneity in the underlying mechanisms of Ca^{2+} regulation during inflammatory pain in the peripheral neuron truly underscores the importance of recognizing the complexity of these two systems. While not without its limitations, the work described here highlights four major components of experimental design critical for interpretation of results. The first is the identification of the tissue of innervation. There is a tremendous amount of evidence demonstrating the differences between primary afferents innervating the visceral system versus somatic and muscle tissues (Raja et al., 1988, Sessle and Hu, 1991, Robinson and Gebhart, 2008). Therefore, when assessing changes in the putative nociceptor cell body, the use of retrograde dyes injected into the target tissue for identification of the subpopulation of interest among all others in the ganglia is a crucial component.

The second is the uses of additional histological and functional markers to further identify the groups within the subpopulation of interest. As described in the Introduction, a substantial amount of work has been done to classify types of nociceptors in the naïve animal. Because evidence suggests that the heterogeneity in pain phenotypes is reflected, at least in part, by the heterogeneity of primary afferents, a better understanding of the qualifications of afferents involved has the potential to yield a more specific the therapeutic approach. However, it is important to note that while nociceptors differentially express a variety of anatomical and biochemical markers, there are important species differences (Price and Flores, 2007). Furthermore, injury-induced changes afferent function (e.g. “silent” nociceptors) and marker expression (Woodbury et al., 2008, Jankowski et al., 2012) makes post hoc identification of the population responsible for the pain signaling more challenging.

Third, while one of the advantages to the use of whole cell patch electrophysiology recordings are the ability to control both intracellular and extracellular milieu, however, this technique has its limitations, especially in regard to intracellular Ca^{2+} regulation. During whole-cell recordings, irreversible 'washout' of diffusible intracellular constituents, such as ATP, phosphorylating molecules, and most importantly intracellular Ca^{2+}, through dialysis can significantly impair the properties and functions of ion channels and complicating data analysis. However, the perforated patch clamp technique avoids this problem by accessing the intracellular space with pore-forming fungicides in the electrode solution allowing the entire cell to be voltage-clamped without disrupting its contents and the integrated activity of all the Ca^{2+} channels, pumps, and exchangers in the membrane can be measured (Inayat et al., 2010). Because of its electrogenic properties, whole cell patch clamp recording of NCX current relies on manipulation of the artificial ionic environment for activation. However, the perforated patch technique allows for the assessment of NCX in a more natural state. Furthermore, using the perforated patch clamp technique combine with fura-2AM imaging allows for the ability to simultaneously study the $[Ca^{2+}]_i$ and the electrophysiological properties of the cell such that the relative contribution of voltage dependent and -independent processes can be assessed that govern intracellular Ca^{2+} homeostasis.

Lastly, the cell body has served as an extremely useful model to study molecules and modulatory mechanisms mediating nociceptor transduction and sensitization, as many of these mechanisms are manifest in the cell body. Furthermore, the soma expresses many molecular entities that are expressed in free nerve endings both at the central and peripheral terminals (Malin et al., 2007). However, as a model, it has limitations. The spatial distribution of cytosolic components is not the same throughout the neuron suggesting different protein-protein

interaction. Furthermore, there appear to be differences in transduction and spike adaptation processes. The underlying differences may be due the lack of non-neuronal peripheral components required in vivo or differential distribution and modulation of transduction molecules. Interpreting injury-induced changes may be most misleading if the cell body is studied in isolation as demonstrated in the work described here, a loss of NCX activity in the cell body, while still important for pain signaling in the presence of inflammation, is not representative of what is happening at either the central or the peripheral terminals. This underscores the importance of corroborating results from cultured neurons with additional approaches attempting to retain an intact terminal field as well as behavior.

5.5 CONCLUSIONS AND FUTURE DIRECTIONS

All together this work emphasizes the importance of the regulation of intracellular Ca^{2+} in the initiation, maintenance and potentially resolution of hyperalgesia in the presence of inflammation. In the future, it will be necessary to figure out what NCX3 is doing on a functional level in the peripheral terminals. Furthermore, upon the discovery of the underlying mechanisms of the inflammation-induced increase in the magnitude of the evoked transient, it will be important to explore the interactions of these two mechanisms both at the cell body and in the terminals. As new technologies come available, it will be essential to look at multiple levels of this heterogeneous nociceptive system simultaneously to decode how changes in the intracellular Ca^{2+} signaling at different levels of the neuron results in functional aspects, such as excitability and neurotransmission at both the central and peripheral terminals for a better understanding of how to target this system effectively in the presence of chronic pain.

BIBLIOGRAPHY

Acosta C, Djouhri L, Watkins R, Berry C, Bromage K, Lawson SN (2014) TREK2 expressed selectively in IB4-binding C-fiber nociceptors hyperpolarizes their membrane potentials and limits spontaneous pain. The Journal of neuroscience : the official journal of the Society for Neuroscience 34:1494-1509.

Aley KO, Levine JD (2002) Different peripheral mechanisms mediate enhanced nociception in metabolic/toxic and traumatic painful peripheral neuropathies in the rat. Neuroscience 111:389-397.

Annunziato L, Pignataro G, Di Renzo GF (2004) Pharmacology of brain Na+/Ca2+ exchanger: from molecular biology to therapeutic perspectives. Pharmacological reviews 56:633-654.

Baccei ML, Kocsis JD (2000) Voltage-gated calcium currents in axotomized adult rat cutaneous afferent neurons. J Neurophysiol 83:2227-2238.

Bautista DM, Siemens J, Glazer JM, Tsuruda PR, Basbaum AI, Stucky CL, Jordt SE, Julius D (2007) The menthol receptor TRPM8 is the principal detector of environmental cold. Nature 448:204-208.

Beirith A, Santos AR, Calixto JB (2002) Mechanisms underlying the nociception and paw oedema caused by injection of glutamate into the mouse paw. Brain research 924:219-228.

Bennett DL (2001) Neurotrophic factors: important regulators of nociceptive function. The Neuroscientist : a review journal bringing neurobiology, neurology and psychiatry 7:13-17.

Berridge MJ (2006) Calcium microdomains: organization and function. Cell Calcium 40:405-412.

Berridge MJ, Bootman MD, Roderick HL (2003) Calcium signalling: dynamics, homeostasis and remodelling. Nat Rev Mol Cell Biol 4:517-529.

Berridge MJ, Lipp P, Bootman MD (2000) The versatility and universality of calcium signalling. Nat Rev Mol Cell Biol 1:11-21.

Bessou P, Perl ER (1969) Response of cutaneous sensory units with unmyelinated fibers to noxious stimuli. J Neurophysiol 32:1025-1043.

Billiau A, Matthys P (2001) Modes of action of Freund's adjuvants in experimental models of autoimmune diseases. Journal of leukocyte biology 70:849-860.

Birinyi P, Acsai K, Banyasz T, Toth A, Horvath B, Virag L, Szentandrassy N, Magyar J, Varro A, Fulop F, Nanasi PP (2005) Effects of SEA0400 and KB-R7943 on Na+/Ca2+ exchange current and L-type Ca2+ current in canine ventricular cardiomyocytes. Naunyn-Schmiedeberg's archives of pharmacology 372:63-70.

Blaustein MP, Lederer WJ (1999) Sodium/calcium exchange: its physiological implications. Physiol Rev 79:763-854.

Boscia F, D'Avanzo C, Pannaccione A, Secondo A, Casamassa A, Formisano L, Guida N, Scorziello A, Di Renzo G, Annunziato L (2013) New roles of NCX in glial cells: activation of microglia in ischemia and differentiation of oligodendrocytes. Advances in experimental medicine and biology 961:307-316.

Bourinet E, Altier C, Hildebrand ME, Trang T, Salter MW, Zamponi GW (2014) Calcium-permeable ion channels in pain signaling. Physiol Rev 94:81-140.

Boyman L, Hagen BM, Giladi M, Hiller R, Lederer WJ, Khananshvili D (2011) Proton-sensing Ca2+ binding domains regulate the cardiac Na+/Ca2+ exchanger. J Biol Chem 286:28811-28820.

Braz JM, Nassar MA, Wood JN, Basbaum AI (2005) Parallel "pain" pathways arise from subpopulations of primary afferent nociceptor. Neuron 47:787-793.

Cao YQ, Mantyh PW, Carlson EJ, Gillespie AM, Epstein CJ, Basbaum AI (1998) Primary afferent tachykinins are required to experience moderate to intense pain. Nature 392:390-394.

Carafoli E, Santella L, Branca D, Brini M (2001) Generation, control, and processing of cellular calcium signals. Crit Rev Biochem Mol Biol 36:107-260.

Carozzi V, Marmiroli P, Cavaletti G (2008) Focus on the role of Glutamate in the pathology of the peripheral nervous system. CNS & neurological disorders drug targets 7:348-360.

Caterina MJ, Julius D (1999) Sense and specificity: a molecular identity for nociceptors. Current opinion in neurobiology 9:525-530.

Caterina MJ, Leffler A, Malmberg AB, Martin WJ, Trafton J, Petersen-Zeitz KR, Koltzenburg M, Basbaum AI, Julius D (2000) Impaired nociception and pain sensation in mice lacking the capsaicin receptor. Science 288:306-313.

Chen SR, Li X, Ebisawa K, Zhang L (1997) Functional characterization of the recombinant type 3 Ca2+ release channel (ryanodine receptor) expressed in HEK293 cells. J Biol Chem 272:24234-24246.

Cheng LZ, Lu N, Zhang YQ, Zhao ZQ (2010) Ryanodine receptors contribute to the induction of nociceptive input-evoked long-term potentiation in the rat spinal cord slice. Mol Pain 6:1.

Chiu IM, von Hehn CA, Woolf CJ (2012) Neurogenic inflammation and the peripheral nervous system in host defense and immunopathology. Nature neuroscience 15:1063-1067.

Cook O, Low W, Rahamimoff H (1998) Membrane topology of the rat brain Na+-Ca2+ exchanger. Biochim Biophys Acta 1371:40-52.

Davis JB, Gray J, Gunthorpe MJ, Hatcher JP, Davey PT, Overend P, Harries MH, Latcham J, Clapham C, Atkinson K, Hughes SA, Rance K, Grau E, Harper AJ, Pugh PL, Rogers DC, Bingham S, Randall A, Sheardown SA (2000) Vanilloid receptor-1 is essential for inflammatory thermal hyperalgesia. Nature 405:183-187.

De Col R, Messlinger K, Carr RW (2008) Conduction velocity is regulated by sodium channel inactivation in unmyelinated axons innervating the rat cranial meninges. J Physiol 586:1089-1103.

DeBerry JJ, Schwartz ES, Davis BM (2014) TRPA1 mediates bladder hyperalgesia in a mouse model of cystitis. Pain.

DiPolo R, Beauge L (2006) Sodium/calcium exchanger: influence of metabolic regulation on ion carrier interactions. Physiol Rev 86:155-203.

Donnerer J, Schuligoi R, Stein C (1992) Increased content and transport of substance P and calcitonin gene-related peptide in sensory nerves innervating inflamed tissue: evidence for a regulatory function of nerve growth factor in vivo. Neuroscience 49:693-698.

Du J, Zhou S, Coggeshall RE, Carlton SM (2003) N-methyl-D-aspartate-induced excitation and sensitization of normal and inflamed nociceptors. Neuroscience 118:547-562.

Duchen MR (1990) Effects of metabolic inhibition on the membrane properties of isolated mouse primary sensory neurones. J Physiol (Lond) 424:387-409.

Eun SY, Jung SJ, Park YK, Kwak J, Kim SJ, Kim J (2001) Effects of capsaicin on Ca(2+) release from the intracellular Ca(2+) stores in the dorsal root ganglion cells of adult rats. Biochemical and biophysical research communications 285:1114-1120.

Evans AR, Nicol GD, Vasko MR (1996) Differential regulation of evoked peptide release by voltage-sensitive calcium channels in rat sensory neurons. Brain research 712:265-273.

Fang X, McMullan S, Lawson SN, Djouhri L (2005) Electrophysiological differences between nociceptive and non-nociceptive dorsal root ganglion neurones in the rat in vivo. J Physiol 565:927-943.

Fang Y, Condrescu M, Reeves JP (1998) Regulation of Na+/Ca2+ exchange activity by cytosolic Ca2+ in transfected Chinese hamster ovary cells. Am J Physiol 275:C50-55.

Fernihough J, Gentry C, Malcangio M, Fox A, Rediske J, Pellas T, Kidd B, Bevan S, Winter J (2004) Pain related behaviour in two models of osteoarthritis in the rat knee. Pain 112:83-93.

Fields RD, Lee PR, Cohen JE (2005) Temporal integration of intracellular Ca2+ signaling networks in regulating gene expression by action potentials. Cell Calcium 37:433-442.

Flake NM, Gold MS (2005) Inflammation alters sodium currents and excitability of temporomandibular joint afferents. Neurosci Lett 384:294-299.

Friel DD, Tsien RW (1994) An FCCP-sensitive Ca2+ store in bullfrog sympathetic neurons and its participation in stimulus-evoked changes in [Ca2+]i. The Journal of neuroscience : the official journal of the Society for Neuroscience 14:4007-4024.

Fuchs A, Rigaud M, Hogan QH (2007) Painful nerve injury shortens the intracellular Ca2+ signal in axotomized sensory neurons of rats. Anesthesiology 107:106-116.

Gauriau C, Bernard JF (2002) Pain pathways and parabrachial circuits in the rat. Experimental physiology 87:251-258.

Gemes G, Bangaru ML, Wu HE, Tang Q, Weihrauch D, Koopmeiners AS, Cruikshank JM, Kwok WM, Hogan QH (2011) Store-operated Ca2+ entry in sensory neurons: functional role and the effect of painful nerve injury. The Journal of neuroscience : the official journal of the Society for Neuroscience 31:3536-3549.

Gemes G, Oyster KD, Pan B, Wu HE, Bangaru ML, Tang Q, Hogan QH (2012) Painful nerve injury increases plasma membrane Ca2+-ATPase activity in axotomized sensory neurons. Mol Pain 8:46.

Gold MS, Thut PD (2001a) Lithium increases potency of lidocaine-induced block of voltage-gated na(+) currents in rat sensory neurons in vitro. J Pharmacol Exp Ther 299:705-711.

Gold MS, Thut PD (2001b) Lithium increases potency of lidocaine-induced block of voltage-gated Na+ currents in rat sensory neurons in vitro. The Journal of pharmacology and experimental therapeutics 299:705-711.

Gracely RH, Lynch SA, Bennett GJ (1992) Painful neuropathy: altered central processing maintained dynamically by peripheral input. Pain 51:175-194.

Grynkiewicz G, Poenie M, Tsien RY (1985) A new generation of Ca2+ indicators with greatly improved fluorescence properties. J Biol Chem 260:3440-3450.

Harper AA, Lawson SN (1985) Conduction velocity is related to morphological cell type in rat dorsal root ganglion neurones. J Physiol 359:31-46.

Hassan AH, Ableitner A, Stein C, Herz A (1993) Inflammation of the rat paw enhances axonal transport of opioid receptors in the sciatic nerve and increases their density in the inflamed tissue. Neuroscience 55:185-195.

Herbert CP, Wright JM, Maclure M, Wakefield J, Dormuth C, Brett-MacLean P, Legare J, Premi J (2004) Better Prescribing Project: a randomized controlled trial of the impact of case-based

educational modules and personal prescribing feedback on prescribing for hypertension in primary care. Family practice 21:575-581.

Hermans AN, Glitsch HG, Verdonck F (1997) Activation of the Na+/K+ pump current by intra- and extracellular Li ions in single guinea-pig cardiac cells. Biochim Biophys Acta 1330:83-93.

Hilge M (2012) Ca2+ regulation of ion transport in the Na+/Ca2+ exchanger. J Biol Chem 287:31641-31649.

Hilgemann DW, Matsuoka S, Nagel GA, Collins A (1992) Steady-state and dynamic properties of cardiac sodium-calcium exchange. Sodium-dependent inactivation. J Gen Physiol 100:905-932.

Hille B (1972) The permeability of the sodium channel to metal cations in myelinated nerve. J Gen Physiol 59:637-658.

Hoesch RE, Weinreich D, Kao JP (2001) A novel Ca(2+) influx pathway in mammalian primary sensory neurons is activated by caffeine. J Neurophysiol 86:190-196.

Hogan QH, McCallum JB, Sarantopoulos C, Aason M, Mynlieff M, Kwok WM, Bosnjak ZJ (2000) Painful neuropathy decreases membrane calcium current in mammalian primary afferent neurons. Pain 86:43-53.

Hucho T, Levine JD (2007) Signaling pathways in sensitization: toward a nociceptor cell biology. Neuron 55:365-376.

Inayat S, Zhao Y, Cantrell DR, Dikin D, Pinto LH, Troy JB (2010) A novel way to go whole-cell in patch-clamp experiments. IEEE transactions on bio-medical engineering 57.

Iwamoto T, Shigekawa M (1998) Differential inhibition of Na+/Ca2+ exchanger isoforms by divalent cations and isothiourea derivative. The American journal of physiology 275:C423-430.

Iwamoto T, Watano T, Shigekawa M (1996) A novel isothiourea derivative selectively inhibits the reverse mode of Na+/Ca2+ exchange in cells expressing NCX1. J Biol Chem 271:22391-22397.

Jackson DL, Hargreaves KM (1999) Activation of excitatory amino acid receptors in bovine dental pulp evokes the release of iCGRP. Journal of dental research 78:54-60.

Jackson JG, Thayer SA (2006) Mitochondrial modulation of Ca2+ -induced Ca2+ -release in rat sensory neurons. J Neurophysiol 96:1093-1104.

Jang JH, Kim DW, Sang Nam T, Se Paik K, Leem JW (2004) Peripheral glutamate receptors contribute to mechanical hyperalgesia in a neuropathic pain model of the rat. Neuroscience 128:169-176.

Jankowski MP, Soneji DJ, Ekmann KM, Anderson CE, Koerber HR (2012) Dynamic changes in heat transducing channel TRPV1 expression regulate mechanically insensitive, heat sensitive C-

fiber recruitment after axotomy and regeneration. The Journal of neuroscience : the official journal of the Society for Neuroscience 32:17869-17873.

Jeon D, Yang YM, Jeong MJ, Philipson KD, Rhim H, Shin HS (2003) Enhanced learning and memory in mice lacking Na+/Ca2+ exchanger 2. Neuron 38:965-976.

Jeyakumar LH, Copello JA, O'Malley AM, Wu GM, Grassucci R, Wagenknecht T, Fleischer S (1998) Purification and characterization of ryanodine receptor 3 from mammalian tissue. J Biol Chem 273:16011-16020.

Ji RR, Samad TA, Jin SX, Schmoll R, Woolf CJ (2002) p38 MAPK activation by NGF in primary sensory neurons after inflammation increases TRPV1 levels and maintains heat hyperalgesia. Neuron 36:57-68.

Julius D (2013) TRP channels and pain. Annual review of cell and developmental biology 29:355-384.

Kao CH, Wang SJ, Chen CY, Yeh SH (1994) Detection of esophageal carcinoma using Tc-99m MIBI SPECT imaging. Clin Nucl Med 19:1069-1074.

Kao JP (1994) Practical aspects of measuring [Ca2+] with fluorescent indicators. Methods Cell Biol 40:155-181.

Karashima Y, Prenen J, Meseguer V, Owsianik G, Voets T, Nilius B (2008) Modulation of the transient receptor potential channel TRPA1 by phosphatidylinositol 4,5-biphosphate manipulators. Pflugers Arch 457:77-89.

Khananshvili D (2013) The SLC8 gene family of sodium-calcium exchangers (NCX) - structure, function, and regulation in health and disease. Molecular aspects of medicine 34:220-235.

Koerber HR, Druzinsky RE, Mendell LM (1988) Properties of somata of spinal dorsal root ganglion cells differ according to peripheral receptor innervated. J Neurophysiol 60:1584-1596.

Koerber HR, McIlwrath SL, Lawson JJ, Malin SA, Anderson CE, Jankowski MP, Davis BM (2010) Cutaneous C-polymodal fibers lacking TRPV1 are sensitized to heat following inflammation, but fail to drive heat hyperalgesia in the absence of TPV1 containing C-heat fibers. Mol Pain 6:58.

Koerber HR, Mendell LM (1988) Functional specialization of central projections from identified primary afferent fibers. J Neurophysiol 60:1597-1614.

Kofuji P, Lederer WJ, Schulze DH (1994) Mutually exclusive and cassette exons underlie alternatively spliced isoforms of the Na/Ca exchanger. J Biol Chem 269:5145-5149.

Kuroda H, Sobhan U, Sato M, Tsumura M, Ichinohe T, Tazaki M, Shibukawa Y (2013) Sodium-calcium exchangers in rat trigeminal ganglion neurons. Mol Pain 9:22.

Laduron PM, Castel MN (1990) Axonal transport of receptors. A major criterion for presynaptic localization. Ann N Y Acad Sci 604:462-469.

Lawand NB, McNearney T, Westlund KN (2000) Amino acid release into the knee joint: key role in nociception and inflammation. Pain 86:69-74.

Lawson SN (2002) Phenotype and function of somatic primary afferent nociceptive neurones with C-, Adelta- or Aalpha/beta-fibres. Experimental physiology 87:239-244.

Lawson SN, Crepps BA, Perl ER (1997) Relationship of substance P to afferent characteristics of dorsal root ganglion neurones in guinea-pig. J Physiol 505 (Pt 1):177-191.

Le Bars D, Gozariu M, Cadden SW (2001) Animal models of nociception. Pharmacological reviews 53:597-652.

Leem JW, Hwang JH, Hwang SJ, Park H, Kim MK, Choi Y (2001) The role of peripheral N-methyl-D-aspartate receptors in Freund's complete adjuvant induced mechanical hyperalgesia in rats. Neurosci Lett 297:155-158.

Leijten PA, van Breemen C (1984) The effects of caffeine on the noradrenaline-sensitive calcium store in rabbit aorta. J Physiol 357:327-339.

Lewin GR, Moshourab R (2004) Mechanosensation and pain. Journal of neurobiology 61:30-44.

Linck B, Qiu Z, He Z, Tong Q, Hilgemann DW, Philipson KD (1998) Functional comparison of the three isoforms of the Na+/Ca2+ exchanger (NCX1, NCX2, NCX3). Am J Physiol 274:C415-423.

Lokuta AJ, Komai H, McDowell TS, Valdivia HH (2002) Functional properties of ryanodine receptors from rat dorsal root ganglia. FEBS Lett 511:90-96.

Lu SG, Gold MS (2008) Inflammation-induced increase in evoked calcium transients in subpopulations of rat dorsal root ganglion neurons. Neuroscience 153:279-288.

Lu SG, Zhang X, Gold MS (2006) Intracellular calcium regulation among subpopulations of rat dorsal root ganglion neurons. J Physiol 577:169-190.

Lu SG, Zhang XL, Luo ZD, Gold MS (2010) Persistent inflammation alters the density and distribution of voltage-activated calcium channels in subpopulations of rat cutaneous DRG neurons. Pain 151:633-643.

Lynn B, Schutterle S, Pierau FK (1996) The vasodilator component of neurogenic inflammation is caused by a special subclass of heat-sensitive nociceptors in the skin of the pig. J Physiol 494 (Pt 2):587-593.

Ma M (2013) Role of calpains in the injury-induced dysfunction and degeneration of the mammalian axon. Neurobiology of disease 60:61-79.

Maggi CA, Tramontana M, Cecconi R, Santicioli P (1990) Neurochemical evidence for the involvement of N-type calcium channels in transmitter secretion from peripheral endings of sensory nerves in guinea pigs. Neurosci Lett 114:203-206.

Malin SA, Davis BM, Molliver DC (2007) Production of dissociated sensory neuron cultures and considerations for their use in studying neuronal function and plasticity. Nature protocols 2:152-160.

Malmberg AB, Chen C, Tonegawa S, Basbaum AI (1997) Preserved acute pain and reduced neuropathic pain in mice lacking PKCgamma. Science 278:279-283.

Mantyh PW, Rogers SD, Honore P, Allen BJ, Ghilardi JR, Li J, Daughters RS, Lappi DA, Wiley RG, Simone DA (1997) Inhibition of hyperalgesia by ablation of lamina I spinal neurons expressing the substance P receptor. Science 278:275-279.

Marsh B, Acosta C, Djouhri L, Lawson SN (2012) Leak K(+) channel mRNAs in dorsal root ganglia: relation to inflammation and spontaneous pain behaviour. Molecular and cellular neurosciences 49:375-386.

Matta JA, Ahern GP (2007) Voltage is a partial activator of rat thermosensitive TRP channels. J Physiol 585:469-482.

McCallum JB, Kwok WM, Mynlieff M, Bosnjak ZJ, Hogan QH (2003) Loss of T-type calcium current in sensory neurons of rats with neuropathic pain. Anesthesiology 98:209-216.

McNearney T, Baethge BA, Cao S, Alam R, Lisse JR, Westlund KN (2004) Excitatory amino acids, TNF-alpha, and chemokine levels in synovial fluids of patients with active arthropathies. Clinical and experimental immunology 137:621-627.

McNearney T, Speegle D, Lawand N, Lisse J, Westlund KN (2000) Excitatory amino acid profiles of synovial fluid from patients with arthritis. The Journal of rheumatology 27:739-745.

Meissner G (1994) Ryanodine receptor/Ca2+ release channels and their regulation by endogenous effectors. Annu Rev Physiol 56:485-508.

Meissner G (2002) Regulation of mammalian ryanodine receptors. Front Biosci 7:d2072-2080.

Merskey HaB, N. (1994) Classification of Chronic Pain. IASP, Seattle.

Michael GJ, Priestley JV (1999) Differential expression of the mRNA for the vanilloid receptor subtype 1 in cells of the adult rat dorsal root and nodose ganglia and its downregulation by axotomy. The Journal of neuroscience : the official journal of the Society for Neuroscience 19:1844-1854.

Michaelis ML, Nunley EW, Jayawickreme C, Hurlbert M, Schueler S, Guilly C (1992) Purification of a synaptic membrane Na+/Ca2+ antiporter and immunoextraction with antibodies to a 36-kDa protein. J Neurochem 58:147-157.

Michel LY, Verkaart S, Koopman WJ, Willems PH, Hoenderop JG, Bindels RJ (2014) Function and regulation of the Na+-Ca2+ exchanger NCX3 splice variants in brain and skeletal muscle. The Journal of biological chemistry 289:11293-11303.

Miller KE, Hoffman EM, Sutharshan M, Schechter R (2011) Glutamate pharmacology and metabolism in peripheral primary afferents: physiological and pathophysiological mechanisms. Pharmacology & therapeutics 130:283-309.

Molinaro P, Viggiano D, Nistico R, Sirabella R, Secondo A, Boscia F, Pannaccione A, Scorziello A, Mehdawy B, Sokolow S, Herchuelz A, Di Renzo GF, Annunziato L (2011) Na+ - Ca2+ exchanger (NCX3) knock-out mice display an impairment in hippocampal long-term potentiation and spatial learning and memory. The Journal of neuroscience : the official journal of the Society for Neuroscience 31:7312-7321.

Morris JL, Konig P, Shimizu T, Jobling P, Gibbins IL (2005) Most peptide-containing sensory neurons lack proteins for exocytotic release and vesicular transport of glutamate. The Journal of comparative neurology 483:1-16.

Namer B, Barta B, Orstavik K, Schmidt R, Carr R, Schmelz M, Handwerker HO (2009) Microneurographic assessment of C-fibre function in aged healthy subjects. J Physiol 587:419-428.

Nealen ML, Gold MS, Thut PD, Caterina MJ (2003) TRPM8 mRNA is expressed in a subset of cold-responsive trigeminal neurons from rat. J Neurophysiol 90:515-520.

Neher E, Sakaba T (2008) Multiple roles of calcium ions in the regulation of neurotransmitter release. Neuron 59:861-872.

Niu CF, Watanabe Y, Iwamoto T, Yamashita K, Satoh H, Urushida T, Hayashi H, Kimura J (2007) Electrophysiological effects of SN-6, a novel Na+/Ca2+ exchange inhibitor on membrane currents in guinea pig ventricular myocytes. Ann N Y Acad Sci 1099:534-539.

Novakovic SD, Levinson SR, Schachner M, Shrager P (1998) Disruption and reorganization of sodium channels in experimental allergic neuritis. Muscle & nerve 21:1019-1032.

Offley SC, Guo TZ, Wei T, Clark JD, Vogel H, Lindsey DP, Jacobs CR, Yao W, Lane NE, Kingery WS (2005) Capsaicin-sensitive sensory neurons contribute to the maintenance of trabecular bone integrity. Journal of bone and mineral research : the official journal of the American Society for Bone and Mineral Research 20:257-267.

Orozco OE, Walus L, Sah DW, Pepinsky RB, Sanicola M (2001) GFRalpha3 is expressed predominantly in nociceptive sensory neurons. Eur J Neurosci 13:2177-2182.

Palty R, Silverman WF, Hershfinkel M, Caporale T, Sensi SL, Parnis J, Nolte C, Fishman D, Shoshan-Barmatz V, Herrmann S, Khananshvili D, Sekler I (2010) NCLX is an essential component of mitochondrial Na+/Ca2+ exchange. Proceedings of the National Academy of Sciences of the United States of America 107:436-441.

Papa M, Canitano A, Boscia F, Castaldo P, Sellitti S, Porzig H, Taglialatela M, Annunziato L (2003) Differential expression of the Na+-Ca2+ exchanger transcripts and proteins in rat brain regions. The Journal of comparative neurology 461:31-48.

Persson AK, Black JA, Gasser A, Cheng X, Fischer TZ, Waxman SG (2010) Sodium-calcium exchanger and multiple sodium channel isoforms in intra-epidermal nerve terminals. Mol Pain 6:84.

Persson AK, Kim I, Zhao P, Estacion M, Black JA, Waxman SG (2013) Sodium channels contribute to degeneration of dorsal root ganglion neurites induced by mitochondrial dysfunction in an in vitro model of axonal injury. The Journal of neuroscience : the official journal of the Society for Neuroscience 33:19250-19261.

Philipson KD, Nicoll DA, Li Z (1993) The cardiac sodium-calcium exchanger. Soc Gen Physiol Ser 48:187-191.

Pierce PA, Xie GX, Peroutka SJ, Green PG, Levine JD (1995) 5-Hydroxytryptamine-induced synovial plasma extravasation is mediated via 5-hydroxytryptamine2A receptors on sympathetic efferent terminals. The Journal of pharmacology and experimental therapeutics 275:502-508.

Popovich PG, Guan Z, Wei P, Huitinga I, van Rooijen N, Stokes BT (1999) Depletion of hematogenous macrophages promotes partial hindlimb recovery and neuroanatomical repair after experimental spinal cord injury. Experimental neurology 158:351-365.

Pottorf WJ, Thayer SA (2002) Transient rise in intracellular calcium produces a long-lasting increase in plasma membrane calcium pump activity in rat sensory neurons. J Neurochem 83:1002-1008.

Price DD, Craggs JG, Zhou Q, Verne GN, Perlstein WM, Robinson ME (2009) Widespread hyperalgesia in irritable bowel syndrome is dynamically maintained by tonic visceral impulse input and placebo/nocebo factors: evidence from human psychophysics, animal models, and neuroimaging. NeuroImage 47:995-1001.

Price DD, Dubner R (1977) Mechanisms of first and second pain in the peripheral and central nervous systems. The Journal of investigative dermatology 69:167-171.

Price TJ, Flores CM (2007) Critical evaluation of the colocalization between calcitonin gene-related peptide, substance P, transient receptor potential vanilloid subfamily type 1 immunoreactivities, and isolectin B4 binding in primary afferent neurons of the rat and mouse. The journal of pain : official journal of the American Pain Society 8:263-272.

Qiu F, Jiang Y, Zhang H, Liu Y, Mi W (2012) Increased expression of tetrodotoxin-resistant sodium channels Nav1.8 and Nav1.9 within dorsal root ganglia in a rat model of bone cancer pain. Neurosci Lett 512:61-66.

Quan D, Wellish M, Gilden DH (2003) Topical ketamine treatment of postherpetic neuralgia. Neurology 60:1391-1392.

Quednau BD, Nicoll DA, Philipson KD (1997) Tissue specificity and alternative splicing of the Na+/Ca2+ exchanger isoforms NCX1, NCX2, and NCX3 in rat. Am J Physiol 272:C1250-1261.

Quednau BD, Nicoll DA, Philipson KD (2004) The sodium/calcium exchanger family-SLC8. Pflugers Arch 447:543-548.

Raja SN, Meyer RA, Campbell JN (1988) Peripheral mechanisms of somatic pain. Anesthesiology 68:571-590.

Rang HP, Bevan S, Dray A (1991) Chemical activation of nociceptive peripheral neurones. British medical bulletin 47:534-548.

Richardson JD, Vasko MR (2002) Cellular mechanisms of neurogenic inflammation. The Journal of pharmacology and experimental therapeutics 302:839-845.

Rigaud M, Gemes G, Weyker PD, Cruikshank JM, Kawano T, Wu HE, Hogan QH (2009) Axotomy depletes intracellular calcium stores in primary sensory neurons. Anesthesiology 111:381-392.

Robinson DR, Gebhart GF (2008) Inside information: the unique features of visceral sensation. Molecular interventions 8:242-253.

Rohacs T (2005) Teaching resources. TRP channels. Sci STKE 2005:tr14.

Rohacs T, Thyagarajan B, Lukacs V (2008) Phospholipase C mediated modulation of TRPV1 channels. Mol Neurobiol 37:153-163.

Sathish V, Delmotte PF, Thompson MA, Pabelick CM, Sieck GC, Prakash YS (2011) Sodium-calcium exchange in intracellular calcium handling of human airway smooth muscle. PloS one 6:e23662.

Scheff NN, Gold MS (2011) Sex differences in the inflammatory mediator-induced sensitization of dural afferents. J Neurophysiol 106:1662-1668.

Scheff NN, Lu SG, Gold MS (2013) Contribution of endoplasmic reticulum Ca(2+) regulatory mechanisms to the inflammation-induced increase in the evoked Ca(2+) transient in rat cutaneous dorsal root ganglion neurons. Cell Calcium 54:46-56.

Scheff NN, Yilmaz E, Gold MS (2014) The Properties, Distribution, and Function of Na+/Ca2+ Exchanger Isoforms in Rat Cutaneous Sensory Neurons. J Physiol [Submitted].

Schulze DH, Polumuri SK, Gille T, Ruknudin A (2002) Functional regulation of alternatively spliced Na+/Ca2+ exchanger (NCX1) isoforms. Ann N Y Acad Sci 976:187-196.

Schwartz ES, La JH, Scheff NN, Davis BM, Albers KM, Gebhart GF (2013) TRPV1 and TRPA1 antagonists prevent the transition of acute to chronic inflammation and pain in chronic pancreatitis. The Journal of neuroscience : the official journal of the Society for Neuroscience 33:5603-5611.

Sessle BJ, Hu JW (1991) Mechanisms of pain arising from articular tissues. Canadian journal of physiology and pharmacology 69:617-626.

Shimosato G, Amaya F, Ueda M, Tanaka Y, Decosterd I, Tanaka M (2005) Peripheral inflammation induces up-regulation of TRPV2 expression in rat DRG. Pain 119:225-232.

Shishkin V, Potapenko E, Kostyuk E, Girnyk O, Voitenko N, Kostyuk P (2002) Role of mitochondria in intracellular calcium signaling in primary and secondary sensory neurones of rats. Cell Calcium 32:121-130.

Shmigol A, Verkhratsky A, Isenberg G (1995) Calcium-induced calcium release in rat sensory neurons. J Physiol 489 (Pt 3):627-636.

Shutov LP, Kim MS, Houlihan PR, Medvedeva YV, Usachev YM (2013) Mitochondria and plasma membrane Ca2+-ATPase control presynaptic Ca2+ clearance in capsaicin-sensitive rat sensory neurons. J Physiol 591:2443-2462.

Sirabella R, Secondo A, Pannaccione A, Molinaro P, Formisano L, Guida N, Di Renzo G, Annunziato L, Cataldi M (2012) ERK1/2, p38, and JNK regulate the expression and the activity of the three isoforms of the Na+ /Ca2+ exchanger, NCX1, NCX2, and NCX3, in neuronal PC12 cells. J Neurochem 122:911-922.

Skerry TM, Genever PG (2001) Glutamate signalling in non-neuronal tissues. Trends in pharmacological sciences 22:174-181.

Solovyova N, Fernyhough P, Glazner G, Verkhratsky A (2002) Xestospongin C empties the ER calcium store but does not inhibit InsP3-induced Ca2+ release in cultured dorsal root ganglia neurones. Cell Calcium 32:49-52.

Staiano RI, Granata F, Secondo A, Petraroli A, Loffredo S, Annunziato L, Triggiani M, Marone G (2013) Human macrophages and monocytes express functional Na(+)/Ca (2+) exchangers 1 and 3. Advances in experimental medicine and biology 961:317-326.

Staud R, Nagel S, Robinson ME, Price DD (2009) Enhanced central pain processing of fibromyalgia patients is maintained by muscle afferent input: a randomized, double-blind, placebo-controlled study. Pain 145:96-104.

Stucky CL, Lewin GR (1999) Isolectin B(4)-positive and -negative nociceptors are functionally distinct. The Journal of neuroscience : the official journal of the Society for Neuroscience 19:6497-6505.

Svichar N, Kostyuk P, Verkhratsky A (1997) Mitochondria buffer Ca2+ entry but not intracellular Ca2+ release in mouse DRG neurones. Neuroreport 8:3929-3932.

Takahashi K, Aoki Y, Ohtori S (2008) Resolving discogenic pain. European spine journal : official publication of the European Spine Society, the European Spinal Deformity Society, and the European Section of the Cervical Spine Research Society 17 Suppl 4:428-431.

Tan PH, Yang LC, Chiang PT, Jang JS, Chung HC, Kuo CH (2008) Inflammation-induced up-regulation of ionotropic glutamate receptor expression in human skin. British journal of anaesthesia 100:380-384.

Tarpley JW, Kohler MG, Martin WJ (2004) The behavioral and neuroanatomical effects of IB4-saporin treatment in rat models of nociceptive and neuropathic pain. Brain research 1029:65-76.

Thayer SA, Miller RJ (1990) Regulation of the intracellular free calcium concentration in single rat dorsal root ganglion neurones in vitro. J Physiol 425:85-115.

Thayer SA, Usachev YM, Pottorf WJ (2002) Modulating Ca2+ clearance from neurons. Front Biosci 7:d1255-1279.

Thurneysen T, Nicoll DA, Philipson KD, Porzig H (2002a) Immunohistochemical detection of the sodium-calcium exchanger in rat hippocampus cultures using subtype-specific antibodies. Ann N Y Acad Sci 976:367-375.

Thurneysen T, Nicoll DA, Philipson KD, Porzig H (2002b) Sodium/calcium exchanger subtypes NCX1, NCX2 and NCX3 show cell-specific expression in rat hippocampus cultures. Brain Res Mol Brain Res 107:145-156.

Tian DH, Perera CJ, Moalem-Taylor G (2013) Neuropathic pain in animal models of nervous system autoimmune diseases. Mediators of inflammation 2013:298326.

Tolkovsky AM, Richards CD (1987) Na+/H+ exchange is the major mechanism of pH regulation in cultured sympathetic neurons: measurements in single cell bodies and neurites using a fluorescent pH indicator. Neuroscience 22:1093-1102.

Usachev Y, Shmigol A, Pronchuk N, Kostyuk P, Verkhratsky A (1993) Caffeine-induced calcium release from internal stores in cultured rat sensory neurons. Neuroscience 57:845-859.

Usachev YM, Marsh AJ, Johanns TM, Lemke MM, Thayer SA (2006) Activation of protein kinase C in sensory neurons accelerates Ca2+ uptake into the endoplasmic reticulum. The Journal of neuroscience : the official journal of the Society for Neuroscience 26:311-318.

Usachev YM, Thayer SA (1997) All-or-none Ca2+ release from intracellular stores triggered by Ca2+ influx through voltage-gated Ca2+ channels in rat sensory neurons. The Journal of neuroscience : the official journal of the Society for Neuroscience 17:7404-7414.

Usachev YM, Thayer SA (1999) Ca2+ influx in resting rat sensory neurones that regulates and is regulated by ryanodine-sensitive Ca2+ stores. J Physiol 519 Pt 1:115-130.

Vaughn AH, Gold MS (2010) Ionic mechanisms underlying inflammatory mediator-induced sensitization of dural afferents. The Journal of neuroscience : the official journal of the Society for Neuroscience 30:7878-7888.

Verdru P, De Greef C, Mertens L, Carmeliet E, Callewaert G (1997) Na(+)-Ca2+ exchange in rat dorsal root ganglion neurons. J Neurophysiol 77:484-490.

Verne GN, Robinson ME, Vase L, Price DD (2003) Reversal of visceral and cutaneous hyperalgesia by local rectal anesthesia in irritable bowel syndrome (IBS) patients. Pain 105:223-230.

Vulchanova L, Olson TH, Stone LS, Riedl MS, Elde R, Honda CN (2001) Cytotoxic targeting of isolectin IB4-binding sensory neurons. Neuroscience 108:143-155.

Walker K, Reeve A, Bowes M, Winter J, Wotherspoon G, Davis A, Schmid P, Gasparini F, Kuhn R, Urban L (2001) mGlu5 receptors and nociceptive function II. mGlu5 receptors functionally expressed on peripheral sensory neurones mediate inflammatory hyperalgesia. Neuropharmacology 40:10-19.

Wan QF, Nixon E, Heidelberger R (2012) Regulation of presynaptic calcium in a mammalian synaptic terminal. J Neurophysiol 108:3059-3067.

Wanaverbecq N, Marsh SJ, Al-Qatari M, Brown DA (2003) The plasma membrane calcium-ATPase as a major mechanism for intracellular calcium regulation in neurones from the rat superior cervical ganglion. J Physiol 550:83-101.

Watanabe Y, Koide Y, Kimura J (2006) Topics on the Na+/Ca2+ exchanger: pharmacological characterization of Na+/Ca2+ exchanger inhibitors. J Pharmacol Sci 102:7-16.

Watkins LR, Hutchinson MR, Milligan ED, Maier SF (2007) "Listening" and "talking" to neurons: implications of immune activation for pain control and increasing the efficacy of opioids. Brain research reviews 56:148-169.

Weiss N, Zamponi GW (2012) Regulation of voltage-gated calcium channels by synaptic proteins. Advances in experimental medicine and biology 740:759-775.

Werth JL, Thayer SA (1994) Mitochondria buffer physiological calcium loads in cultured rat dorsal root ganglion neurons. The Journal of neuroscience : the official journal of the Society for Neuroscience 14:348-356.

Werth JL, Usachev YM, Thayer SA (1996) Modulation of calcium efflux from cultured rat dorsal root ganglion neurons. J Neurosci 16:1008-1015.

Woodbury CJ, Kullmann FA, McIlwrath SL, Koerber HR (2008) Identity of myelinated cutaneous sensory neurons projecting to nocireceptive laminae following nerve injury in adult mice. The Journal of comparative neurology 508:500-509.

Woodbury CJ, Zwick M, Wang S, Lawson JJ, Caterina MJ, Koltzenburg M, Albers KM, Koerber HR, Davis BM (2004) Nociceptors lacking TRPV1 and TRPV2 have normal heat responses. The Journal of neuroscience : the official journal of the Society for Neuroscience 24:6410-6415.

Xie W, Strong JA, Ye L, Mao JX, Zhang JM (2013) Knockdown of sodium channel NaV1.6 blocks mechanical pain and abnormal bursting activity of afferent neurons in inflamed sensory ganglia. Pain 154:1170-1180.

Yilmaz-Rastoder E, Gold MS, Hough KA, Gebhart GF, Williams BA (2012) Effect of adjuvant drugs on the action of local anesthetics in isolated rat sciatic nerves. Reg Anesth Pain Med 37:403-409.

Zhang X, Xu ZO, Shi TJ, Landry M, Holmberg K, Ju G, Tong YG, Bao L, Cheng XP, Wiesenfeld-Hallin Z, Lozano A, Dostrovsky J, Hokfelt T (1998) Regulation of expression of galanin and galanin receptors in dorsal root ganglia and spinal cord after axotomy and inflammation. Ann N Y Acad Sci 863:402-413.

Zhang XL, Mok LP, Katz EJ, Gold MS (2010a) BK(Ca) currents are enriched in a subpopulation of adult rat cutaneous nociceptive dorsal root ganglion neurons. Eur J Neurosci 31:450-462.

Zhang XL, Mok LP, Katz EJ, Gold MS (2010b) BKCa currents are enriched in a subpopulation of adult rat cutaneous nociceptive dorsal root ganglion neurons. Eur J Neurosci 31:450-462.

Zhang XL, Mok LP, Lee KY, Charbonnet M, Gold MS (2012a) Inflammation-induced changes in BK(Ca) currents in cutaneous dorsal root ganglion neurons from the adult rat. Mol Pain 8:37.

Zhang XL, Mok LP, Lee KY, Charbonnet M, Gold MS (2012b) Inflammation-induced changes in BKCa currents in cutaneous dorsal root ganglion neurons from the adult rat. Mol Pain 8:37.